NTNU – Trondheim
Norwegian University of
Science and Technology

3D geophysical and geological modelling of the Karasjok Greenstone Belt

Jon Are Aagård Skaar

Geology
Submission date: December 2014
Supervisor: Allan George Krill, IGB
Co-supervisor: Jörg Ebbing, NGU

Norwegian University of Science and Technology
Department of Geology and Mineral Resources Engineering

Abstract

The Karasjok Greenstone Belt (KGB) is a linear segment of rift-related metavolcanic and metasedimentary rocks and forms the northeastern prolongation of the Paleoproterozoic Central Lapland Greenstone Belt in the Fennonscandian shield. Due to the few exposures and lack of surface data data in the Finnmarksvidda area, the internal structures within the KGB are poorly understood. This thesis is therefore a part of the project Mineral Resources in Northern Norway (MINN), governed by the Geological Survey of Norway (NGU). Its purpose is to integrate geophysical and geological data in order to present a new 3D crustal model of the northern part of the KGB, to better understand the crustal architecture.

The new 3D model presented in this thesis covers an area of 20 x 30 km, to depths of 10 km, just north of Karasjok. It is based on 3D density modelling of newly acquired high resolution Airborne Gravity Gradient data, integrated with new geological field observations and supplemental petrophysical data. As a first step in developing the new 3D model, a qualitative structural interpretation of curvature analysis of gravity gradient and aeromagnetic data, was followed up by field mapping of key structures. The results from these investigations were used as inputs to constrain the 3D model. This multiscale approach has allowed establishing a link between near-surfaces and deeper, regional structure of the belt. By utilizing the second and third order invariants of the gravity tensor during the modelling, it has been possible to constrain the 3D model shapes and geometries of the main structures within the KGB.

The results of the study show that the KGB makes up an east-dipping crustal feature, positioned between the Archean Jergul Gneiss Complex (JGC) and the Paleoproterozoic collisional mélange, the Tanaelv Migmatite Belt (TMB). The model suggests that the KGB is rather shallow, making up a 3 km deep structure. The first order structures were caused by west-vergent thrusting, formed during a regional D_1 deformation phase. These structures reflect imbricate stacking and internal folding, reassembling a fold-and-thrust belt. Later deformation phases reactivated these thrust structures, initiating transpressional and strike-slip movement, in addition to folding. Steep NE-SW trending faults have been identified as important structures, indicating a prolonged deformation history. These faults are attributed to complex dextral rotation, explaining the arcuate structural grain towards the southern part of the study area.

The developed 3D crustal model suggests that the volcanic units within the Bakkilvarri Fm. are less voluminous than previously interpreted. The volcanics are concentrated in the eastern part of the belt, forming a NW-SE linear structure. The 3D model shows that outcropping tonalities in the northeastern parts of the area are recognized as crustal scale structures, either representing thrust emplaced basement complex, or a deformed intrusive unit. This complex explains the circular-shaped negative gravity and magnetic anomaly. The mafic and ultramafic intrusions are

generally shallow features, and were most likely emplaced before, or during an early stage of the main thrusting.

This study shows that careful integration of geological and geophysical data can vastly improve the 3D understanding of complex, poorly exposed terranes. Integrated 3D density modelling using airborne gravity gradient data and rotational invariants helps to refine and establish realistic 3D subsurface models.

Samandrag

Karasjok Grønnsteinsbelte (KGB) er eit lineært segment av rift-relaterte metavulkanitter og metasedimentære einingar og utgjer den nordvestlege delen av dei Paleoproterosoiske suprakrustalane i det Fennoskandiske skjoldet. KGB er ansett som den nordlege forlenginga av Sentral-Lapland Grønnsteinsbelt. På grunn av dårleg blotningsgrad og mangel på overflatedata er dei interne strukturane i KGB dårleg forstått. Denne oppgåva er gjennomført som ein del av Mineralressursar i Nord-Noreg (MINN), styrt av Noregs Geologiske Undersøking. Hensikta med oppgåva er å integrere geofysiske og geologiske data for å utvikle ein ny 3D skorpemodell av den nordlege delen av KGB.

Den nye 3D modellen utgjer eit området på 20 x 30 km, til eit djup på 10 km, rett nord for Karasjok. Den nye modellen er utvikla ved hjelp av 3D tettleiksmodellering av nye høgoppløyselege flygradiometrimålingar, integrert med petrofysikk, flymagnetiske data og geologiske observasjonar. For å avgrense 3D modelleringa har det blitt gjennomført kvalitative strukturtolkingar av kurtvaturanalyser av gravitasjonstensoren og flymagnetiske data, saman med oppfølgingsarbeid i felt. Denne integrerte framgangsmåten har gjort det mogeleg å korrelere djupare og grunnare strukturar internt i grønnsteinsbeltet. Ved å utnytte til andre og tredje ordens invariant av gravitasjonstensoren, har det vore mogleg å avgrense tredimensjonale strukturer og geometriar til hovudelementa innan KGB i 3D modelleringa.

Resultata frå dette studiet viser at Karasjok Grønnsteinsbelt utgjer ein austhellande skorpestruktur , plassert mellom den Arkeiske Jergulgneissen og det Seinproterosoiske Tanaelvbeltet. Den nye 3D modellen viser at grønnsteinsbeltet er ein grunn struktur som strekker seg til om lag 3 km djup. Feltobservasjonar og strukturelle tolkingar av potensialfeltdata viser at hovudstrukturane er danna som ei resultat av vestleg skyving, under den regional deformasjonsfasen D1. Basert på dei generelle strukturelle trendande, er dei tolka til å vere imbrikasjonsstabling og folding, som reflekterer strukturar frå eit folde-og skyvebelte. Dei komplekse strukturelle trendane observert i dag vart danna som eit resultat av kompleks reaktivering av gamle D1-strukturar. Dette initierte mest sannsynleg transpresjon og sidelengsbevegelsar langs gamle D1-skyvesoner. Dei nye tolkingane i området viser at NA-SV orienterte forkastingar utgjer viktige skorpestrukturar, og er mest sannsynleg relatert til fleire generasjonar med reaktivering. Desse strukturane er relaterte til ein dekstral rotasjon og kan difor forklare den bueforma strukturelle orienteringa mot dei sørlege delane av beltet.

Den nye 3D geologiske modellen viser at dei vulkanske einingane innan Bakkilvarri Fm. utgjer ein mindre del av beltet enn tidlegare anteke. Desse er hovudsakleg konsentrert i den austlege delen av beltet, der dei utgjer ein NV-SA lineær struktur. 3D modellen viser at utgåande tonalitter i den nordaustlege delen av beltet utgjer storskala skorpestrukturar. Dei er tolka til å anten vere innskyvde underlagsdekker eller deformerte intrusive kompleks. Desse kompleksa forklarar dei sirkulære neg-

ative gravitasjons og magnetiske anomaliane. Mafiske og ultramafiske intrusjonar utgjer generelt grunne strukturar. Resultata her viser at dei mest sannsynleg vart danna rett før eller på eit tidleg stadium i hovuddeformasjonsfasen.

Dette studiet viser at integrert tolking av geofysikk og geologi kan auke 3D forståinga av komplekse og dårlege blotta terran. 3D modellering av flytyngdegradientdata og rotatsjonsinvariantar bidreg til å forbetre 3D skorpemodellar.

Acknowledgment

This master thesis has been carried out at the Department of Geology and Mineral Resources Engneering at the Norwegian University of Science and Technology (NTNU), Trondheim. The thesis is written in collaboration with the Geological Survey of Norway (NGU). Prof. Allan G. Krill (NTNU) has been the main supervisor. Prof. Jörg Ebbing (Prev. NGU, now University of Kiel, CAU) has been the external supervisor.

Many have contributed during this project. First of all, I would like to express my gratitude to Allan Krill and Jörg Ebbing for help and guidance throughout this project. I am grateful to Jörg Ebbing for presenting me the opportunity to get involved in the Mineral Resources in Northern Norway-project (MINN) and at NGU. Thank you for your support during the project and the fruitful discussions about interpretation and modelling.

I would also particularly express my gratitude to the Continental Shelf Geophysics group at NGU, for including me in their team and supporting me throughout the project. In particular, I want to personally thank Odleiv Olesen for his support and the help to finance my field work, conference visits and trip to CAU. I am also grateful to Marco Brönner and Laurent Gernigon for the guidance and help during the last semester of this thesis.

I would also like to thank my family for supporting me throughout the years at NTNU.

At the end, I would also like to thank all my classmates at NTNU, in particular all the 6. graders who did not finish the study normed time. The years in Trondheim would not have been the same without you!

14/12- 2014 Trondheim

Jon Are Skaar

Contents

Chapter 1

Introduction

The Precambrian Fennoscandian Shield is made up a variety of Archean to Paleoproterozoic crustal blocks, and reflects a prolonged history of crustal remobilization and continent growth (Gaàl and Gorbatschev, 1987; Daly et al., 2001, 2006; Korja et al., 2006; Cagnard et al., 2011). Common to many other Precambrian shields, the Fennoscadian shield is mainly dominated by reworked Archean rocks and Paleoproterozoic rift-related metasedimentary and volcanic suits (Gaàl et al., 1989; Lehtonen et al., 1998). The main Paleoproterozoic greenstone terrane within the Fennoscandia, the Central Lapland Greenstone Belt (CLGB), is regarded as one of the largest known greenstone terranes, reflecting over 600 million years of geodynamic development (Figure 1.1 (a)) (Lehtonen et al., 1998; Hanski et al., 2001; Hanski and Huma, 2005). In Norway, the Karasjok Greenstone Belt (KGB) makes up the northwestern prolongation of the CLGB (Often, 1985; Braathen and Davidsen, 2000). The KGB can be traced as an almost 100 km wide belt from the Lakselv Valley, throughout the northern Finland (Figure 1.2).

Archean and Paleoproterozoic greenstone belts throughout the world have shown to be favorable areas for valuable mineral deposits, with large scale base metal and precious mineralization (Eilu et al., 2007; Weihed et al., 2005). The most common mineral deposits are related to magmatic activities and deformation influence by fluid flows, creating large potentials for Ni-Cu-PGE, hydrothermal gold, Fe-Ti, iron oxide copper gold (IOCG) and volcanogenic massive sulfide (VMS) deposits (Nilsson and Often, 2005; Airo and Mertanen, 2008; Weihed et al., 2005; Sandstad et al., 2012). An example is the Suurikuusikko deposit within the CLGB, which stands out as a world class gold deposit, with a total resource of 7.36 Moz (Patison et al., 2007). To evaluate the possibilities for mineralization, it is essential to have a well constrained geological and structural understanding of the area. As a result, there has been a large interest for investigating and mapping greenstone belts, for evaluation of the economical potential.

The Paleoproterozoic greenstone belts in the Fennonscandian shield are often heavily covered with Quaternary sediments, and few outcrops are exposed (Olesen and Solli, 1985; Midtun, 1988; Olesen and Sandstad, 1993). This hampers regional geological field mapping and development of coherent geodynamic models. Consequently, the use of geophysical methods have become fundamental in order to understand the geological framework in poorly exposed regions (Olesen and Sandstad, 1993; Betts et al., 2007; Aitken et al., 2008; Airo and Mertanen, 2008). Aeromagnetic and airborne gradiometry (AGG) surveys stand out as the most effective and cheapest geophysical methods to cover large areas with high resolution surveys.

1.1 Background of the thesis

The Finnmarksvidda area has been considered for a long time to be a potential area for large scale mineral deposits. However, the Finnmarkvidda area remains under-explored compared to other Archean and Paleoproterozoic greenstone terranes in the world, such as the Yilgarn Craton and Superior Province of Canada (Weihed et al., 2005). In the 1980's, the Geological Survey of Norway (NGU) launched a large regional mapping program in the Finnmark area. This program led to a significant improvement of the regional geological understanding in the area. However, due to the lack exposures and basic geological data, several important questions still persist. Since then, there has be a demand for a systematic, regional overview and quantification of the mineral potential, in order to enhance the prospectivity mapping.

In 2011, the Geological Survey of Norway initiated a national program for mapping of mineral resources in Northern Norway (MINN-project). The main aim of the program was to gain sufficient geological, geophysical and geochemical data to support and promote further prospectivity. One of the main goals of the MINN-project was to cover the northern parts of Norway with high resolution airborne geophysical data. During a time span from 2007-2012, the entire Finnmarksvidda was covered with high resolution aeromagnetic and radiometric data. In 2011, the first onshore Airborne Gravity Gradient in Norway was acquired over the northern parts of the KGB.

This thesis is a part of the recent investigations of the Karasjok region on Finnmarksvidda. The work of this thesis is based on the newly acquired high resolution aeromagnetic and AGG data, collected as a part the MINN-project.

1.2 Aim of the thesis

The aim of this master thesis is to integrate geophysical, petrophysical and geological data in order to develop a new 3D geological and geophysical model of

the northern part of the Karasjok Greenstone Belt (KGB), and is a part of the MINN-project, governed by the Geological Survey of Norway.

The development of the new 3D model is based on 3D density modelling of newly acquired Airborne Gravity Gradient data, constrained by petrophysical data, potential field analysis and field mapping. The development of the 3D model is limited by the outline of the AGG survey, making up a 20 x 30 km block within the Iddjajav'ri area, just north of Karasjok (Figure 1.1 (b)). An additionally part of this study is to enhance the geological understanding of the area, by integrating the high resolution geophysical data and geological field observation, to identify and extrapolate lithological and structural features under quaternary sediment cover. This is used as further constrains for 3D model.

By developing a new 3D crustal model of the area, this thesis aims to establish the link between deep structures of the greenstone belt to the observable structures at the surface. This allows for an investigation of important regional structures and lineaments, and can be used to enhance the understanding of the structural architecture of the KGB. By proposing a more detailed 3D model of the geological and structural setting in the Iddjajav'ri area, it is possible to evaluate the tectonic evolution and mineral potential in the area.

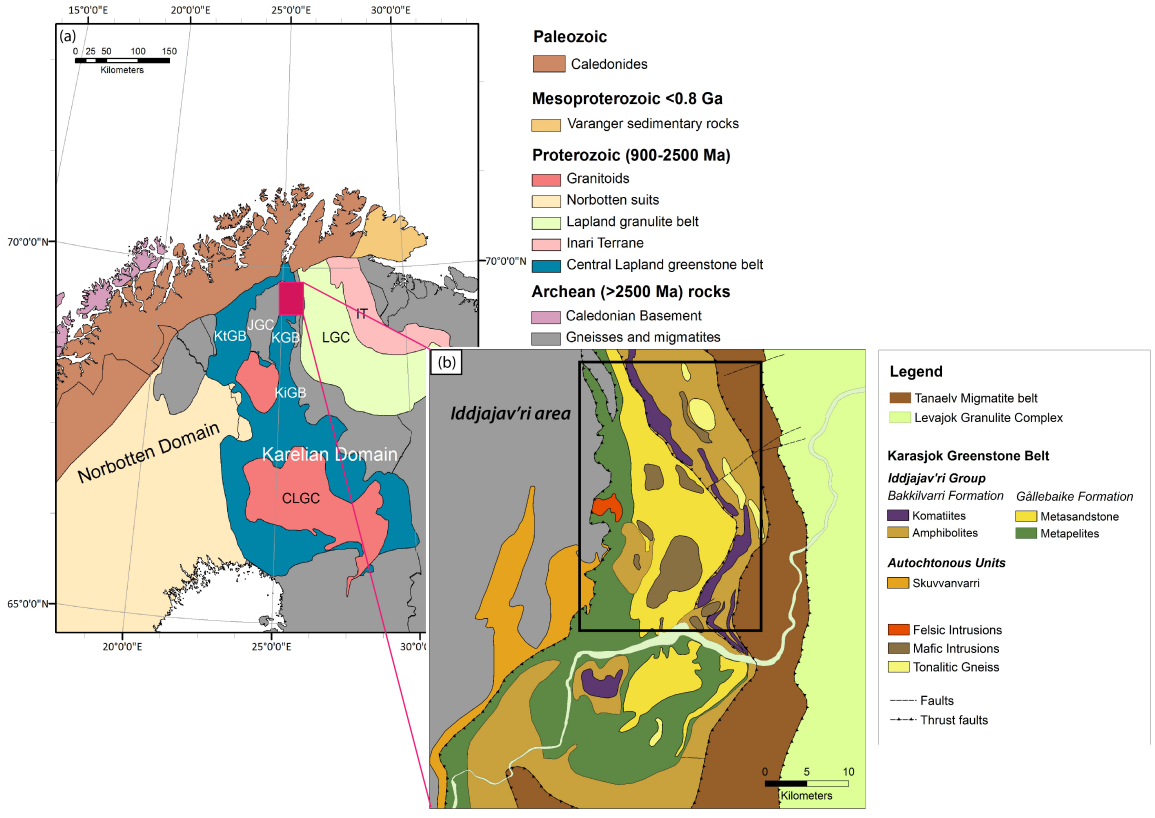

Figure 1.1: (a) Regional tectonic map of the northern part of the Fennonscandian shield, modified after Koistinen et al. (2002). (b) Simplified bedrock map the Karasjok-Iddjajav'ri area, based on the map by Often (1985) and Henriksen (1986). The tectonostratigraphy is based on the interpretation defined by Often (1985) and Siedlecka et al. (1985). Abbreviations: CLGC: Central Lapland Granitoid Complex; IT: Inari Terrane; JGC: Jergul Gneiss Complex; KGB: Karasjok Greenstone Belt; KiGB: Kittilä Greenstone Belt; LGB: Lapland Granulite Belt

1.3 Study Area

The 20 to 40 km wide, NNW-SSE trending Karasjok Greenstone Belt (KGB) is located in easternmost part of the Finnmarksvidda, and is separated from the Kautokeino Greenstone Belt (KtGB) by the Archean Jergul Gneiss Complex (JGC) (Figure 1.1, 1.2) (Krill, 1985; Gaàl and Gorbatschev, 1987; Henriksen, 1991). The KGB sits west of the tectonically overlying Tanaelv Migmatite Belt (TMB) and Levajok Granulite Complex (LGC). The Paleoproterozoic supracrustal complex was emplaced between two large gneiss domes, JGC in the west and Baisvarri Gneis Complex (BGC) in the east (Krill, 1985; Gaàl et al., 1989; Cagnard et al., 2011). The main effort of this work is concentrated within the Iddjajav'ri area, north of Karasjok (Figure 1.1 (b)).

Several large scale Au-Cu and Ni-Cu-PGE deposits have been discovered in Finnish parts of the CLGB since the 80's (Eilu et al., 2007; Weihed et al., 2005). Consequently, the greenstone and schists belts stand out as promising areas for mineral potential (Airo and Kurimo, 1999; Lehtonen et al., 1998; Airo and Mertanen, 2008). The Geological Survey of Finland (GTK) has initiated several explorations projects in the central parts of the CLGB, resulting several large gold discoveries (Patison et al., 2007). However, the Norwegian parts of the KGB remain underexplored. Over 20 years with sporadic exploration have indicated that the Karasjok area is related to high mineral potential, and shows promising indications for possible orogenetic gold and Ni-Cu-PGE deposits (Often, 1985; Nilsson and Often, 2005). However, no of the current prospects have shown sufficient grades or size to be economically profitable.

The Finnmarksvidda area is heavily covered by glacial drifts from the last ice age. As a result, there are few exposures and outcrops in the area, and traditional geological mapping is challenging. Though efforts was carried out during the 80's (Henriksen, 1986), the geology and structural evolution are still poorly constrained. Consequently, the geological interpretation of the study area mostly rely on geophysical mapping and interpretation.

1.4 Previous work

Several geological and geophysical investigations have been conducted in the Karasjok area. The largest coordinated mapping program in Kautokeino-Karasjok area was conducted during a time period from 1982-1992, by NGU. The aim of the program was to remap the area with high resolution geological maps and geophysical data, in order to improve the tectonic understanding and assess the mineral potential of the area (Often, 1985; Krill, 1985; Olesen and Solli, 1985).

The geological mapping of the study area was carried out in a period from 1977-1983, by a variety of contributers ((Henriksen, 1986) and reference therein). The

final map was produced by Henriksen (1986). Furthermore, a regional geological investigation was conducted by Krill (1985), in order to constrain the metamorphic evolution Karasjok-Levajok area.

A summary report compiled by Nilsson and Often (2005) presents an overview of Ni-Cu-PGE occurrences in the Precambrian Finnmark. In this report, the most promising prospects within the Iddjajav'ri area, is defined by the Gallujav'ri intrusion (Figure 3.1). The most recent prospecting campaign in the area was initiated in 2007 by Store Norske Gull AS. Since then, several possible prospects have been drilled in the area, without any profitable results.

The most thorough geophysical study in the area was performed over a series of years as a part of the Finnmark-program, and the results were published in a series of NGU reports (Midtun, 1988). A summary paper from the entire Karasjok area was published by Midtun (1988). This publication summarized the results of the regional interpretation from the Karasjok area, conducted during the Finnmark Program. Results showed that the KGB represent an isoclinal, recumbent fold, between the Archean basement complex and the Tanaelv Migmatite Belt. Their results did not include any tectonic contact between the Gållebaike and Bakkilvarri Fm. The cross section was interpreted to be a large scale, upright antifor. The basement core of the antiform explained the negative gravity anomaly. Several smaller sections were modelled by using only magnetic data.

Midtun (1988) modelled both a regional and a more local E-W gravity profiles in the northern part of the Iddjajav'ri area (his Figure 7 and Profile E). The regional profile extended further west, towards the KtGB. The regional profile showed that the KGB formed an east dipping structural feature, emplaced between the Jergul Gneiss Complex in the west, and Tanaelv Migmatite Belt in the east. The local profile indicated that the KGB made up a synform-antiform pair, with a updome of the JGC. The study concluded that the area was mainly influenced by compressional tectonics, and possibly made up a foreland-thrust belt, supporting the regional interpretation by Krill (1985) and Gaàl et al. (1989).

As a part of the acquisition of the new AGG data in the Iddjajav'ri area, Ellis and Ebbing (2013) inverted the AGG data set using the VOXI alogrithm developed by Geosoft. The recovered density and susceptbility model was improved by utilizing the Iterative reweighted inversion (IRI) technique (Ellis et al., 2012).

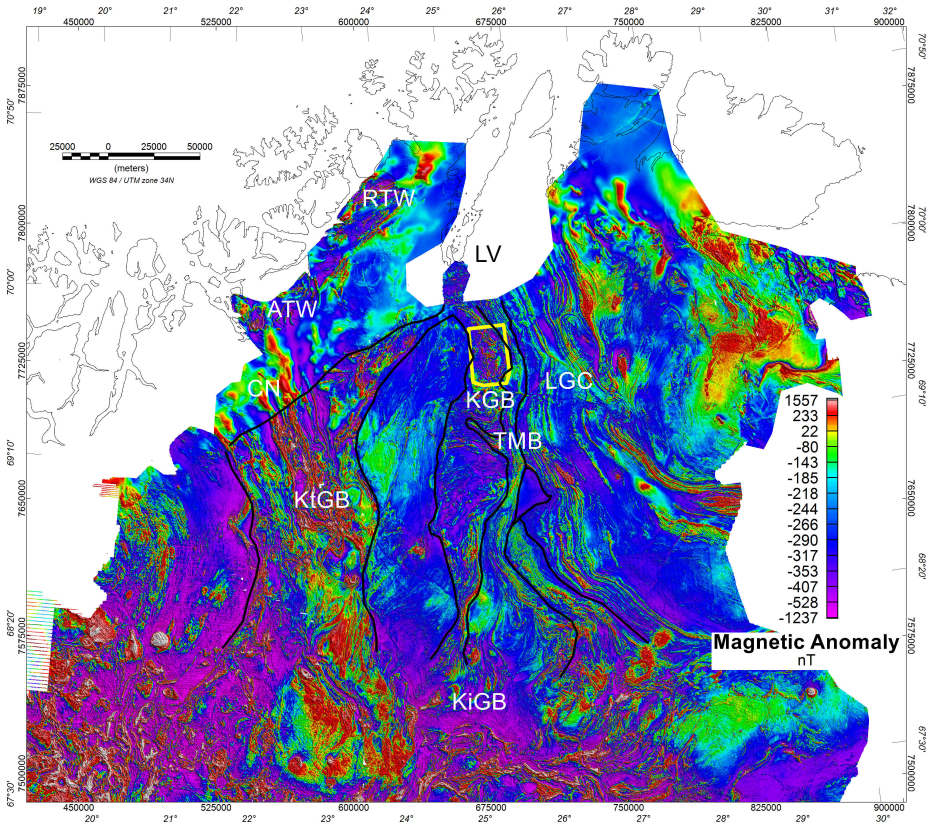

Figure 1.2: Compiled regional high resolution aeromagnetic data, collected from the MINN-project, the Geological Survey of Finaland and Sweden. Section 5.2.2 describes the processing and compilation details. Yellow window marks the study area for this thesis. Tectonic domains after Krill (1985), Olesen and Sandstad (1993) and Koistinen et al. (2002). Abbreviations: Alta Tectonic Window, CN: Caledonian Nappes, JGC: Jergul Gneiss Complex, KGB: Karasjok Greenstone Belt, KiGB: Kittilä Greenstone Belt, KtGB: Kautokeino Greenstone Belt, LGC: Levajok Granulite Complex, LV: Lakselv Valley, RTW: Repparfjord Tectonic Window.

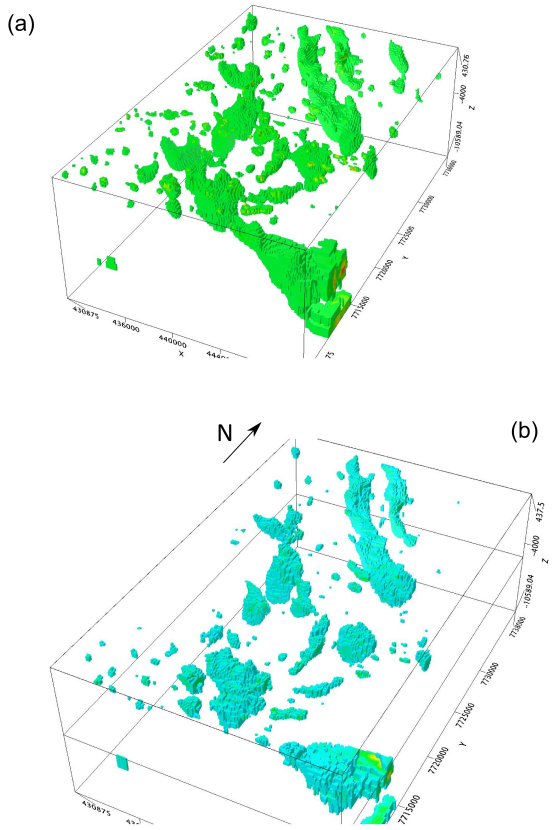

Figure 1.3: Results from the property inversion by Ellis and Ebbing (2013). (a) The recovered density distribution, where the model has been clipped for values below 150 kg/m^3. (b) The recovered susceptibility distribution from the Magnetization Vector Inversion (MVI). Only values over 0.05 (normalized units) are shown. Note the large, NW-SE trending body seen in both of the inversion results. The body correlates to the observed mafic to ultramafic volcanic belt within the Bakkilvarri Fm. Isolated anomalies further west are mostly caused by mafic and ultramafic intrusions.

Pure property, voxelized inversions algorithms have the advantage that no a priori information is needed in order to recover density and susceptibility models (Zhdanov et al., 2004). This allows a first, coarse model to be recovered from the measured data. However, reliable interpretations of pure property inversions require geological ground truth and petrophysical constrains, as the recovered property models represent a smoothed model of complex geology. The recovered models from the VOXI inversion revealed more complex structures related to the distribution of the main volcanic units within the KGB (Figure 1.3 (a), (b)).

Chapter 2

Potential field background

Gravity and magnetic fields are vector fields that obeys Laplace equation in source free space (Kellogg, 1929). These vector fields describe forces that influence at any point in space, due to density distribution for the gravity field, or magnetiztion distribution for the magnetic field. Extensive treatments of theory behind these methods can be found in Blakley (1995) and Kellogg (1929).

Both gravity and magnetic methods have been extensively used for investigations and modelling of shallow and deep structures (Blakley, 1995). The main goal potential field methods measurements is to reduce the signal so it only reflects the geophysical signature of the desired the target source. The anomaly field is therefore regarded as the deviation from a regional normal field.

2.1 Gravity

The gravitational field occurs due to the mutual attractions between two bodies with masses, following Newton's Law of Gravitation (Kellogg, 1929). By applying the superposition principle, the gravity field caused by a mass is described by the integral equation:

$$\mathbf{g}(P) = \gamma \int_R \rho(Q) \frac{\hat{\mathbf{r}}}{r^2} dv \tag{2.1}$$

where $\hat{\mathbf{r}}$ is the unit vector between the origin of the volume of mass, Q, and the observation point P (Blakley, 1995).

By reducing the measured gravity field, gravity surveys can detect lateral density variation in the upper mantle and crust, dependent on the scale of survey. Traditionally, the most common component used in gravity interpretation is the vertical gravity, as this is measured in normal gravity surveys.

The gravity field is derived from the first order derivative of the gravity potential, while the second order derivatives yield the gravity gradients (Kellogg, 1929).

The gravity gradients form a second rank tensor, and can be described by the matrix:

$$\Gamma = \nabla \mathbf{g} = \begin{bmatrix} g_{xx} & g_{gxy} & g_{xz} \\ g_{yx} & g_{yy} & g_{yz} \\ g_{zx} & g_{zy} & g_{zz} \end{bmatrix} \tag{2.2}$$

Consequently, the tensor is independent of the choice of coordinate system. As the gravitational potential follows Laplace's equation, five of the nine gradients are independent. The gradient tensor is symmetric and its trace, or the first order invariant, given by $Tr(\Gamma) = g_{xx} + g_{yy} + g_{zz}$ equals zero, when the field is harmonic, and obeys Laplace's equation, i.e. in source free regions (Blakley, 1995; Pedersen and Rasmussen, 1990). As a consequence, there are only five independent gradients.

The vertical gravity gradient response from a point source, has a decay rate of $1/r^3$, similar to magnetic field (Heiland, 1940). However, in reality the decay rate for complex geological structures are dependent on their shape, depth and dimension (Hinze et al., 2013). Consequently, the gravity gradients are more sensitive to shallower sources, i.e. emphasize higher frequencies over lower, and are therefore image the near surface geology better compared to vertical gravity measurements. This makes the gravity gradient surveys more suitable for interpretations of shallow geology and structures, as the signal does not contain, in this case, unwanted contribution from long wavelength sources, and the problem of separating the regional field from the residual field is not so prominent.

The gravity gradients can be measured directly through gravity gradiometry. Gravity gradiometry was first introduced by Baron von Eötvös and during the 1920's and 30's, termed the torsion balance method (Rybar, 1923; Heiland, 1940). Torsion methods proved to be a valuable measuring method, and measurements were successfully implemented in oil and mineral exploration (Rybar, 1923; Slotnick, 1932; Evjen, 1932).

The airborne gravity gradiometry system (AGG) FALCON was developed during the 1990's by BHP Billiton, and first applied in commercial surveys in 2001 (Lee, 2001; Dransfield, 2007). The FALCON system is based on a rotating gravity gradiometry instrument that measures the horizontal components of the gravity field, i.e. the g_{xy} and g_{uv}, where $g_{uv} = \frac{1}{2}(g_{xx} - g_{yy})$ (Lee, 2001). The horizontal gradients are transformed in order to calculate the five independent gravity components. For the more details regarding the technical background of AGG technology, the reader is referred to Dransfield (2007), Carlos et al. (2013) and references therein. Although the tensor gravity technique is know for more that 15 years, only two full tensors surveys have been flown onshore in Norway. However, Full Tensor Gradient (FTG) surveys have been acquired in the Barents Sea, both by airborne and ship measurements.

2.1.1 Geometric properties of the equipotential field and curvature analysis

The horizontal components of the gravity field measured by the AGG system, the g_{xy} and g_{uv}, are often called the curvature gradients. In order to understand the properties of these components and their applications in curvature analysis, this section briefly summarizes the relations between gravity gradients and the geometry of the equipotential field.

Changes in the gravity field can be attributed to variations of its equipotential surface, that further can be attributed to changes in curvature of an surface. Given an arbitrary point P at the surface S, the tangent plane yields the x- and y-axis, while the z-axis is defined as the normal vector to the tangent plane, i.e. gravity field lines (Hofmann-Wellenhof and Mortiz, 2005). Hence, the curvature C is given as the tangent plane to the point P, which is continuous as long as the surface S is smooth and is differential (Slotnick, 1932). The tangent surface is therefore described by

$$z = \frac{R^2}{2}\left(\frac{\partial^2 z}{\partial x^2}\cos^2(\theta) + \frac{\partial^2 z}{\partial x \partial y}\sin\theta\cos\theta + \frac{\partial^2 z}{\partial y^2}\sin^2\theta\right) \tag{2.3}$$

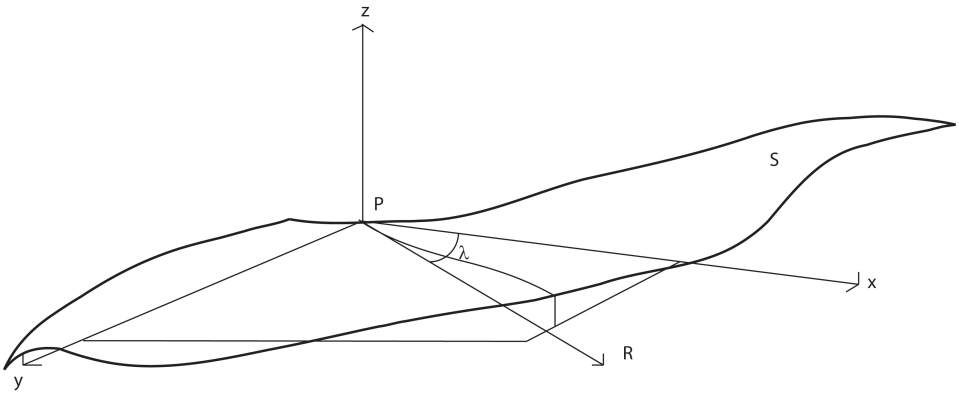

Figure 2.1: The equipotential surface S, given at a point P

where R is the radii vector of the tangent plane. From differential calculus and expansions of the Taylor series and using the definition of curvature, curvature of the tangent plane is given

$$k = -\left(\frac{\partial^2 z}{\partial x^2}cos^2\theta + 2\frac{\partial z}{\partial xy}sin\theta cos\theta + \frac{\partial^2 z}{\partial x^2}sin^2\theta\right) \tag{2.4}$$

From derivation of equation 2.4 to find the angles where the function reaches its maximum, it clear that solution yields two principle direction of the equipotential surface. As the solution for the extreme points of equation 2.4 yields a

trigonometric solution, it is reasonable to conclude that one of the curvatures is a maximum, and the other a minimum, where the two solutions are perpendicular to each other. Applying the statement above to equation 2.4, the maximum and minimum curvature of the surface is given by

$$K_1 = \frac{\partial^2 z}{\partial x^2} \tag{2.5}$$

$$K_2 = \frac{\partial^2 z}{\partial y^2} \tag{2.6}$$

which then is the radii of the principle curvature (Slotnick, 1932; Heiland, 1940).

As the K_1 and K_2 are the extreme values of the curvature, they represent the radii of principle curvature (Slotnick, 1932). Consequently, these components can be used to derive different properties of the curvature of a surface. The average value of the maximum and the minimum curvature is therefore a constant and yields the mean curvature, given by

$$K_m = \frac{1}{2}\left(\frac{\partial^2 z}{\partial x^2} + \frac{\partial^2 z}{\partial x^2}\right) \tag{2.7}$$

The differential curvature is found by subtracting the maximum and minimum curvatures, given by 2.5 and 2.6.

$$K_d = \frac{1}{2}\left((\frac{\partial^2 z}{\partial x^2} + \frac{\partial^2 z}{\partial y^2})^2 + 4(\frac{\partial^2 z}{\partial xy})^2\right)^{0.5} \tag{2.8}$$

The relation between the curvature of a arbitrary surfaces and the gravitational equipotential surface is obtained by defining the gravity potential U to the surface z, by an implicit relation

$$U(x, y, z) = c \tag{2.9}$$

As z is implicitly defined by the gravity potential, the equation above can be used to derive the expressions for the curvatures of the gravitational equipotential surface. This can be used to link the differential curvature to the second derivative of the potential, yielding

$$K_d = \frac{\sqrt{g_{uv}^2 + 4g_{xy}^2}}{g_z} \tag{2.10}$$

and to the mean curvature

$$K_m = \frac{(g_{xx} + g_{yy})}{2g_z} \tag{2.11}$$

Therefore, the measured components g_{xy} and g_{uv} in AGG surveys are proportional to the components of the differential curvature (equation 2.4). As the

differential curvature is zero for a spherical surface, it is a measurement of the deviation from a spherical surface (Hofmann-Wellenhof and Mortiz, 2005; Zhdanov et al., 2004). Furthermore, the geometric properties of the equipotential fields are therefore independent of coordinate systems, and give a clear physical quantity of the tensor. As proven with inversion results, the horizontal gradients have higher resolving power than the vertical gradient alone (Zhdanov et al., 2004).

2.1.2 Application of the gravity tensor and curvature

Traditionally, the vertical gravity gradient has been the most used component during interpretation (Marson and Klingele, 1993). Due to its physical properties, it is the most straightforward gradient to interpret, as it is directly related to the shape of the source body. Consequently, the vertical gravity gradient yields easily interpretable information about the size and depth extent of the source body.

Compared to the vertical gradient, the horizontal components of the tensor contain additional information, as they are more sensitive to changes in strike and shape of source bodies. This has been extensively shown by conventional filtering techniques (Cordell and Grauch, 1982; Blakley and Simpson, 1986). As the horizontal derivatives of the field induce a phase shift compared to the vertical component, they are more difficult to interpret and include in modelling procedures. Additionally, the conventional filtering and interpretation of single derivative components may lead to misinterpretation of structures, as the source signal is only measured though one of the directions.

In order to take advantage of the different components of the gravity tensor, the properties of the equipotential field can be utilized through the different curvature properties, following the mathematical derivation described above. As the geometric properties, i.e. the curvature, are independent of the coordinate system and include all gradient directions, they contain information not readily observable from the individual gradient components. The analysis of the different curvature components (i.e. variants of the horizontal components) has been used since the early 30's, and are not a new interpretation technique (Rybar, 1923; Heiland, 1940).

A much used quantity during the early days of torsion balance, were the gravity curvature or curvature magnitude, defined as (Slotnick, 1932)

$$g(k_1 - k_2) = \sqrt{g_{uv}^2 + 4g_{xy}^2} \tag{2.12}$$

which is then proportional to the differential curvature (Rybar, 1923). The gravity curvature is often referred to the horizontal directive tendency (HDT) (Heiland, 1940). This term is adopted in this thesis. As the equipotential surface of the point mass is spherical, the HDT is measurement of the deviation of the density distribution from of a point source. The HDT can therefore be used to outline the complexity and somewhat the regional extent of anomalies, as deep regional

features tend to have a smoother signal than shallower, short wavelength anomalies (Blakley, 1995).

The total horizontal gradient of the vertical gravity (often termed the total horizontal derivative (THDR)) can be defined by

$$THDR = \sqrt{\left(\frac{\partial g_z}{\partial x}\right)^2 + \left(\frac{\partial g_z}{\partial y}\right)^2} \tag{2.13}$$

The THDR calculates the slope of the measured field. It is based on direction of the largest changes, either ascent or descent, throughout the field. As a result, the maximum values of the THDR are located at the edges of anomaly bodies. This makes the THDR a very efficient filter to outlines edges of anomalous bodies and their structural trends (Blakley and Simpson, 1986; Cordell and Grauch, 1982). Yet, care should be taken when interpreting the THDR, as peak values of dipping bodies and contacts are shifted away from their actual position. In addition, overlapping anomalies can create complex signatures that are not related to true lithological contacts.

By combining different curvatures, it is possible to define local shapes of the equipontial field. Cevallos et al. (2013) illustrates the combination of the mean curvature and the differential curvature, and terms it the shape index (SI). This is defined as

$$SI = \frac{2}{\pi} \arctan\left(\frac{2K_m}{K_d}\right) \tag{2.14}$$

using the expression derived for the mean and differential curvature from (equations 2.10 and 2.11), the equation becomes

$$SI = \frac{2}{\pi} \arctan\left(\frac{g_{zz}}{\sqrt{g_{uv}^2 + 4g_{xy}^2}}\right) \tag{2.15}$$

Consequently, the shape index can be used to determine different morphologies of the equipotential surface. As observed from equation 2.15, the shape index is normalized variant of the HDT, with similarities to other local phase filters, as the tilt derivative and TDX (Miller and Singh, 1994; Cooper and Cowan, 2006).

Pedersen and Rasmussen (1990) introduced the calculations of second and third invariants, to describe the gravity and magnetic tensor. The invariants are rotational invariant and are therefore not dependent on the coordinate system. The second and third order invariants are defined as:

$$I_1 = \sqrt{g_{xx}g_{yy} + g_{yy}g_{zz} + g_{yy}g_{zz}} - (g_{xy}^2 + g_{yz}^2 + g_{xz}^2) \tag{2.16}$$

$$I_2 = g_{xx}(g_{yy}g_{zz} - g_{yz}^2) + g_{xy}(g_{yz}g_{xz} - g_{xy}g_{zz}) + g_{xz}(g_{xy}g_{yz} - g_{xz}g_{yy}) \tag{2.17}$$

The invariants utilize the components of the tensor and can therefore resolve 3D geological features not readily observable from single gradient components (Murphy and Brewster, 2007). The second and third invariants do not contain any more information than the gradients themselves, they represent an efficient way to integrate all tensor components in gravity gradient interpretations. In this study, the second and third order invariants have been applied in both the structural interpretation and during the modelling procedure.

2.2 Magnetics

The Earth's magnetic field can broadly be described as a dipole field, located at the center of the Earth. The remaining parts are caused by a non-dipole field, which include the crustal field. Changes in the magnetic field, which is measured in aeromagnetic surveys, reflect the spatial distribution of magnetic material. Magnetization of a causative body can be described as a single dipole, where the total magnetization is caused by the sum of all magnetic dipole moments, i.e. $\mathbf{M}dv = \mathbf{m}$. Consequently, the magnetic potential is given by

$$V(P) = -C_m \mathbf{M} \cdot \nabla_P \frac{1}{r} dv \tag{2.18}$$

From the Helmholtz theorem, the magnetic field are given by the gradient of the scalar field

$$\mathbf{B}(P) = \nabla V(P) \tag{2.19}$$

Most magnetic surveys measure the total field strength, or also referred to as the total magnetic intensity (TMI). The most common instruments measure the sum of both the vertical and horizontal components. In order to reflect magnetic anomalies from the Earth's crust, it is necessary to reduce the field, to obtain the residual magnetic intensity (RMI), ΔT, given by the equation

$$\Delta T = |\mathbf{T}| - |\mathbf{F}| \tag{2.20}$$

The RMI reflects anomalies caused by variations in magnetic properties within the crust and upper mantle. Magnetization of materials can be caused by both induced magnetization and/or remanent magnetization, which is inherited from earlier events. The dominant magnetization component is therefore described from the ratio between susceptibility and remanence. The induced magnetization is given by the relation

$$\mathbf{M}_{ind} = \chi \mathbf{H} \tag{2.21}$$

where $\mathbf{H}$ is the inducing field and χ is the susceptibility of the material (Clark, 1997). Hence, the total magnetization observed from the subsurface is given by

$$\mathbf{M} = \mathbf{M}_{ind} + \mathbf{M}_{rem} \tag{2.22}$$

Induced magnetization is set up parallel to the Earth's magnetic field. The Curie temperature of magnetite is often used as the thermal limit for magnetic anomalies. In most geodynamic settings, the maximum depth is often located at the crust-mantle transition, approximately depths of 30-40 km.

The magnetization intensity of geological bodies are a function of their magnetic mineralogy, which mainly varies with the distribution of iron in either oxides or silicates. In general, induced intensity measured in aeromagnetic surveys is controlled by the amount of magnetite content in rock units (Clark, 1997; Henkel, 1991), as paramagnetic minerals only yield weak responses. Stable Fe-mineral phases is dependent both of the primary composition, as well as later metamorphic and chemical alterations (Clark, 1997; Grant, 1985a).

In addition, compositional variations control the susceptibility and remanence. Consequently, varying degrees of deformation and alteration can create different magnetic signatures from the same lithological compositions (Airo, 2005, 2007), or by the amount of remanent magnetization present. In addition, burial depth, dip, geometry of the source body, together with the orientation of present day field, control the amplitude, wavelength and shape of the anomaly field (Clark, 1997; Paterson and Reeves, 1985; Hinze et al., 2013). As a result, interpretation of magnetic anomalies are more complex than for gravity.

Remanent magnetization can be acquired by several complex processes. However, natural thermal remanence (NRM) is considered as the most effective contribution measured in aeromagnetic surveys (Dunlop and Ozdemir, 1997; Clark, 1997). The effect of the remanent magnetization on magnetic anomalies is dependent on the declination and inclination of the imprinted magnetization. The relation between the induced and remanent magnetization is given by the Koenigsberger-ratio, also known as the Q-ratio

$$Q = \frac{\mathbf{M}_{rem}}{\mathbf{M}_{ind}} \tag{2.23}$$

In cases where Q-ratios are above one, remanent magnetization should be taken into account when interpreting aeromagnetic data (Clark, 1997; Schmidt et al., 2007; McEnroe and Brown, 2004). In cases where remanent magnetization is reversed relative to the induced magnetization, the magnetic anomalies are heavily skewed or shifted from the induced direction, even if Q-ratios are below one.

2.3 Filtering and image enhancement of potential field data

It is a well known fact that application of conventional filtering techniques greatly enhances interpretation and integration of potential field data. In this study, several techniques have been used as complementary tools for interpretation of depth, structural trends and shape of potential field anomalies within the area. The

filtering and image enhancements have been done using the Discrete Fast Forward Algorithm in the Geosoft Montaj MAGMAP extension (Geosoft, 2005b), which is based on the alogrithms developed by (Bhattacharyya, 1966) and (Parker, 1973). A brief outline of the filtering techniques and their application is presented in this chapter.

2.3.1 Field continuation and transformations

Spectral filtering is a common filtering technique to distinguish shallower features from the deeper. By removing spectral energy related to either deeper or shallower sources, wavelength filtering allows to enhance the field caused by either local or regional anomalies (Gunn et al., 1997; Jaques et al., 1997).

Upward continuation is a low-pass filtering technique that reassembles the observed field at a higher elevation than the actual survey. As a result, the filtering suppresses high frequency signals, over the longer. The technique utilizes the fact that the observation point is from the source body, and therefore contains lower frequency components.

Pseudo Gravity Regional features and of the magnetic anomalies were enhanced by applying the pseudo-gravity (PsG). The pseudo-gravity transforms the magnetic field to an equivalent gravity field, as if the density distribution within in each magnetic domains, is proportional to the magnetization. The transformation requires that the magnetization is piecewise constant, and that no remanent magnetization is present (Blakley, 1995). The pseudo-gravity was used for mapping larger magnetic bodies, as the filter enhances the regional trends, and attenuates the near surface, short wavelength anomalies. In addition, the pseudo gravity was useful to map the correlation between magnetic and gravity sources in the area.

2.3.2 Derivative filtering

The application of different derivative filters can be applied to study the subtle features in potential field data, if not directly measured. The first vertical derivative (VD1) enhances vertical changes of the observed field. It has the function as a high pass filter and increases the spatial resolution of near surface geological structures, as these signals have higher frequency and changes faster, signals from deeper sources. Due to the dynamic range of the anomaly signal, shallower or high intensity anomalies will dominate over more subtle features, as the signature will vary with the effective amplitude. As a result, more subtle features do not provide strong enough signal to be detected.

In order to map more subtle features, a number to balanced or local phase filters can be applied (Cooper and Cowan, 2006; Miller and Singh, 1994). This study

mostly used the amplitude normalizing properties of the tilt derivative (TDR). The TDR yields similar results as the VD1, but are amplitude normalization between negative and positive $\frac{1}{2}\pi$. The TDR is given by the equation

$$TDR = \arctan \frac{\frac{\partial g_z}{\partial z}}{\sqrt{\left(\frac{\partial g_z}{\partial x}\right)^2 + \left(\frac{\partial g_z}{\partial y}\right)^2}} \tag{2.24}$$

Furthermore, the TDR is negative outside sources while positive over sources. The zero contour outlines the boundaries of magnetic and gravity sources, given that the contact is vertical. Discussions and limitations of the method are addressed by e.g. Verduzco et al. (2004) and Cooper and Cowan (2008). The TDR is particularly useful for mapping deeper and more subtle features, not readily seen from the first VD1 or anomaly grids. Consequently, the TDR filter is efficiently applied to highlight structural trends, and more subtle anomalies.

2.4 Structural interpretation of potential field data

There is a strong correlation between potential field analysis and structural analysis, as both aim to interpret overprinting structures, kinematics and 3D architecture of geological features (Aitken et al., 2008; Aitken and Betts, 2009). The ability to correlate potential field data with classical geological approach can therefore be used to interpret structures in poorly exposed terranes, and correlate regional features, not readily observable from field mapping Betts et al. (2007).

Gravity and magnetic anomalies can be described by their tone, texture, shape and pattern, each characteristic to features of the source bodies (Jaques et al., 1997; Gunn et al., 1997). The tone is mainly a function of the amount of magnetite for the case of magnetic surveys, or the bulk density for gravity surveys. The tone can be described as the amplitude of the signal, shown as a tonal color in gridded data. The textural qualities are relate to the short wavelength component of the anomaly, also called relief.

Careful interpretation of potential field data integrated with geological field observations, allows to delineate lithological variations, folds, faults, fractures and large scale shear zones (Gunn et al., 1997; Betts et al., 2003). Due to the higher degree of variations of susceptibility between lithologies and more surface-near sensitivity, the magnetic data is more useful for recognition and mapping smaller structures and detailed, near-surface geology (Airo, 2005; Aitken et al., 2008). Magnetic anomalies are generated either by petrophysical variations between or within lithologies, or by structural features between rocks with different magnetizations (Grant, 1985a). By having a firm understanding of the magnetization pattern, structural features and geological contacts can be established with higher degrees of confidence.

In general, faults and shear zones are recognized by: offsets or displacements of reference structures, discordances of linear structures, linear minimas, due to magnetite destruction or linear to slightly curved magnetic gradients (Henkel and Guzmàn, 1977; Henkel, 1991; Clark, 1997). Large shear zones are often related with a linear signature, either positive or negative, dependent on the fluid processes within the shear zones (Henkel and Guzmàn, 1977). Locally thrusted structures can lead to a repetition of magnetic horizons, similar to the magnetic layering. In areas with low angle thrusts, asymmetric patterns can occur, due to the superposition of different magnetizations. The observed anomaly depends on the magnetization contrast between the foot wall and hanging wall. In general, such anomalies can be identified by discordant structures and more curved minimas, than for brittle dislocations (Henkel, 1991; Airo and Mertanen, 2008).

Folds can be recognized as repetitions of magnetic horizons, or identification of fold axes and limbs if the folds plunge. Separation between faults and upright, tight folds can be difficult, due to their similar signal. In cases where there are clear magnetization contrasts, the dip of folds or faults can be interpreted from the asymmetric anomaly curve. Shallow dipping fold axis can often be recognized by magnetic form lines, where the separate limbs can be observed. In general, systematic linear parallel magnetic features can be attributed to a single tectonic event, either as primary or secondary magnetic foliation, or as a result of combined folding and faulting, which often can be observed in compressional deformation events.

The recognition of domains with different magnetic and gravimetric character, can therefore be used to interpret units or zones with either marked different lithological or structural evolution. The domain based approach can be utilized to separate domains, with common structural evolution, similar to methods used in structural geology (Betts et al., 2003; Aitken et al., 2008).

2.5 Forward Modelling

Several different approaches and strategies for forward and inverse modelling have been developed during the last decades. It is not the aim of this thesis to give a summary of the different approaches. The reader is referred to Blakley (1995) and Hinze et al. (2013) for an extensive outline on modelling approaches. This sub-chapter outlines the basics behind the forward modelling techniques, used in this thesis. To appreciate the result and correctly assess the validity of the modeling results, it is important to understand the foundations behind the forward algorithms.

The forward modelling used in this work was carried out by two main softwares; Intreprid GeoModeller and IGMAS+ (Interactive Geophysical Modeling ASsistant).

2.5.1 GeoModeller

GeoModeller is primarily a 3D geological modeling software, allowing the integration of both geological and geophysical data to solve the forward and inverse problem. The geological model is performed by rule-based modeling, based on a kriging algorithm, similar to e.g Leapfrog.

In order to interpolate between the data points and create a smooth 3D model, the alogrithm requires spatial information (x, y and z position) for both lithological contacts and structural data (Calcagno et al., 2008). The geoloical surfaces are calculated as implicite surfaces, using the potential field interpolation method. Lithological interfaces are therefore interpolated where the potential for one unit is larger than the other. Consequently, the quality of the model is highly dependent on the quality and amount of input spatial data. The interpolation is rule based, i.e. it follows the predefined stratigraphical order that is controlled by the user.

To calculate the forward response of the model, each lithological unit or formation is defined with petrophysical properties. The forward modeling routine is based on a voxel representation of the volume, where each voxel is assign a lithology, and consequently with related petrophysical properties (Calcagno et al., 2008). The forward calculation can either be done in the spatial domain with a convolution algorithm, or by 3D Fast Fourier Transform. As a result, the calculated potential field response is lithoconstrained, as each voxel may only be defined as a single lithology.

2.5.2 IGMAS+

IGMAS+ is an interactive 3D gravity and magnetic forward modelling software. The software is based on triangulation and interpolation between predefined modeled vertical cross sections. The geometries of layers and bodies are defined and modified in the 2D cross sections. The 3D geometries of the bodies are defined by triangulated planes between the top and the bottom of defined layers (Götze and Lahmeyer, 1988; Schmidt and Götze, 1998). Consequently, by defining a sufficient number of cross sections, the amount of interpolation between sections is reduced, and more detailed structures can be made. Each polyhedron is predefined with even distributed density, susceptibility and remanent magnetization. The calculated 3D forward gravity and magnetic field of the model is calculated by the surface integral for all triangulated polyhedrons. The use of vertices and triangulation allow for interactive changes of the shapes and petrophysical properties of the defined layers.

The use of absolute densities, and to match the calculated data to the observed, it is common to apply a constant or DC shift. As IGMAS+ models a complete 3D cube, extended at a certain distance in each direction, it is not necessary to apply DC shifts to the calculated data. Consequently, the software allows for geological modeling of the regional field, i.e. if the model is created deep enough to reflect

the contributions of the observed data.

Chapter 3

Geological and tectonic setting

The Finnmarkvidda area is the northern extension of the Karelian Province, mainly dominated by reworked Archean rocks and Paleoproterozoic rift-related meta-sedimentary and volcanic suits (Gaàl et al., 1989; Lehtonen et al., 1998; Hanski and Huma, 2005). The Kautokeino-Karasjok area includes three large Archean basement complexes, separating the high-grade terranes and supracrustal granite-greenstone belts (Krill, 1985; Often, 1985; Olesen and Sandstad, 1993). The Paleoproterozoic supracrustal meta-sedimentary-volcanic terranes are made up by the Kautokeino Greenstone Belt (KtGB) in the west and Karasjok Greenstone Belts (KGB) in the east. The NW-SE trending greenstone belts are considered to be the northernmost extension of the larger Central Lapland Greenstone Belt (CLGB)(Figure 1.1).

The sedimentary-volcanic units within the KGB extend from Lakselv valley in the north, through the Finnmarksvidda, and can be traced into the central Finnish Lapland, where it bifurcates and reaches both the eastern and western Finnish border (Barbey et al., 1984; Ward et al., 1989; Lehtonen et al., 1998). The greenstone belt can be traced both towards the eastern and western borders of Finland. The southernmost extension of the CLGB is structurally limited by the large shear zone, the Sirkka Line (Gaàl et al., 1989; Väisänen, 2002). The KtGB also displays similar N-S trending features, branching into the larger, more complex volcanic and schist belts in Finland, later intruded by large scale granitoid intrusions (Olesen and Solli, 1985; Lehtonen et al., 1998).

Isotopic datings have shown early Proterozoic ages of the supracrustal features, while the basement complexes are dated as Archean age (Krill et al., 1985; Lehtonen et al., 1998; Hanski et al., 2001). The northern extension of the Paleoproterozic terranes, towards the Lakselv area, are overlain by autochthonous rocks of the Dividal Group and allochtonous thrust nappes, emplaced during the Caledonian Orogeny

(Olesen et al., 1990; Davidsen, 1994; Roberts, 2003). Relics of Paleoproterozoic greenstone terranes can also be observed in structural windows at several locations in the Troms and Finnmark areas (Pharaoh and Peatce, 1984; Roberts, 2003).

3.1 Tectonostratigraphy and lithologies

Stratigraphic definitions and lithological correlations within poorly exposed and polyphase deformed Paleoproterozoic terranes are difficult. The Finnmarkvidda terrane is no exception. Due to the lack of radiometric age dating, exposures and reliable relations between the different lithologies, the stratigraphic relations are still poorly constrained. As a result, different stratigraphies have been developed, based on different interpretations and study areas (Figure 3.3). Within the northern part of the KGB, Davidsen (1994) and Pharaoh and Walsh (1987) defined local stratigraphy for the Lakselv area. In the southern parts, a tectonostratigtaphic relation was defined mainly by Often (1985) and Siedlecka et al. (1985). The stratigraphic correlation between the well exposed Lakselv area and the southern part is not fully understood, and several questions persists regarding the variations in both lithology and structural trends.

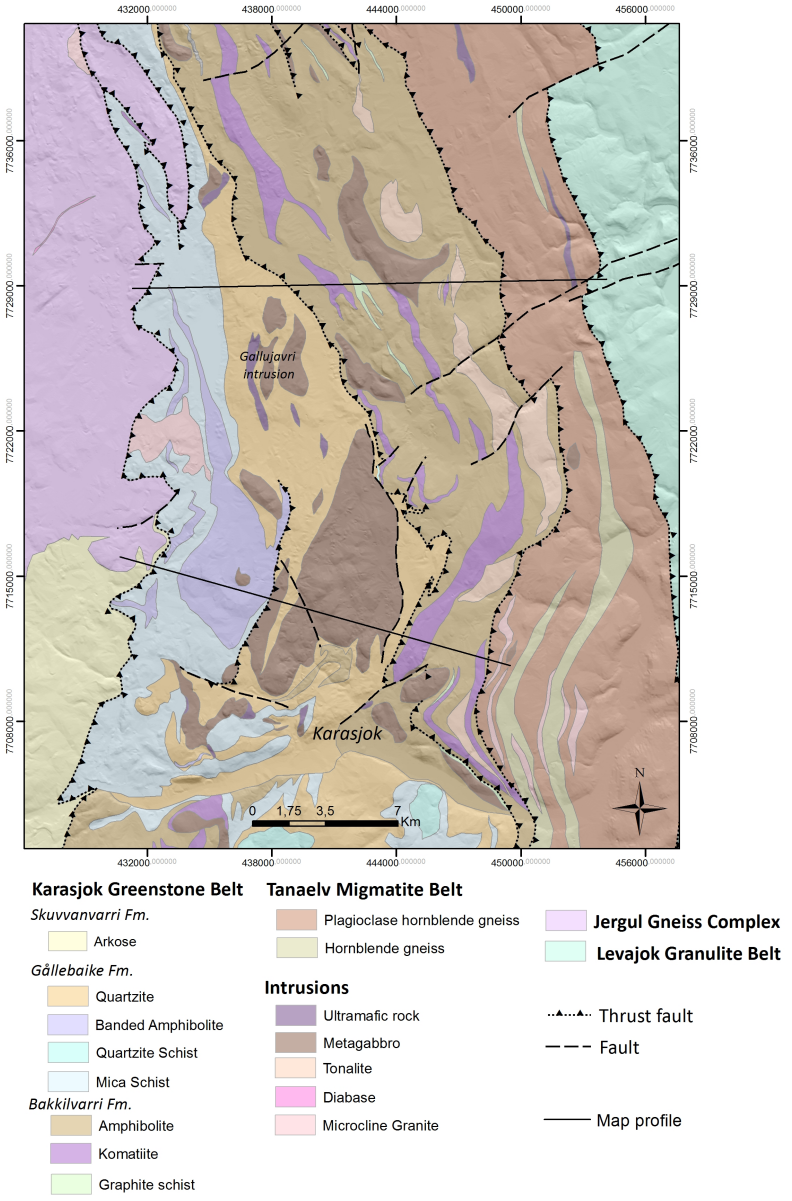

Figure 3.1: Geological map of the Iddjajav'ri area, based on Henriksen (1986) and Nilsen (1986).

Often (1985) and Siedlecka et al. (1985) defined the main features of the KGB to be made up by five main lithological formations (Figure 3.3). The two lowest formations; Voumegielas and Skuvvanvvari Formations, can only be observed in the vicinity of the Jergul Gneiss Complex. The main feature of the KGB is the several km thick, Iddjavarri group, that consists of three main formations; the lowermost Gålibaiki Formation, the Bakkilvarri Formation and the uppermost Råt'zigarri Formation.

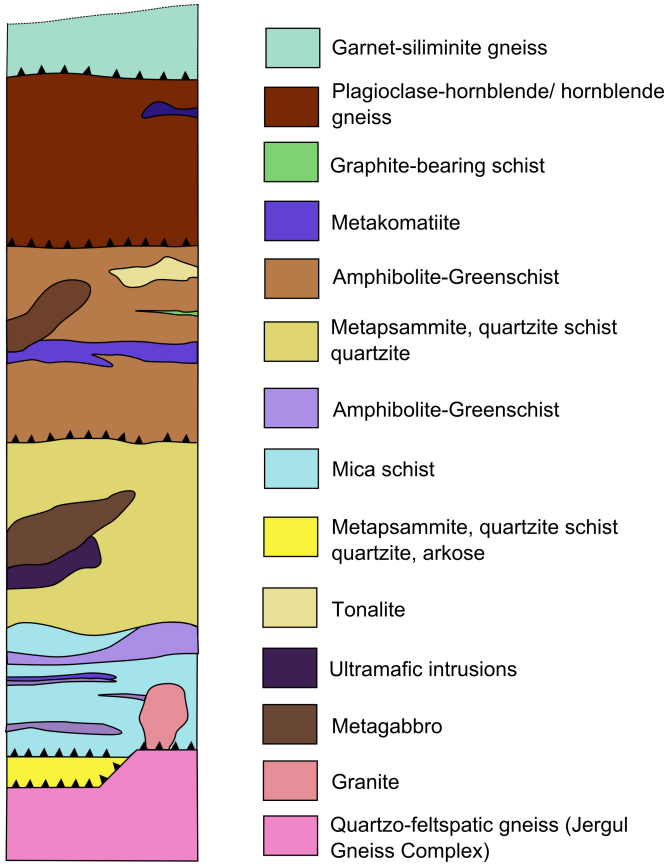

Figure 3.2: Schematic stratigraphic column from the Iddjajav'ri, from Often (1985) and Henriksen (1986)

3.1.1 The Jergul Gneiss Complex

The Jergul Gneiss Complex (JGC) forms a N-S trending basement complex, separating the KtGB and KGB (Krill, 1985; Midtun, 1988; Olesen and Sandstad, 1993) (Figure 1.1). The gneiss complex consists mainly of tonalitic to granitic gneisses.

Additionaly, diabase dikes have been observed within the complex, mainly occuring as NE-SW and NW-SE trending features (Olesen and Sandstad, 1993). Age dating have shown Archean ages, and the JGC is defined as the oldest known rock in Norway (M. Marker, pers.comm., Aug 2014).

3.1.2 Karasjok Greenstone Belt

The supracrustal units within the KGB has been divided into five formations by Often (1985), where the three uppermost main sedimentary-volcanic sequences were grouped into the Iddjajav'ri Group. Often (1985) interpreted the two lowermost formations to be tectonically separated from the Iddjajav'ri group.

The Voumegielas Fm. is primarily made up by foliated ampibolites, interpreted to be relics from mafic and komatiitic volcanism (Often, 1985; Barbey et al., 1984), and is the lowest unit of the supracrustal rocks within the KGB. It is interpreted to have a gradual transition to the above lying Skuvvanvarri Formation. The observations of the Voumegiela Fm. are limited to the northernmost part of the KGB, in the Skoganvarre area as well and the Lakselv area. This has not been confirmed within the sequence in the Iddjajav'ri area.

The Skuvvanvarri Fm. consists mostly of clastic lithofacies, i.e. sandstones, feldspar-rich quartzites, mudstones and conglomerates (Siedlecka et al., 1985). The Skuvvanvarri Fm. shows some preserved primary sedimentary structures in the northern extension, the Skoganvarre area Pharaoh and Walsh (1987). The formation rests with an angular unconformity on the JGC, which is interpreted to be the primary depositional contact, indicating an autochtonous, terrigenous origin (Often, 1985; Siedlecka et al., 1985). Nevertheless, the contact against the JGC is often disturbed by felsic intrusions and thrusting (Krill, 1985). The eastern contact towards the Iddjajav'ri group appears to be of tectonic origin, and is separated by the NNW-SSE trending thrust fault, termed Guvvajav'ri thrust by Henriksen (1991). This thrust is observed throughout the entire study area (Often, 1985).

Iddjajav'ri Group

The main lithologies within the survey area are made up by the Iddjajav'ri Group. Often (1985) divided the rocks within the Iddjajav'ri Group into to main three formations; the Gållebaike, Bakkilvarri and Raitegår'zi Formations. Within the KGB, the Iddjajav'ri Group is the most widespread, and has been interpreted to be the main rock unit of the belt.

The Gållebaike Fm. is defined as the lower most formation in the Iddjajav'ri Group, and consists of mixed lithologies, ranging from metapsammites and metapelites

to amphibolites and thin layers of metakomatiites. The lowermost part of the formation is made up by mica schists and fuschite-bearing schist, with 5-10 m thick beds of amphibolites. The upper parts show a transition to sandstones and feldspar-rich quartzites (Often, 1985; Siedlecka et al., 1985). Smaller areas are marked by thick occurrences of amphibolites and volcano-related sediments, e.g. tuffites or calcite-rich sediments (Henriksen, 1991). These are particularly concentrated at the Jalgesvadda hill. The transition from the Gållebaike to the Bakkilvarri Formation has been interpreted to be transitional, but is locally influenced by thrusting within the Iddjajav'ri area (Often, 1985; Henriksen, 1991).

The Bakkilvarri Fm. is considered to be a thick sequence of monotonous amphibolites and ultramafic volcanic rocks (Barnes and Often, 1990; Often, 1985). The volcanic lithologies within the Bakkilvarri Formation have been divided into two main sequences; (a) metakomatiites and (b) thoeliitic amphibolites (Pharaoh and Peatce, 1984; Often, 1985; Henriksen, 1991). Barnes and Often (1990) and Pharaoh and Walsh (1987) concluded that these lithologies showed a clear relation to shallow water eruptions, due to their unusual high Ti composition. The abundance of the komatiites are unusual within the KGB, compared to other greenstone belts, where this type of magmatism only forms a minor phase of the sequence (Barnes and Often, 1990). Radiometric dating of a komatiite sample in the northern part of the Bakkilvarri Fm. showed an age of 2085 $\pm$ 85 Ma (Krill et al., 1985). The komatiites have been interpreted to have been formed during the rifting phase, possibly related to a mantle plume (Barnes and Often, 1990; Lehtonen et al., 1998; Hanski and Huma, 2005). Similar komatiites can be observed as a perseving belt of ultramafics from the Finnmark region, through Salla and Sodankylä and into Russia (Lehtonen et al., 1998; Hanski and Huma, 2005).

The Råt'zigarri Fm. is interpreted as the uppermost formation of the KGB, and consists mainly of aluminous mica schists and mafic to intermediate volcanics (Often, 1985; Siedlecka et al., 1985). The formation is only observed south of the Karasjokka River, and have not been observed within the Iddjajav'ri area. The volcanics of the Råt'zigarri Formation shows similar composition to the units that are observed in the Bakkilvarri. The most pronounced difference from the Bakkilvarri Fm. is the greater influx of clastic sediments. Initially, the Råt'zigarri formation was intepreted to be conformably deposited on the Bakkilvarri Formation (Often, 1985; Siedlecka et al., 1985), but Braathen and Davidsen (2000) interpreted the Råt'zigarri Formation to represented tectonically emplaced unit, termed the Råt'zigarri Nappe.

3.1.3 Tanalev Migmatite Belt

The narrow NNW-SSE trending Tanaelv Migmatite Belt consists mainly of high grade metamorphic gneisses, and shows large variations in lithologies throughout the area. Two main lithology groups are; mafic hornblende gneisses and a tonalitic to granodioritic gneiss variations. These rocks can now be observed as mylonitic mafic hornblende gneisses, where they often display mylonitic texture, indicative to high strain shearing (Krill, 1985; Daly et al., 2006). Furthermore, the TMB are observed to have wide distribution of different magmatic units, ranging from microcline granites to more mafic gabbroic bodies and anorthosites. Initially, the TMB was interpreted to be relics from sediments deposited at a continental margin, but is now recognized as a tectonic melange of several lithodomains, sheared and emplaced during the closing stage of the Lapland-Kola Orogeny (Gaàl et al., 1989; Krill, 1985; Daly et al., 2006).

3.1.4 Levajok Granulite Complex

Levajok Granulite Complex (LGC) corresponds to a highly metamorphosed unit of the Paleoproterozoic metasedimentary sequence, located east of the TMB. The LGC is considered as the northernmost prolongation of the Lapland Granulite Belt (Barbey et al., 1984; Gaàl et al., 1989; Daly et al., 2006). The belt consists mainly of high-grade garnet and garnet-sillimanite gneisses, interpreted to be high-grade metamorphosed relics of Al-rich sediments, dated from 2.0 Ga to 1.9 Ga (Daly et al., 2001; Korja et al., 2006). The LGC is not present within the study area, and is therefore not extensively described here.

3.1.5 Intrusions

Several mafic to ultramafic intrusions can be observed throughout the stratigraphical units in the KGB (Figure 3.1). The intrusions show large petrological variations, ranging from ultramafic to granitic compositions. The mafic and ultramafic intrusions occur dominantly as isolated satellite intrusions, without any clear relation to each other. Due to their apparent differences regarding crystallization and emplacement, their regional coherence and tectonic correlation are not well constrained (Nilsson and Often, 2005; Henriksen, 1991). The timing of the magmatic events have not been constrained, but a large gabbroic intrusion just south of Karasjok center have been interpreted to be synorogentic due to their field relation to adjacent sandstones (Elvebakken et al., 1985; Often, 1985). The intrusions are also remarkably little influenced by mechanical deformation, and show mostly primary textures. However, primary the composition is often altered and indicates mid to upper greenschist metamorphism (Barnes and Often, 1990; Nilsson and Often, 2005; Henriksen, 1991).

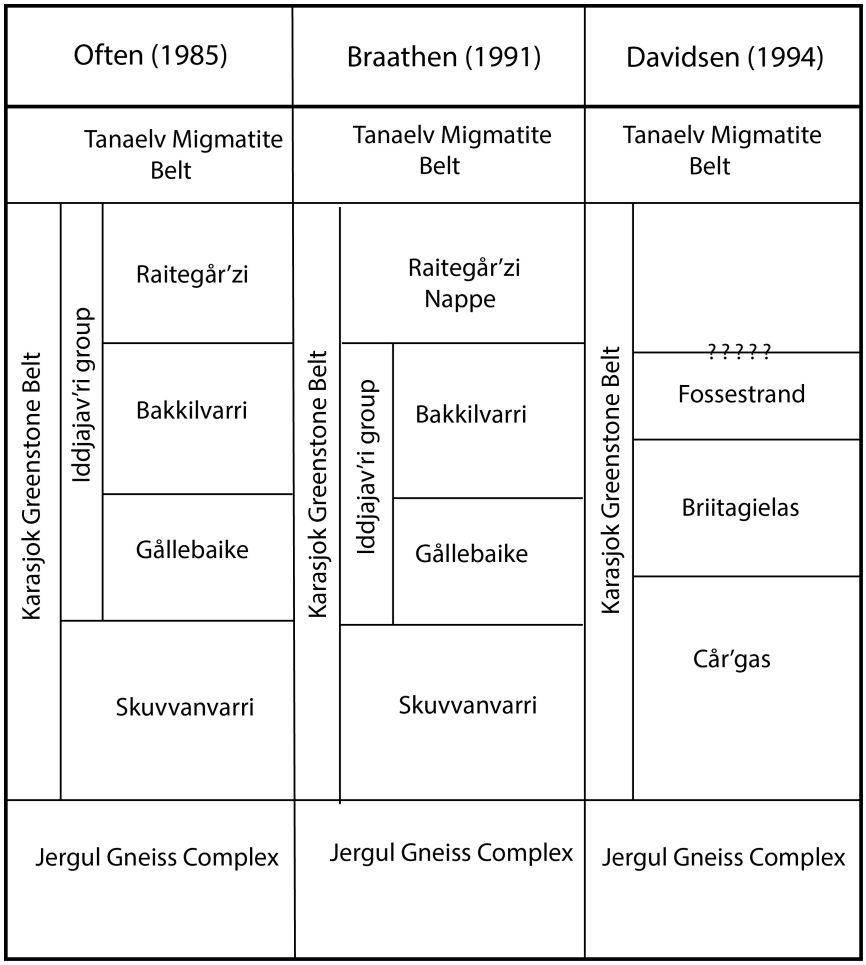

Figure 3.3: Summary of different stratigraphical interpretation from the Karasjok-Lakselv area.

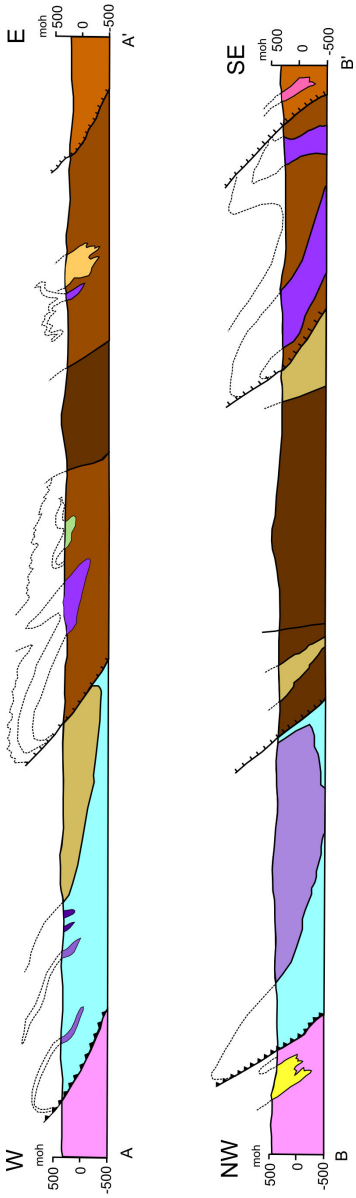

Figure 3.4: Cross sections illustrating the present geological model of the area, from Henriksen (1986). Similar legend as for the geological map in Figure 3.1.

Diabase dikes are observed in the southern part of the KGB, but have not been seen in the Iddjajav'ri area. Granites can be observed both within the JGC, and are related to the shear zone separating the Gållebaike Fm. and the JGC (Henriksen, 1991; Braathen and Davidsen, 2000). Due to their crosscutting relations and the existence of Gållebaike Fm. xenolithis, they have been interpreted to be post-orogentic.

Several tonalites to granodiorites have been mapped in eastern part of Iddjajav'ri, constituting a north-south trending belt (Often, 1985; Henriksen, 1991). A larger sheared granodiorite lens can be observed in the northwestern part of the Iddjajav'ri area, interpreted to be either reworked intermediate intrusives or tectonically emplaced. Henriksen (1991) and Pharaoh and Walsh (1987) proposed that the intermediate gneisses could be detached fragments of a reworked basement, emplaced either by detachement folding or large scale shearing. These interpretations have not been confirmed by radiometric datings.

3.2 Structural geology and tectonic setting

3.2.1 Structures and deformation phases in the Karasjok area

The general structural interpretation is based on a compressional tectonic model, where the KGB sits between the JGC and TMB, in a recumbent isoclinal synform (Often, 1985; Midtun, 1988). In total, four deformation phases have been observed in the KGB (Braathen and Davidsen, 2000; Henriksen, 1991). Three phases of ductile deformation phases have been defined as D_1, D_2 and D_3. The fourth deformation phase has been recognized as mainly a post-orogentic, brittle deformation phase. As a result of the poor degree of exposures, structural observations are limited.

D_1 created the most dominant foliation observed within the Iddjajav'ri area, showing a NW-SE strike direction (Henriksen, 1991). The foliation dips towards the east, and is recognized by an east-plunging L_1 stretching lineation (Henriksen, 1991; Braathen and Davidsen, 2000). The F_1 fold phase is marked by large, mesoscale recumbent isoclinal synform, showing westward vergence. These folds have been well documented in the Lakselv area (Davidsen, 1994; Braathen and Davidsen, 2000). Braathen and Davidsen (2000) interpreted that the TMB was thrusted on top of the KGB in the late stages of the D_1 phase. Often (1985) described the transition between the Gållebaike and Bakkilvarri formation as originally gradual. However, the D_1 phase caused local thrusting in the Iddjajav'ri area (Henriksen, 1991; Often, 1985). Furthermore, structural interpretations from Often (1985) and Braathen and Davidsen (2000) indicate that the isoclinal folding caused the updoming of basement structures within the KGB.

		Style
	Extrusion of mafic and ultramafic volcanic rocks	
D1	S1, Isoclinal to tight F2 folds, shearing and thrusting	Ductile , penetrative
D2	Tight F2 folds, S2 crenulation clevage, local shearing along overturned F2 folds	Ductile, non-penetrative
D3	Open folding av earlier structure	Ductile, non-penetrative
D4	Brittle, NE-SW and NW-SE trending faults	Brittle non-penetrative

Figure 3.5: Current model for the structural evolution and tectonic model of the KGB, based on Henriksen (1991) and Braathen and Davidsen (2000).

The D_2 is marked by mesoscale folding, superimposed and reorientation of the initial S_1 foliation and F_1 folds. The F_2 folds are reported plunge toward E and NNE, with upright to overturned axial planes dipping towards the east (Henriksen, 1991). The S_1 foliation was transposed parallel to the F_2 fold limbs. D_2 shear zones have also been mapped at the base of the greenstone belt (Braathen and Davidsen, 2000). On the basis of several overprinting features, Braathen and Davidsen (2000) considered the possibility that some of the large scale D_2 basement thrusts (The Storfossen Thrust in the Karasjokka area), were reactivations of original D_1 shear zones, created during early over-thrusting. In addition, several small scale, D_2 thrusts appear to be concentrated at upper of lower limbs of folded ultramafic, creating rootless and isolated fold hinges and limbs, related to actinolite-chlorite phyllonites (Henriksen, 1991; Braathen and Davidsen, 2000).

The D_3 phase is recognized as having similar structures as the D_2, but have been defined by a shift in the compressional direction (Braathen and Davidsen, 2000). As a result, the F_3 folds are observed to superimpose on the F_2 folds and D» thrusts. Several D_2 shear zones were most likely reactivated and/or affected by folding during the D_3 phase (Braathen and Davidsen, 2000). Krill (1985) interpreted the F_3 folds to cause the down-folding of the TMB in a mesoscale syncline within the southern parts of the belt.

Changing deformation conditions are recognized by the brittle D_4 phase. The last known deformation phase is dominated by steeply inclined, NE-SW and NW-SE, large scale joints and brittle faults (Henriksen, 1991; Braathen and Davidsen, 2000). The D_4 phase is observed both through field observations and in regional geophysics through out the Fennoscandian Shield (Henkel, 1991; Olesen and Sandstad, 1993; Cagnard et al., 2011).

3.2.2 Regional tectonic models

The tectonic evolution of the northern Fennoscandia is complex, and several details regarding the nucleation of Paleoproterozoic crust are still unknown (Daly et al., 2006; Korja et al., 2006; Weihed et al., 2005). This section does not aim to describe the entire Paleoproterozoic evolution in the area. However, an outline of the tectonic outline of the KGB is presented, in order to create a regional framework for this study. As mentioned above, little work has been done in the eastern parts of the Finnmarksvidda, since the late 80's. Consequently, the tectonic evolution of KGB is poorly constrained. As there are few reliable ages from the KGB in the Finnmarksvidda area, regional tectonic models are based on work from the southern parts of the CLGB.

The main crustal architecture that can be observed today is interpreted to originate from the Lapland-Kola orogen (Daly et al., 2001, 2006). In more recent time, this orogeny has been interpreted to constitute a part of the larger and more regional scale Svecofennian orogeny, which influenced most of the Fennoscandia from 1.92 Ga to 1.77 Ga (Korja et al., 2006; Cagnard et al., 2011). The Lapland-Kola orogen has also been termed the Svecokarelian in earlier literature (Barbey et al., 1984; Krill, 1985), following older stratigraphical interpretations of the northern Fennoscandia (Gaàl and Gorbatschev, 1987; Lehtonen et al., 1998). However, as proposed by Gaàl and Gorbatschev (1987), the definition of a Svecokarelian Orogeny was based on misleading age datings and should therefore be abandoned. Consequently, the work in this thesis follows the nomenclature as presented by Korja et al. (2006) and Cagnard et al. (2011), where closure of the Kola ocean and subsequent continent-continent collision is termed as the Lapland-Kola orogen.

The supracrustal rocks of the KGB are interpreted to have been deposited on felsic Archean basement during several episodes of rifting, crustal thinning, which ultimately lead to the opening of a small ocean, termed the Kola ocean, around mid-Paleoproterozoic times (Krill, 1985; Daly et al., 2001). Krill (1985) proposed that the rifting initiated approximately 2.1 Ga for the units within the Karasjok area. However, investigations from the Finnish parts of the CLGB have shown that the supracrustal rocks within the CLGB were deposited during several episodes of rifting events, dated to 2.4, 2.2. and 2.0 Ga, reflecting a 400 Ma timespan (Lehtonen et al., 1998; Hanski, 2001). Several studies within the CLGB have shown that most of the supracrustal rocks were related to the 2.4 and 2.2 Ga rift events. These sediments were mainly a mix of clastic and mafic to ultramafic volcanics, deposited in an intracratonic basin (Ward et al., 1989; Hanski and Huma, 2005). Opening of the Kola ocean and creation of oceanic crusts constrained to approximately 2.0 Ga (Daly et al., 2001). Comparably, the Bakkilvarri komatiites have been dated to 2085 $\pm$ 85 Ma by Krill et al. (1985). Early structural studies concluded that the KGB was mainly influenced by compressional tectonics due to non-conformable emplacement, as part of the basin-inversion and initiaion of the Kola-Lapland orogeny

at 1.91-1.79 Ga (Krill, 1985; Gaàl and Gorbatschev, 1987). The Lapland-Kola orogen is interpreted as a subduction and intra-continental collision (Marker, 1985; Krill, 1985; Daly et al., 2006) of the LGC, which is interpreted as relics of Al-rich sediments deposited in the Kola ocean.

During the main collisional event, the LGC was thrusted westward and emplaced on top of the KGB (Cagnard et al., 2011). During the main metamorphic events, the Karasjok-Levajok area reached up to granulite facies, with an inverse thermal gradient towards the east (Krill, 1985). The core of the KGB shows temperature ranges from 380 °C in the western extension, to about 620 °C in contact with TMB, reaching up to amphibolite facies (Krill, 1985; Cagnard et al., 2011). Braathen and Davidsen (2000) interpreted that the KGB acted as a regional detachment zone, and caused higher degree of folding and faulting during the D_1 and D_2 phases, than within the TMB and LGC. Braathen and Davidsen (2000) interpreted that the TMB was emplaced at late stage during the D_1 phase. South of the Karasjokka river, the TMB is down-folded, creating a tongue-shape geometry. Such rotational deformation is not observed in the northern part of KGB, where most structures follows a NNW-SSE linear trend (Henriksen, 1991).

The Lapland-Kola orogen lacks the presence of typical UHP-terranes, caused by erosion and uplift (Cagnard et al., 2011; Daly et al., 2006). In addition, there has not been observed any relics of oceanic crust within the Karasjok-Lakselv region. Within the CLGB, the Kittilä Group has been interpreted to represent a part of the oceanic crust, thrusted on top the lower autochonous Sodankylä and Savukoski Groups (Hanski and Huma, 2005). The Kittilä group has been dated to 1987 $\pm$ 36 Ma (Hanski, 2001).

In general, the Archean geodynamic development of greenstone belts show to end member styles, what is referred to as "horiztonal" tectonics and "vertical" tectonics (de Wit, 1998). Archean greenstone belts in Australia and Canada are well documented examples of vertical tectonics, where gravitational instabilities due to a high thermal gradient and convective crustal overturn caused dome-and-keel structures (de Wit, 1998). The KGB differs from older Archean greenstone belts situated in e.g. Australia or on the African continent, where circular domes and basins dominates the variations between gneiss domes and greestones (Cagnard et al., 2011). Linear fold and thrust belts show signs of large degrees of crustal shortening, which indicates that horizontal tectonics were more important than horizontal. Cagnard et al. (2011) points out that the Lapland-Kola orogen was a mixed-hot orogen, i.e. a transition between the Archean ultra hot orogens, and the modern cold orogen.

Chapter 4

Results from geological field investigations

The KGB has undergone several phases of ductile deformation. The timing of the different deformation phases, and their tectono-metamorphic evolution are still poorly constrained, mainly due to the lack of exposures within the area. However, structural field observations and interpretations yield important constrains and information about the structural styles and expected geometries within the study area. These observations and interpretations are valuable a priori information when interpreting aeromagnetic and AGG data, in addition as constrains for the 3D geophysical modeling.

In order to unravel some of the structural evolution, and resolve some of the key question from the qualitative structrual interpretation, key areas with reasonable degree exposure were investigated. Field mapping was carried out in two periods, with a total of three weeks during the summers of 2013 and 2014. Due to the lack of outcrops within the area, the strategy was to visit already known outcrops in order to obtain lithological and structural observations, in addition to collection of rock samples for petrophysical measurements. The main effort of the structural investigations was put in the southern part of the study area, as this turned out to be the most exposed and accessible area. As these observations alone do not make a sufficient basis to interpret the different deformation phases and their timing, the main results are presented from each investigated area.

A total of 156 field localities were visited, (See Figure 4.1) and about 50 hand samples were collected. As most of the outcrops have average size of less than two square meters, the focus of the geological mappings was mainly to establish structural relations through mapping of microstructures and strain variations within different the rock units.

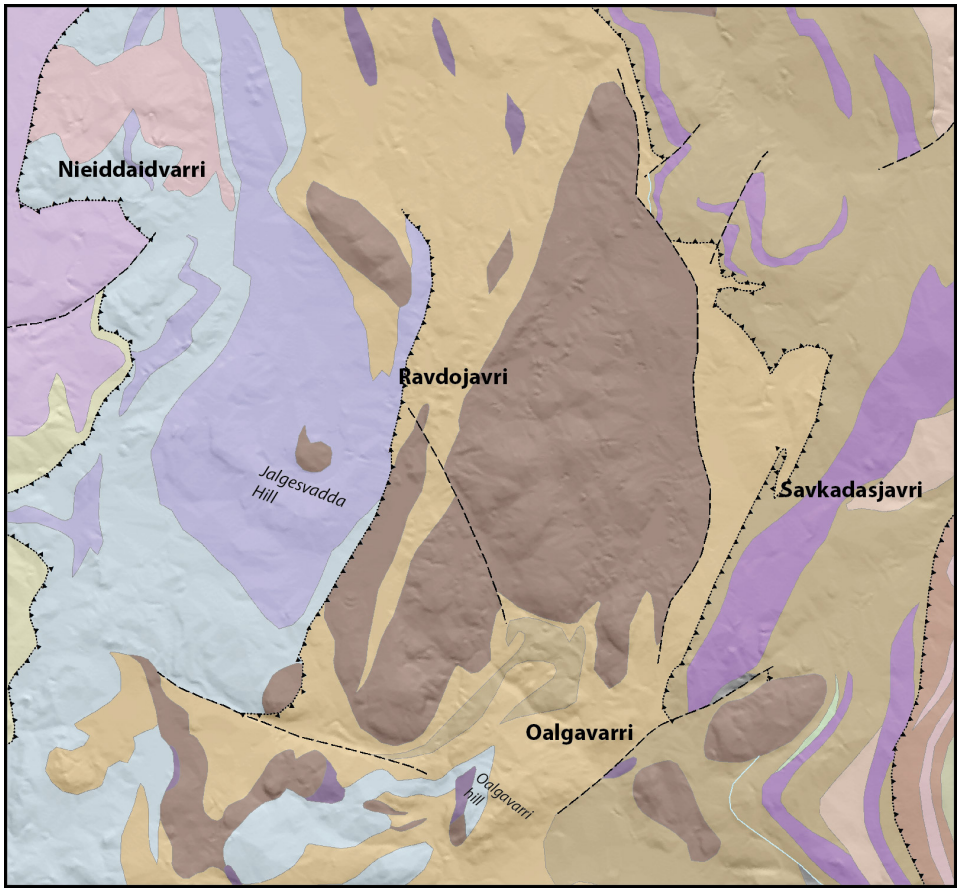

Figure 4.1: Overview of the areas for field investigations. Names in italics show local names on topographic hills used in the structural description. Geological map and tectonostratigraphy are simplified from Henriksen (1986), Often (1985) and Siedlecka et al. (1985). See Figure 3.1 for legend.

4.1 Structural observations

4.1.1 Oalgevarri Area

The Oalgevarri area reflects the upper stratigraphies within the Gållebaike Fm. (Figure 4.1, 3.2), including quartzite, quartzite schists and massive to banded amphibolites. The observed structures are mainly dominated by a penetrative ductile foliation, particularly well developed in less competent lithologies (Figure 4.2 (d) and Figure 4.3 (c) and (d)). In the western part of the study area, the foliation is dominated by steep, NW and SE-dipping L-S fabric, particularly well developed

within quartzites, quartzite schists and mica schists (Figure 4.5). The penetrative foliation is defined by reorientation of primary lithological banding, forming a composite $S_{0/1}$ foliation (Figure 4.2 (a)). The quartzite schists are often interbedded with 1-2 m thick layers of massive quartzite.

The western parts of the area are recognized by upright, open to tight folds, plunging towards the ENE (Figure 4.2 (a)). These F_2 folds appear to have transposed the $S_{0/1}$ foliation parallel to the axial planes in the fold limbs. Throughout the area, an axial planar foliation is preserved in fold hinges of folded mica-rich quartzite schists, forming a high angle to the $S_{0/1}$. These F_2 folds appear as km-scale features within the western part of the Oalgevarri area, where the entire Oalegevarri Hill (Figure 4.1), stand out as a km-scale fold structure.

Primary bedding has been identified by mud cracks and ripple marks. These outcrops appear to be openly folded, around a SSE plunging axis. Compared to the flattening within fold hinges elsewhere, they appear to be very little deformed. A study by Elvebakken et al. (1985), interpreted the sequence as shore-face deposits.

Intrafolial folds can rarely be observed within the quartzite schists (Figure 4.2 (a)). In some outcrops, relics of earlier foliations are preserved at high angle to the $S_{0/1}$, possibly reflecting relics of primary bedding. In the westernmost part of the area, parasitic upright and open S-folds are commonly observed within the area (Figure 4.2 (b)). Their fold axes plunge shallowly towards the NE. The quartzitic schists are often related to a penetrative lineation, parallel to the main fold axis, reflecting an intersection lineations. The observations of fold axes and stereoplot analysis suggest that the Oalgevarri Hill is related to a km-scale, moderately NE-plunging fold (Figure 4.6).

The eastern part of the Oalgevarri area is marked by a change in structural trends (Figure 4.5; 4.6). The metasedimentary litholoiges are primarily dominated by more mica-rich quartzite schists, influenced by open to tight, ENE plunging folds. Towards the overlying amphibolites, the gneisses are often observed with asymmetric folding, showing both NW and SE-vergence.

Whereas the quartzite schists are mostly dominated by upright fold structures, the amphibolites appear to have accommodated more strain, and are often strongly foliated. The foliation dips mostly towards the NW or SE (Figure 4.6). The foliation is defined by rotated and flattened actinolite minerals, along with elongated quartz lenses. Measured fold axes plunge steeply towards the WNW (Figure 4.6). The amphibolites are often related to asymmetric folding, where a partly developed discrete crenulation cleavage is common in outcrops with more intense folding. In most outcrops, the amphibolites are observed with non-coaxial deformation structures (Figure 4.3 (d)). Asymmetric folding within the amphibolites are in general south-vergent.

M- to km-scale fold structures, similar to those developed in the Gållebaike quartzite schists, are not observed within the Bakkilvarri amphibolites. Outcrops

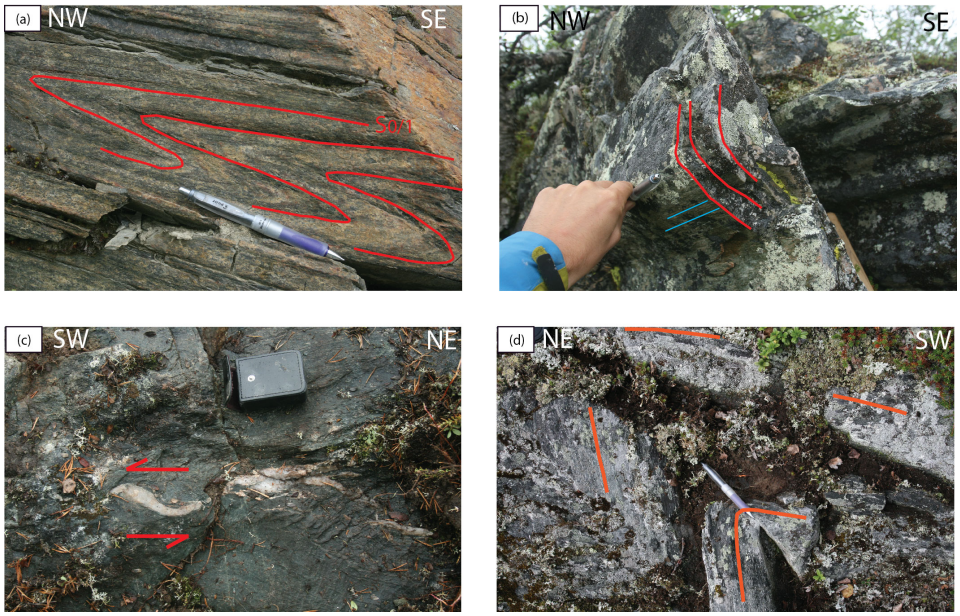

Figure 4.2: Field observations of different styles of ductile structures within the Oalgevarri area. (a) Isoclinal, asymmetric NW verging fold, transposing the penetrative fabric in a quartzite schist. Picture taken just beneath a tectonic contact to a mafic intrusion. Picture taken towards a vertical wall. (b) Upright, parasitic S-folds, folding penetrative foliation (red lines) observed in a quartzitic schist. A penetrative lineation (blue lines) is developed parallel to the fold axis. Pencil marks the shallowly dipping fold axis towards the NE. (c) Sinistral quartz sigma clast within a pervasively sheared amphibolite. (d) Asymmetric, steeply dipping F_2 folds within an intensly foliated amphibolite. Note axial plane parallel to the pencil and relatively steeply dipping fold axis towards the NE. Partly developed, discrete crenulation cleavege is observed within the fold limbs, indicating NE-vergence. Picture taken looking down on a sub-horizontal pavement.

adjacent or close to the contact between amphibolites and quartzite schists are often related to highly strained amphibolites, with partly developed mylonitic foliation (Figure 4.2 (c), 4.3 (d)). The quartzite and quartzite schists display more brittle related structures, and contain slivers and patches of mafic mineral assemblages (Figure 4.3 (c)). These observations are remarkably consistent throughout the Oalgevarri area, and is suggestive to a tectonic contact between the two Bakkilvarri and Gållebaike Fm.

Localized high strain zones are often observed, in particular within the amphibolites, and show in many cases a well developed mylonitic foliaton (Figure 4.3 (b) and (d)). The dip of the foliation ranges from shallowly, to steeply dipping, and

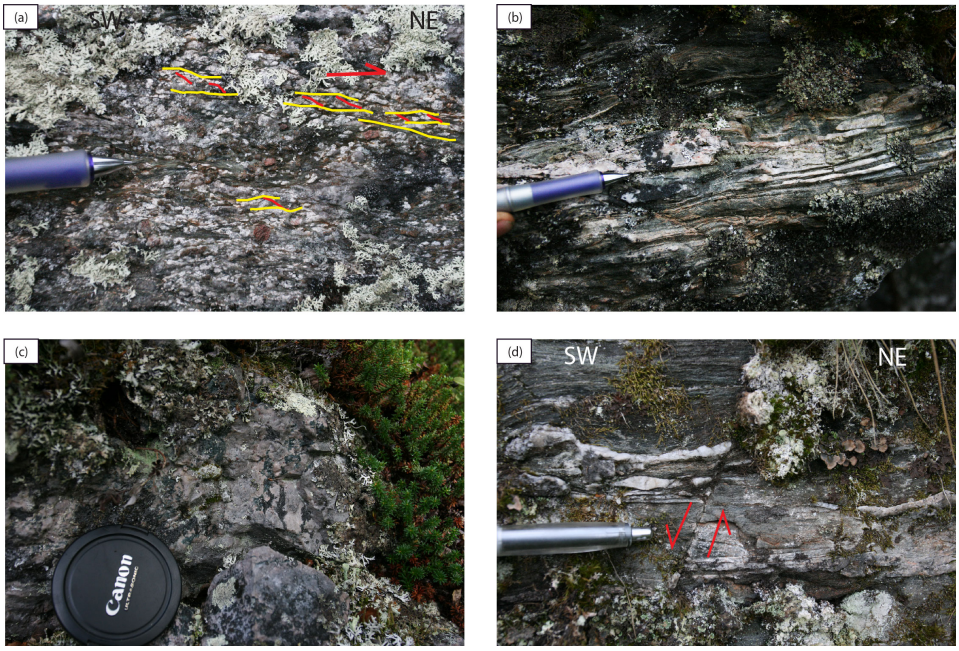

Figure 4.3: Field observations of different styles of ductile structures within the Oalgevarri area. (a) Dextral extensional crenulation cleavage developed in mica schist. Note the large garnet grains within a more fine grained matrix. (b) Strongly foliated hbl-plg-bt gneiss. The outcrop is located just below the contact to an amphibolite unit. (c) Deformed quartzite located just below the contact to strongly foliated amphibolite. Note the intermingled amphibolite within the quartzite matrix. (d) Penetrative, strongly foliation amphibolite. Note the brittle fault cross cutting the main foliation, indicating brittle reactivation.

deformation structures suggest non-coaxial flow (Figure 4.2 (c), 4.3 (a)). Several of the high strain zones are overprinted by southward oriented brittle faults, indicating extensional movement (Figure 4.3 (d)). Towards the eastern contact to Bakkilvarri Fm., several outcrops reveal strongly foliated garnet-mica schists. From the foliation, stretching lineation and kinematic indicators, these garnet-mica schists indicate NE sense of shear (Figure 4.3 (a)).

Mafic to ultramafic units occur mainly as lense shaped bodies within the metasedimentary packages. At the southwestern part of the Oalgevarri hill, the contact between quartzitic schists and the intrusives is influenced by ductile movement (Figure 4.4). This is expressed by smaller zones of completely recrystallized metagabbros, where kinematic indicators show NW-vergent thrusting. The quartzite schists do not show any recrystalized structures.

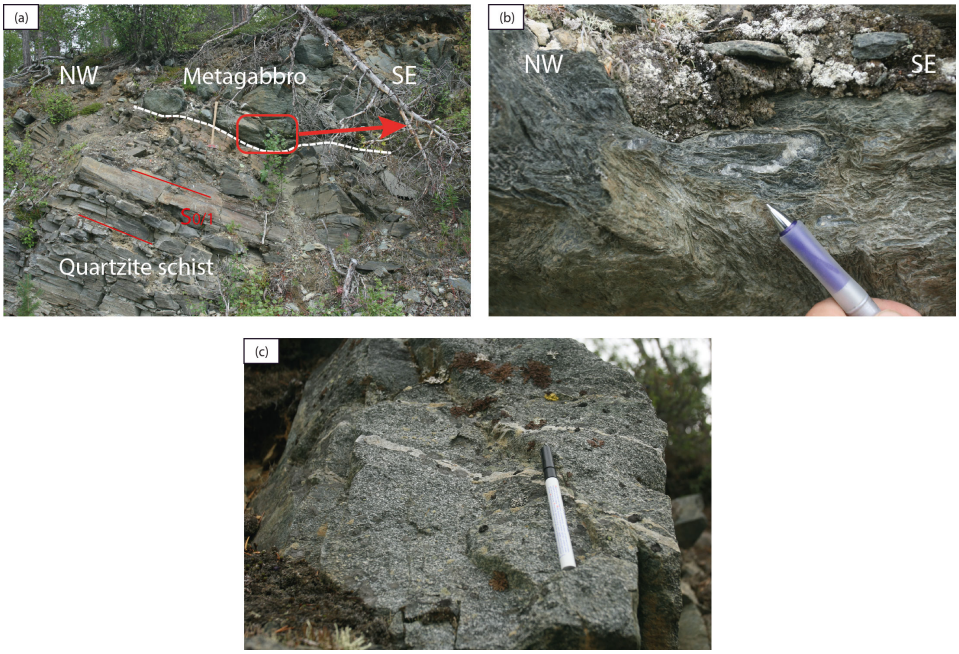

Figure 4.4: Indications for thrust movement along the contact between the quartzite schist and metagabbro, just west for the Oalgevarri Hill. (a) Overview photo showing the contact (white dashed lines), between the quartzite schist and metagabbro. (b) Strongly foliated and recrystalized metagabbro at the contact. The quartzite schist appears to be significantly less deformed and foliated than the metagabbro. (c) Textures within the metagabbro observed 3 m above the contact. A penetrative folation of oriented plagioclase and pyroxene can be observed within throughout the metagabbro. Shear sense indicators suggest of top to the NW kinematics.

4.1.2 Ravdojavri area

The Ravdojavri area is characterised by of several large intrusions hosted within the supracrustal rocks (Figure 4.1). The largest intrusion in the area is made up by the Stuorra Gourpmet intrusion, making up a apparent km-scale intrusion (Henriksen, 1991). The inner parts of the intrusions appear mainly undeformed, but hydrothermal alterations are common. Some ultramafic intrusions are completely altered to serpentinite.

The area is mainly dominated by quartzite schists and quartzites, folded together with smaller units of mica schists and banded to massive amphibolites. The metasedimentary rocks are dominated by a pervasive, composite $S_{0/1}$ foliation, defined by alignments of mica-rich domains between elongated quartz-plagioclase

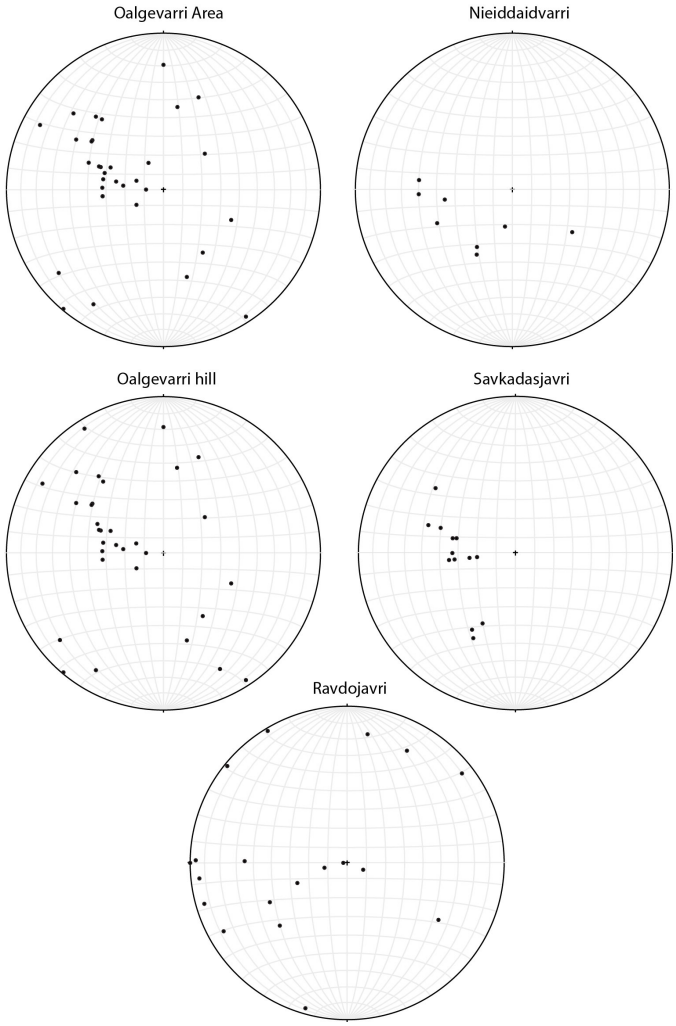

Figure 4.5: Stereoplots showing poles to foliation from the different areas. Note that the Oalgevarri area has been divided into two parts, where the Oalgevarri hill has its own stereoplot, to illustrate the open folding. A reduced number of Oalgevarri hill observations have been included in the Oalgevarri area plot.

layers. The composite foliation indicates a parallel reorientation of the primary bedding.

The quartzite schists are folded by tight, NE plunging folds (Figure 4.7 (b)). The mica-layers are folded into cm-scale folds, forming a axial plane S_2 creunlation cleavage. In the limbs, this crenulation cleavage appears as the dominant foliation, overprinting the $S_{0/1}$ foliation. This cleavage forms a crenulation lineation, parallel

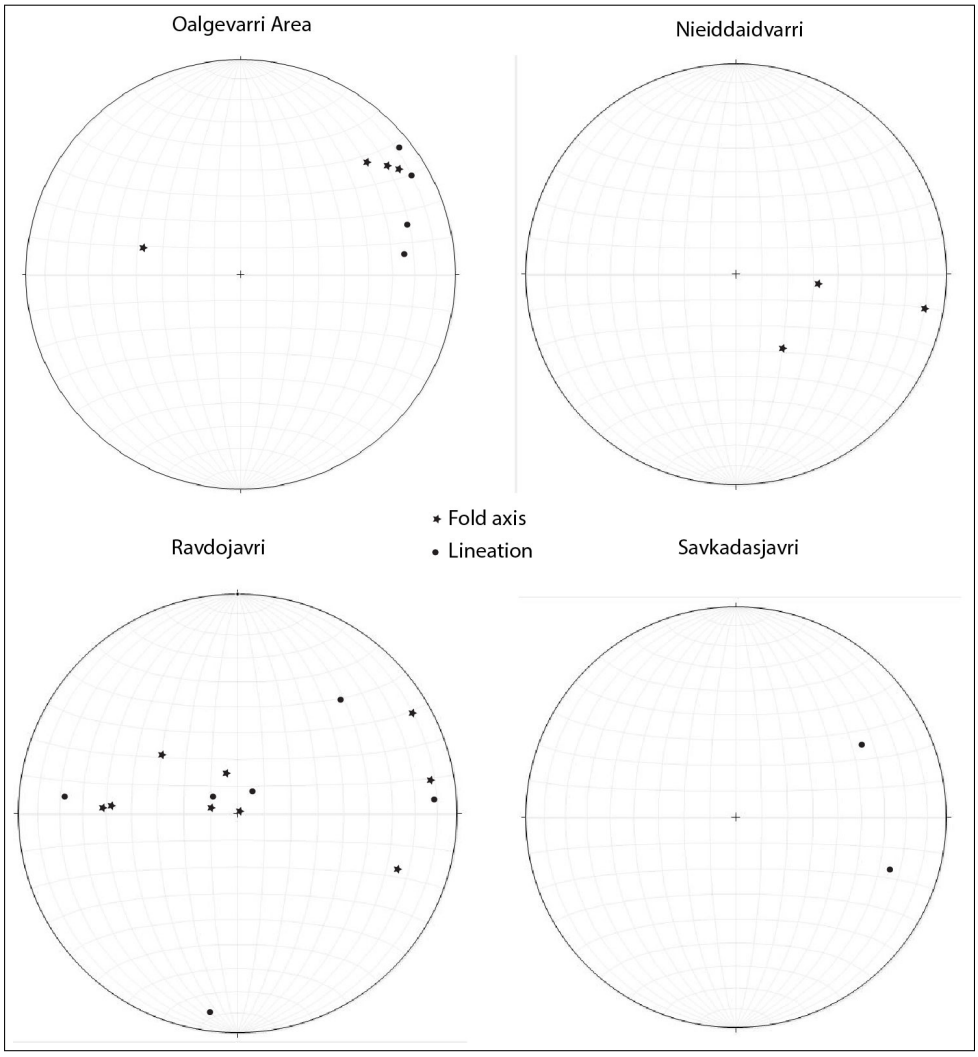

Figure 4.6: Stereoplots showing lineations and fold axes from the different areas.

to the fold axis. In addition, a second crenulation cleavage can be observed, making up a high angle to the $S_{0/1}$ (Figure 4.7 (a)). This is responsible for a near vertical plunging crenulation lineation. The crenulation lineation is also perpendicular to the NE-plunging fold axis. Furthermore, these quartzite schists seem to be refolded around a near vertical, NW to SE plunging fold axis (Figure 4.6). In an outcrop along the main road to between Karasjok and Lakselv, the folds related to the steeply plunging fold axis appear to post-date the gently, NE-plunging folds, and are almost parallel to the second crenulation cleavage. This may be indicative to a

third deformation phase, overprinting F_2 folds.

Outcropping amphibolites are recognized by well developed kink or chevron folds (Figure 4.7 (d)). In the most intensely kink folded amphibolites, a discrete to penetrative crenulation cleavage overprints the earlier foliation, forming a distinct S_2 foliation. In the Ravdojavri area, the kink and chevron folds in the amphibolites appear to plunge moderately towards the NW (Figure 4.6 , 4.7 (d)).

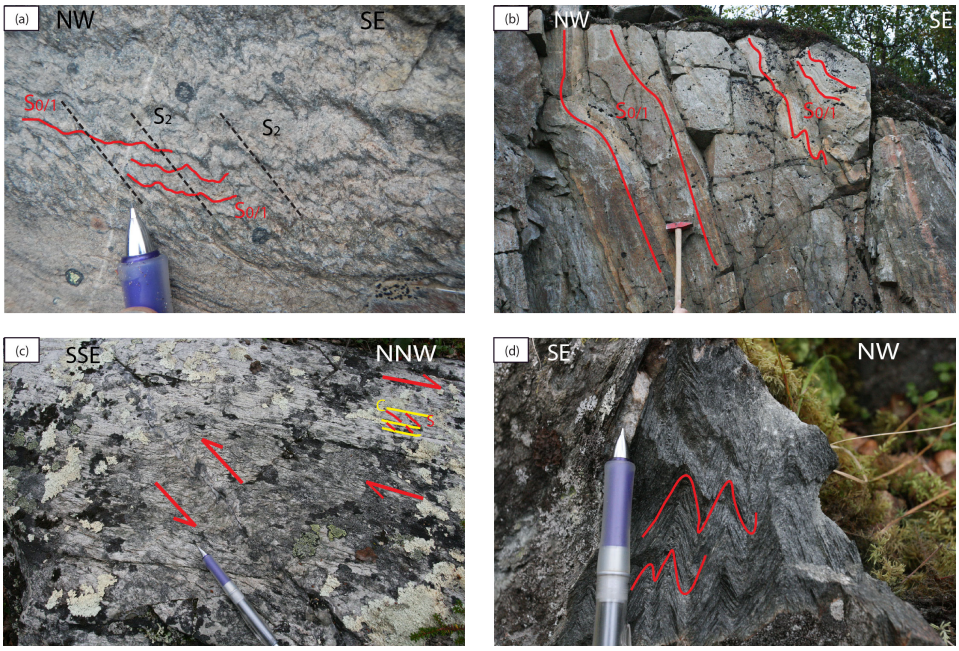

Figure 4.7: Field observations from the Ravdojavri area. (a) Well developed axial plane foliation that cuts the composite $S_{0/1}$ in quartzite schists. The photograph is taken perpendicular on a horizontal surface within the outcrop shown in (b). (b) Parasitic S-folds in a quartzite schists. (c) Mylonitic foliation within quartzite schists, indicating NW sense of shear. Note the flanking fold indicating opposite sense of shear. Photograph taken perpendicular to a horizontal rock pavement. (d) Kink folds in a foliated amphibolite, with moderately plunging fold axis.

Outcropping quartzite schists reveal NW-SE striking penetrative mylonitic foliation, in addition to an apparent mineral stretching lineation (Figure 4.7 (c)). This mylonitic foliation dips steeply towards the NE, and the stretching lineation is seen as elongated quartz and feldspar grains, and plunges gently towards the NE. The sense of shear can be derived from composite shear fabrics and indicates top to the NE kinematics (Figure 4.7 (c)). However, the high strain zone appears to be influenced by additionally SW strike slip component, inferred from flanking folds and S-C' structures (Figure 4.7 (c)). The mylonitic foliation dips almost with 80

°, further supporting the possibility of strike-slip kinematics. The lack of outcrops in the area limit the possibility to map the extent of the zone.

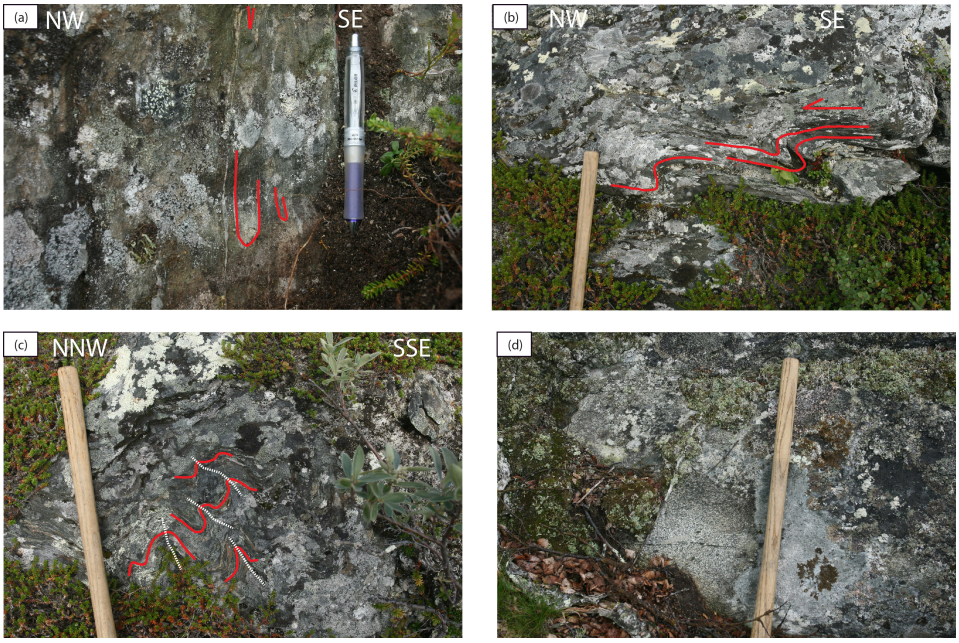

Figure 4.8: Structural observations from the amphibolites at the Jalgesvadda hill. (a) Rootless intrafolial folds, parallel to the foliation. Picture taken in the NW limb a macroscopic, tight fold. (b) Asymmetric, sinistral, NW verging folds. (c) Irregular folding of an earlier foliation and quartz veins, similar to the observation at (a). (d) The gabbro observed within the center of the Jalgesvadda Hill complex. A pronounced lineation could be observed, made up by alligned plagioclase and pyroxene.

The measured fold axes in the area show large variation in plunge (Figure 4.6). For instance, at the Jalgevadda hill, the folds are mostly irregular and show asymmetric fold patterns. The fold styles vary from plunging upright to plunging inclined, and are generally tightly folded. Observations of asymmetrical folds indicate NW-vergence (Figure 4.8 (b) and (c)). Most measured fold axes plunge steeply towards the SE and NW. These folds are generally disharmonic (Figure 4.8 (b)). In addition, rootless, intrafolial folds are commonly observed within the amphibolites (Figure 4.8 (a)). These observations clearly show that the folds within the Ravdojavri area have different orientation and plunge, compared to observations from the km-scale folding at the Oalgevarri hill.

The structures at the Jalgesvadda hill suggest a non-coaxial component during progressive deformation. Asymmetric drag folds and plunging inclined folds, indi-

cate that these structures were formed during NW verging shear movement. Yet, it is clear that the structures observed at the Jalgesvadda hill show quite different characteristics, than the compressional structures located around the Oalgevarri hill.

4.1.3 Nieiddaidvarri area

The Nieddiaidvarri area is located at the very base of the KGB, though the actual contact is not observable (Figure 4.1). The area is dominated by mica schists, with thinner interbedded units of quartzites and amphibolites. Structurally, the area is marked by a pervasive ductile foliation (Figure 4.10). The main, penetrative foliation dips moderately to gently towards the NW and NE (Figure 4.10 (a) and (b)).

Mica schists are in general strongly foliated. In areas with more intense folding, a discrete crenulation cleavage is developed, overprinting the main penetrative foliation. Towards the contact to the JGC, the mica schists appear to be dominated by an anastomosing, strong foliation, where asymmetrical folding suggests W-vergent sense of shear (Figure 4.10 (a) and (b)). Further away from the contact to the JGC, the mica schists are dominated by irregular, disharmonic folding (Figure 4.10 (a) and (b)), plunging steeply towards the ESE (Figure 4.6).

Differences in deformation can readily be observed between lithologies, even within single outcrops. In particular, quartzite and quartzite schists appear to be significantly less deformed and strained compared to rocks such as mica schists and amphibolites. The quartzite schists have a poorly developed foliation and are generally recognized by open, gentle folds. Within similar outcrops, mica schists and amphibolites show an anastomosing, phyllonitic foliation (Figure 4.10 (a), (c)).

Several shear sense indicators can be observed throughout the area; vergence of asymmetrical folds, shear fabrics and winged porfyroclasts (Figure 4.10 (c)). In general, the sense of shear indicates NW movement. Figure 4.10 (c) show an example of NW-vergent feldspar sigmoid clast, within a qtz-hbl-bt gneiss. These observations are suggest that the contact between the JGC and KGB are influenced by NW-vergent thrusting. From overprinting relations, the NE-plunging folding appear to have occurred after the development of the main foliation. However, the calculated fold axis from the observed foliation suggests a NE-plunging fold axis. This may indicate a third folding phase.

Strongly developed foliation within the area can be exemplified by a granitic gneiss, observed just above the contact to the JGC (Figure 4.10 (b)). Henriksen (1991) interpreted this as a granitic intrusion. Field observations show that the granite is recognized by a pervasive, mylonitic foliation, dipping moderately towards the east. It consists of highly strained clasts of quartz and plagioclase, within in a finer matrix, suggesting significant stretching. In addition, penetrative ribbon and stretching lineation plunges perpendicular to the foliation (Figure 4.10

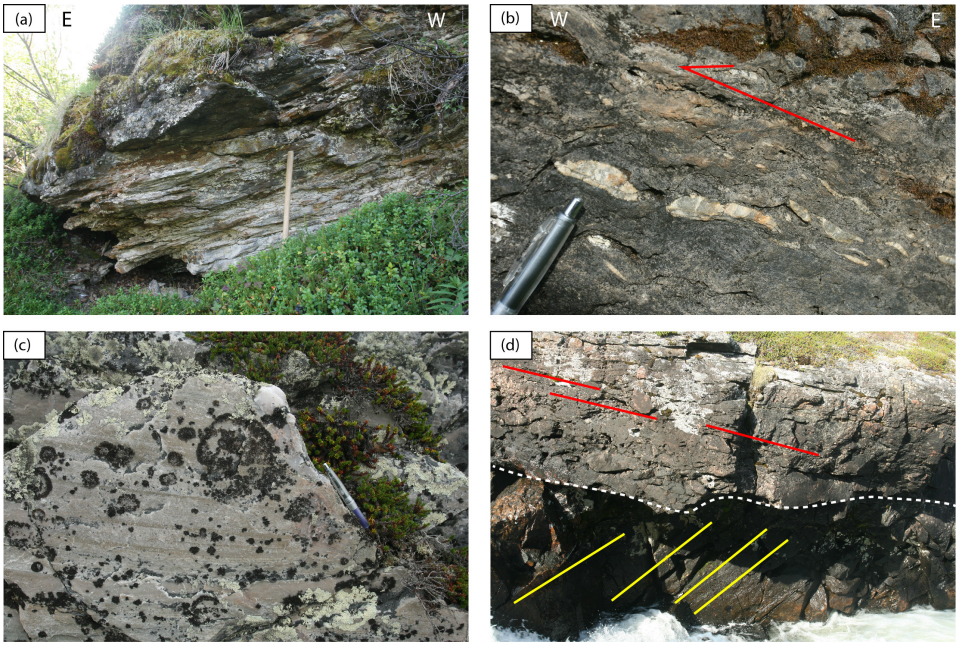

Figure 4.9: Exposures from the lower parts of the KGB, illustrating the nature of the contact. Pictures taken from different places along the belt. (a) Strongly foliated mica schist at the contact to the Skoganvarre Fm. (b) Kinematic indicators showing west-vergent movement in the lower units of the KGB. (c) The Skuvvanvarri quartzite, location just west of the contact to the Gållebaike Fm. (d) The Skålvoll-locality, showing basal conglomerate from the Skuvvanvarri Fm. (red line show foliation), in contact with the JGC (yellow line). The dashed line indicates the contact.

(b)). An outcrop south in the area shows a disconcordant contact between the granitic gneiss, and an adjacent bt-qtz-plg gneiss. This observation, along with observed xenoliths of metasedimentary rocks within the granitic gneiss, suggests that the body represents an intrusion. Due to the highly strained textures and general eastward dip, it is reasonable to assume that the body was emplaced before or early the main deformation phase. The granitic gneiss appears in addition to be refolded by ESE plunging folds.

4.1.4 Savkadasjavri area

The Savkadasjavri area is mostly dominated by outcropping lithologies from the Bakkilvarri Fm. (Henriksen, 1986), though outcrops are sparse. The main lithologies are garnet-rich amphibolites and chlorite-actinlites rockes, most likely origi-

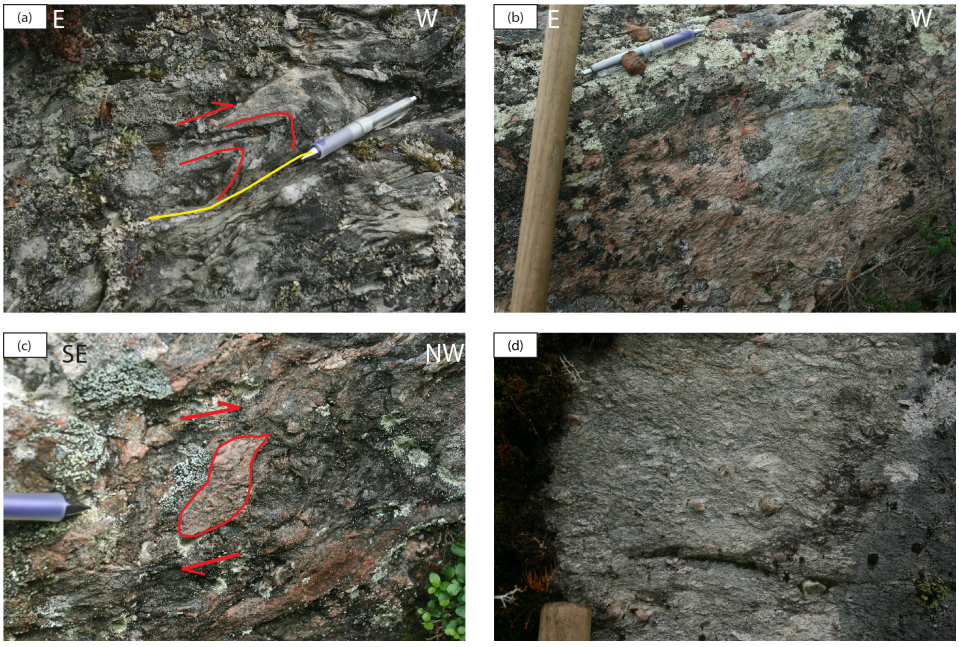

Figure 4.10: Field observations from the Nieiddaidvarri. (a) West-vergent asymmetrical folding witihin mica schists, with developed wavy bedding. Outcrop located just above the contact to the JGC (b) Strongly foliated granititc gneiss, with ribbon lineations. (c) Strongly foliated qtz-hbl-bt gneiss. Outcrop located just above the contact to the JGC. The sigma clast indicates NW-vergent sense of shear. (d) Foliated mica schist, with large garnet clasts.

nated from thoeliitic and komatiitic lavas or volcanoclastic sediments (Often, 1985). The lithologies are dominated by a penetrative E to SE-dipping foliation, defined by reoriented amphibolite grains and elongated feldspar domains. Within the chlorite-rich rocks, a moderately east-plunging mineral lineation can be observed (Figure 4.5, 4.6).

Changes in the strike of the penetrative foliation towards the northern part of the study area, together with observed fold axes, suggest that the rocks are folded by km-scale folding (Figure 4.6). Poles to the bedding in the area reveal that the large-scale fold structure is most likely characterized by a ENE plunging fold axis (Figure 4.6). An outcrop in the southern part of the investigated area shows gentle to open upright folds with NW-dipping fold axes (Figure 4.11 (a)). Hence, it appears that the area is influenced by two fold trends.

Amphibolites cropping out along the underlying contact with the metapsammites, show a penetrative, ductile foliation. Kinematic indicators such as sigma clasts and asymmetric NW-vergent folds indicate non-coaxial top-to-the NW move-

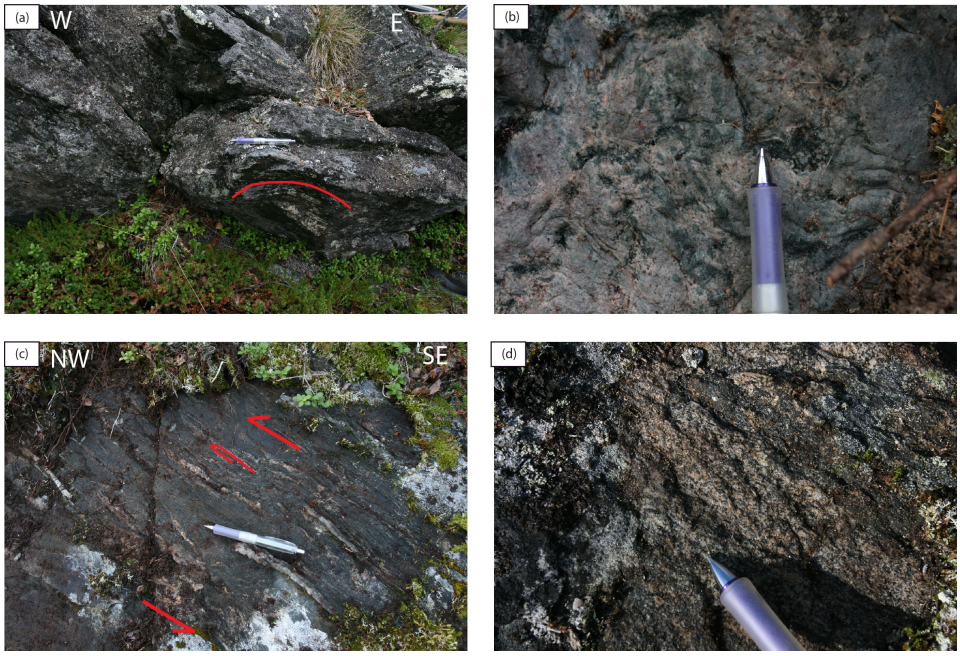

Figure 4.11: Field observations from the Savkadasjavri.(a) Outcropping actinolite-chlorite rock, showing a open, gentle NW plunging fold axis, with an apparent upright axial surface (b) Deformed quartzite with intermingled clasts of amphibolite, just at beneath the contact to the Bakkilvarri amphibolites. (c) Mylonitic foliation above the contact to the Gållebaike Fm. Kinematic indicators show NW verging kinematics. Picture taken towards a rock wall. (d) Foliated tonalite within the Bakkilvarri Fm.

ment (Figure 4.11 (c)). An interesting feature within the outcrop is isoclinal, rootless folds marked by earlier refolded foliation and quartz veins. Metapsammites exposed below the contact between the Bakkilvarri and Gållebaike Fm. are highly deformed, with tectonically intermingled clasts of amphibolite (Figure 4.11 (b)).

Isolated outcrops of foliated tonalitic gneisses can be observed within the Savkadasjavri. These outcrops occur scattered in the area, and it has not been possible to determine their field relations to the amphibolites and actinolite-chlorite rocks. Though, the appearance of these rocks shows signs of deformation and alteration (Figure 4.11(d)).

4.2 Conclusion and implications

The structural observations and interpretations from the area indicate a long and complex tectonic evolution. It is readily observable that strain has been heterogeneously distributed in the area. In particular, it appears that the amphibolites are significantly more deformed, than the quarzite schists. Moreover, several of the large scale features suggest that they have been reactivated, causing complex overprinting structures. There is also a complex relationship between thrust zones and fold structures. During deformation, it appears that strain was progressively concentrated into shear zones. However, the width of these shear zones remains unclear. Within the Gållebaike Fm. km-scale folding is evident, and appears to control the lithological distribution in the area.

During the field investigations, it has been challenging to verify the map scale extent of the S_1, isolclinal folding, mostly due to the limited possibilities to follow km-scale structures in the field. Field observations of intrafolial folds appear to be the most certain observation of such fold phase. This is also supported by the general ENE-dipping, penetrative foliations.

Field observations indicate that the mafic and ultramafic intrusions are pre or syn-orogentic, as they follow the main structural trends of the supracrustal rocks. The granite observed within the Nieiddaidvarri seems to intrude the adjacent host rock. However, its mylonitic and highly strained texture indicates that it has been influenced by one or several ductile phases. Consequently, these interpretations suggest that the granite is a pre-thrusting structure. The mafic to ultramafic intrusions are less deformed in their interior parts, whereas the contacts appear to be strained. Additionally, hydrothermal alterations have influenced several of the mafic bodies.

No primary contacts were found between the Bakkilvarri and Gållebaike Fm. The amphibolites appear to have obtained large amounts of strain near the contacts to the quartzite schists. Structural observations within the Savkadasjavri area indicate that the Bakkilvarri amphibolites have been thrusted on top of the Gållebaike Fm, supporting earlier interpretation of local west-ward thrusting within the Iddjajav'ri area (Henriksen, 1986). It is also noteworthy to observe that the contact between the amphibolites and quartzite schists within the Oalgevarri area are influenced by thrusting, indicating that local thrusts faults were developed internally within the units in the Gållebaike Fm.

The results from the different areas suggest a second fold phase, responsible for the transposition of the main foliation into limbs to E-NE plunging folds. Most measured fold axes indicate that F_2 folds are mostly upright and gently plunging. Furthermore, refolding of apparent F_2 folds indicate a third fold phase. Additionaly, field observations within the Nieddidivarri indicate that the thrust contact to the JGC is folded by possibly F_2 folds

The depth and extent of the thrust between the Gållebaike and Bakkilvarri Fm.

remains uncertain. It cannot be ruled out that the local thrusting only represents a thrust repetition, and that the Gållebaike Fm. is present in the eastern side of the belt, even though there are no field evidence for this. Braathen and Davidsen (2000) used observation of S- and Z- folds and repetition of lithologies as indicator of recumbent, isoclinal F1 folding. Within the study area, it has not been possible to verify this with confidence. However, these evidence could be overprinted by local thrusting, as seen between the Gållebaike and Bakkilvarri Fm.

Field observations of the tonalite within the Bakkilvarri Fm. are not conclusive to rule out either that they represent intrusions or local slivers of a basement units, as suggested by Henriksen (1991) and Midtun (1988). The tonalites have a well developed penetrative foliation, and are therefore suggestive to pre-date the main deformation phase. However, as their age are not constrained, it is still unknown if they represent relics of an intermediate basement complex, or pre-collisional intrusive.

Chapter 5

Petrophysical and Geophysical data

The aim of the chapter is to describe the acquisition and processing of the data used for the potential field interpretation and modelling. That includes the petrophysical, aeromagnetic, and gravity gradient data.

5.1 Petrophysical data

Preexisting petrophysical measurements from the Finnmark area were collected from the extensive petrophysical database manged by Geological Survey of Norway (Olesen et al., 2010). The Geological Survey of Norway has systematically conducted petrophysical sampling in the Finnmark area, along with routinely measurements on bedrock samples from geological mapping effort. See Olesen et al. (2010) and references therein for more detailed description. 1800 samples were extracted from the Karasjok area, covering almost 1220 km^2.

Lithological units usually show large fluctuation in magnetic susceptibilities, even at outcrop scale. As aeromagnetic surveys measure the magnetization of large rock packages, it is important to have a sufficient large dataset to evaluate the average properties of each rock units. In addition, it is also important to asses the statistical susceptibility distribution of each rock unit, as similar lithological units often are recognized by bi- and trimodal susceptibility distribution. An important fact during petrophysical sampling in sparsely outcropped terranes, are the over-representation of exposed lithological units. In addition, the distribution of outcrops may bias the dataset, since areas with no or few outcrops are not represented.

About 16 new samples were collected for petrophysical measurements during field trips in 2013 and 2014. The samples were measured with respect to density,

susceptibility and remanent magnetization, at the petrophysical lab at the NGU. In addition, several in-situ measurements were carried out at available outcrops in the field using a hand held susceptibility meter with an 20x20 cm induction coil. An average of ten measurements were made at each outcrop, to obtain the average susceptibility, due the several order variations of magnitude just within meters. The average was further used to represent the lithology that observed at the outcrop. The lab and field measurements were analyzed separately.

The acquired petrophysical data were merged with the regional database. The general overview of the petrophysical properties of the different units in the area, is presented in Table 5.4. To investigate the relation between lithological observations and petrophysical properties, density, susceptibility and Q-ratio were plotted in two types of bimodal plots; density vs susceptibility, and Q-ratio vs susceptibility (Figure 5.5, 5.6).

Measured remanence was only available for about 1/3 of the total samples from the DRAGON database. Q-ratios were not calculated for samples with susceptibilities below 0.0015 SI, as the inaccuracy of the measurements becomes poor for samples with low susceptibility. The Q-ratios were calculated by using the IGRF 2011 in Karasjok, yielding a strength of 53 674 nT.

From the petrophysical database, about 17 samples had measured NRM components. The measurements of the NRM orientation were plotted on equal area stereoplots. Where sufficient data existed for similar outcropping domains and units, the average inclination and declination for all measurements per unit were further summarized on a single stereoplot, using a 95 % confidence interval. Where only few measurements existed, the Q-ratio, the remanent magnetization intensity and the stereogram results were investigated to asses the possible effects on the interpretation of the magnetic data.

5.1.1 Susceptibility

The measured susceptibility from Karasjok area shows large variations, even within in each formation and lithology (Figure 5.1, 5.3, 5.2). The transition from coarse grained to fine grained magnetite is generally indicative to higher stable remanence, increase of multi domains magnetite (Clark, 1997; Grant, 1985a). Monocline pyrrhotite are stable carriers of strong remnant magnetization, and from the magnetic anomaly map, it would be difficult to distinguish remanence from either magnetite or pyrrhotite. Exploration experience gained by the GTK show that magnetite are recognized by a negative in-phase component in the FDEM data (Airo, 2005; Airo and Mertanen, 2008).

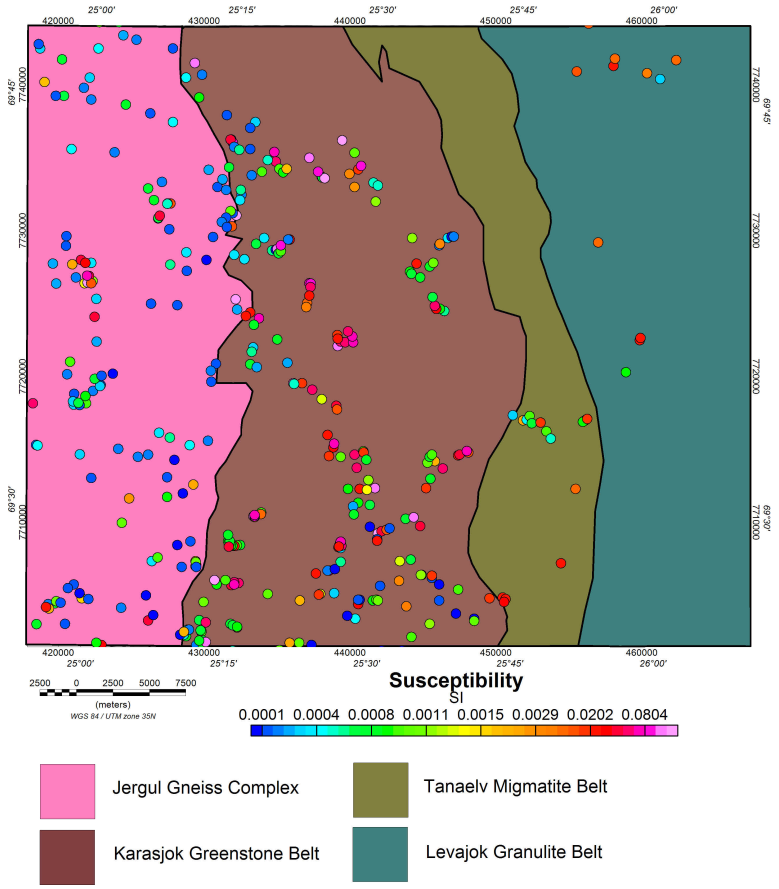

Figure 5.1: Overview of the geographical distribution of susceptibility in the study area.

Gållebaike Fm.

In general, the Gållebaike formation is marked by lower susceptibilities, which reflects the low magnetite content in the main sedimentary lithologies (Figure 5.5, 5.4).

Generally, the susceptibilities of the quartzites and quartzite schists are concentrated in the range 0.0001 to 0.001, with an arithmetic mean of 0.007 SI. The main population is concentrated below 0.001 SI, but a few high susceptibility increase the average. Field observations indicate that the high susceptibility metapsammitic units occur mainly in two generations; a quartzite schists with abundant amounts of magnetite, concentrated in black, finely laminated beds, and as impure hbl-bt-qtz gneisses where no signs of the primary bedding is observed. The magnetite rich quartzite schists are concentrated as local features in the study area, but impure

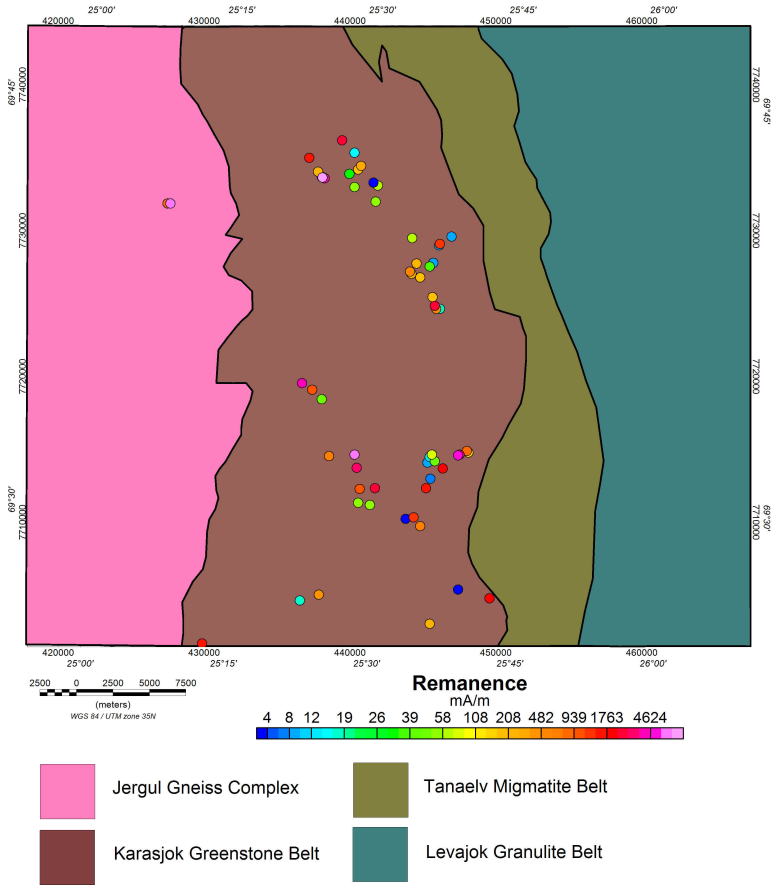

Figure 5.2: Overview of the geographical distribution of measured remanent magnetization in the study area. Geological outline based on Often (1985).

hbl-bt-qtz gneisses tends to be concentrated around mafic to ultramafic intrusions. The deposits can therefore be results of secondary metamorphic processes, or as isolated deposits areas where magnetite has been concentrated in the sediments.

Mica schists and pelitic rocks within the Gållebaike Fm. show generally higher susceptibilities than the psammites and quartzites. They have more continuous distribution, and a lager high sucseptibility population. In general, the susceptibilities are bimodal, where the modes are concentrated in paramagnetic and ferromagnetic susceptibilities. The low magnetic units are gathered around 0.005 SI, whereas the high magnetization units are concentrated around 0.06 SI. Field observations show that sheared pelites are related to high susceptibilities. Yet, these observations are only supported by a few outcrops. Similar results have also been seen from the KtGB (Olesen and Solli, 1985; Olesen and Sandstad, 1993).

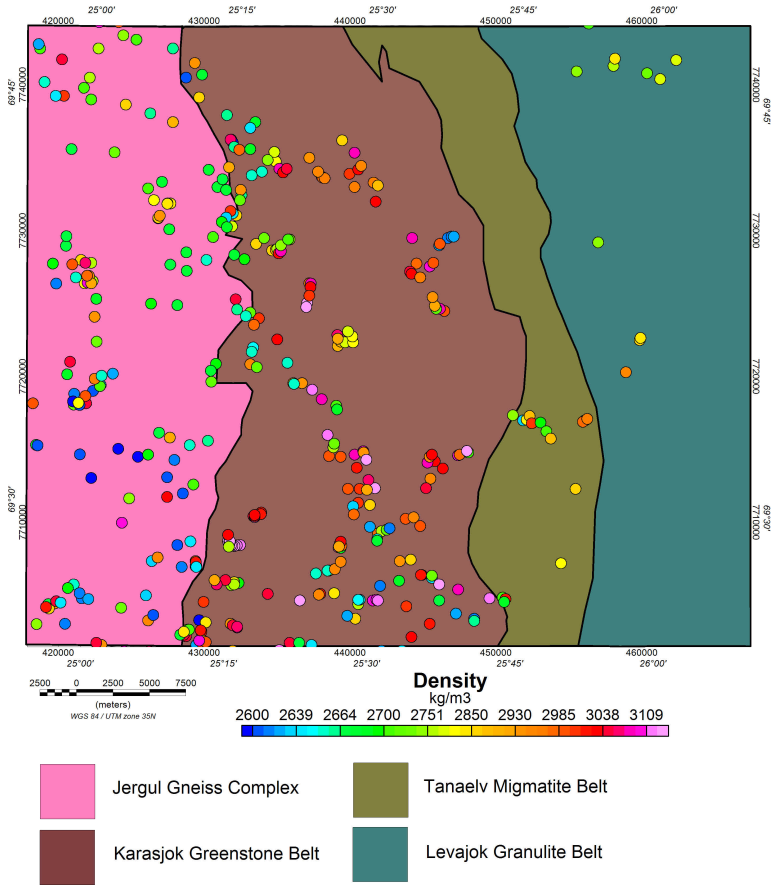

Figure 5.3: Overview of the geographical density distribution in the study area.

The volcanics within the Gållebaike show high susceptibility, with arithmetic mean above 0.02 SI, and maximum values above 0.1 SI (Figure 5.4). Figure 5.5 (a) indicates a bimodal distribution, where the main population concentrates around 0.001 SI. The higher susceptibility variants are grouped with an average value of 0.05 SI (Figure 5.5 (a)). The low susceptibility are most likely due to the low metamorphic grade within the lower parts of the Gållebaike Fm, as growth of magnetite is limited within the greenschist facies.

Geological unit	Susceptibility [SI] min-max		Standard deviation	Q-Value min-max		Mean density [kg/m3] min-max		Standard deviation [kg/m3]
Jergul Gneiss Complex	0,0043		0,0311	0,8		2675		75
n=278	0,00001	0,1879		0,03	0,3	2520	2981	
Skuvvanvarri	0,0022		0,0086	1,3		2675		79
n=135	0,00001	0,08218		0,05	13,8	2510	3030	
Gållebaiki								
Amphibolite	0,0421		0,1134	0,5		2927		130
n=126	0,00009	0,92197		0,01	4,3	2572	3160	
Metapsammites	0,0074		0,0268	0,3		2670		77
n=101	0,00001	0,1884		0,01	3,1	2510	3170	
Pelites	0,0222		0,0337	0,3		2749		90
n=100	0,00001	0,15371		0,02	3,1	2580	3072	
Bakkilivarri								
Amphibolite	0,0160		0,0559	0,4		3016		98
n=176	0,0002	0,5177		0,03	4,6	2720	3400	
Komatiite	0,0421		0,0579	0,6		2981		90
n=97	0,00007	0,23215				2711	3218	
Metasediments	0,0135		0,0475	1,7		2785		136
n=45	0,00003	0,29393		0,06	8,1	2600	3159	
Tanaelv Migmatite Belt								
Acidic Gneisses	0,0260		0,0302	0,3		2717		99
n=76	0,00006	0,15351		0,02	1,5	2570	3051	
Mafic Gneisses	0,0146		0,0363	0,3		2939		157
n=57	0,00047	0,24525		0,03	1,3	2664	3636	
Mafic intrusions	0,0255		0,0592	0,7		3007		137
n=66	0,00005	0,43129		0,02	3,8	2650	3224	
Ultramafic intrusions	0,0575		0,0441	1,5		2996,8		141
n=55	0,00019	0,12971		0,3	7,3	2769	3330	
Felsic Intrusions	0,0027		0,0031	0,2		2669		47
n=46	0,00005	0,43129		0,38	0,04	2580	2781	

Figure 5.4: Summary of the measured petrophysical parameters

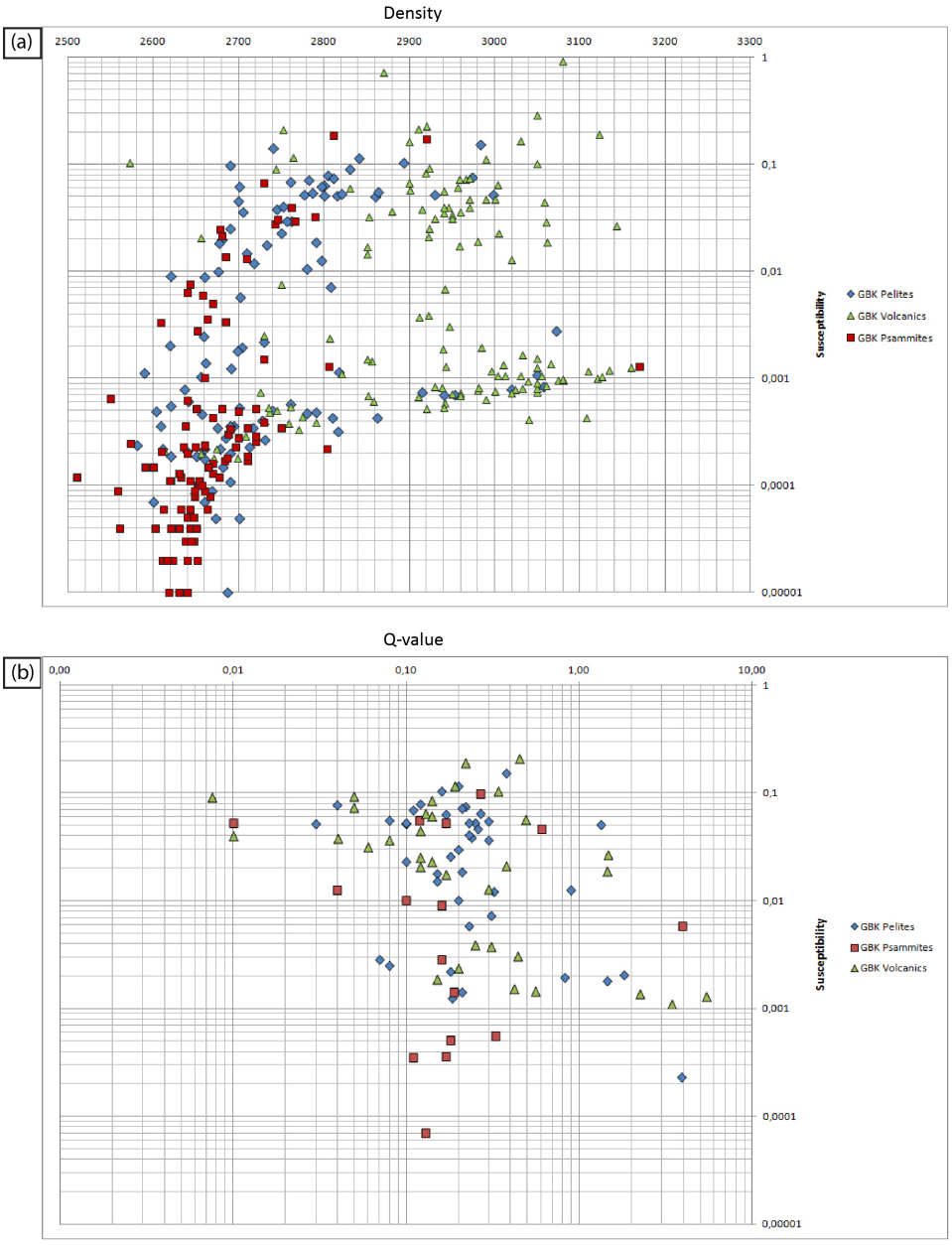

Figure 5.5: Petrophysical cross plots of rocks from the Gållebaike formation. (a) Susceptibility-density plot and (b) susceptibility - Q-ratio plot.

Bakkilvarri Fm.

The sedimentary rocks within the Bakkilvarri formation, mainly mica schists, black schists and graywacks, are in general related to low susceptibilities (Figure 5.6 (a)). The average value is 0.001 SI, but the main population is concentrated towards lower values. The average is skewed due to a high few, high susceptibility samples. These observations are consistent with earlier petrophysical investigations from similar lithologies within the CLGB (Midtun, 1988; Airo and Mertanen, 2008; Olesen and Sandstad, 1993; Grant, 1985b). The Bakkilvarri komatiites show bimodal susceptibility distribution. Similar observations are reported from the Lakselv Valley (B. Davidsen, pers.com., May, 2014), and within the Savukoski Group (Airo and Mertanen, 2008). The difference in magnetic properties appears to be caused by compositional variations, where the high magnetized units have coarse grained magnetite as main magnetite mineralogy (Airo, 1995; Grant, 1985a). The low magnetic units are therefore caused by the concentration of Fe in silica-phases, or higher amounts of monocline ferrimagnetic pyrrhotite (Airo, 2005; Clark, 1997). However, samples with low remanent magnetization indicate that iron is mainly concentrated in the silica-phase (Grant, 1985a).

In addition, hydrothermally influenced komatiitic bodies are often related to altered mineralogy, where the susceptibility is controlled by the amount desctruction of ferrimagnetic minerals (Airo, 2005; Airo and Mertanen, 2008). The mineralogy of altered komatiites is mainly dominated by hydrous minerals, e.g. talc and actinolite (Henriksen, 1991; Often, 1985; Airo, 2005). Such bodies were originally highly magnetic, dominated by coarse grained magnetite yielding high susceptibilities. Polyphase chemical alterations and mechanical deformations have re-mobilized the Fe-distribution, and destroyed primary ferrimagnetic minerals, lowering the susceptibility. However, the komatiites stand out as the most magnetic units within the Bakkilvarri Fm.

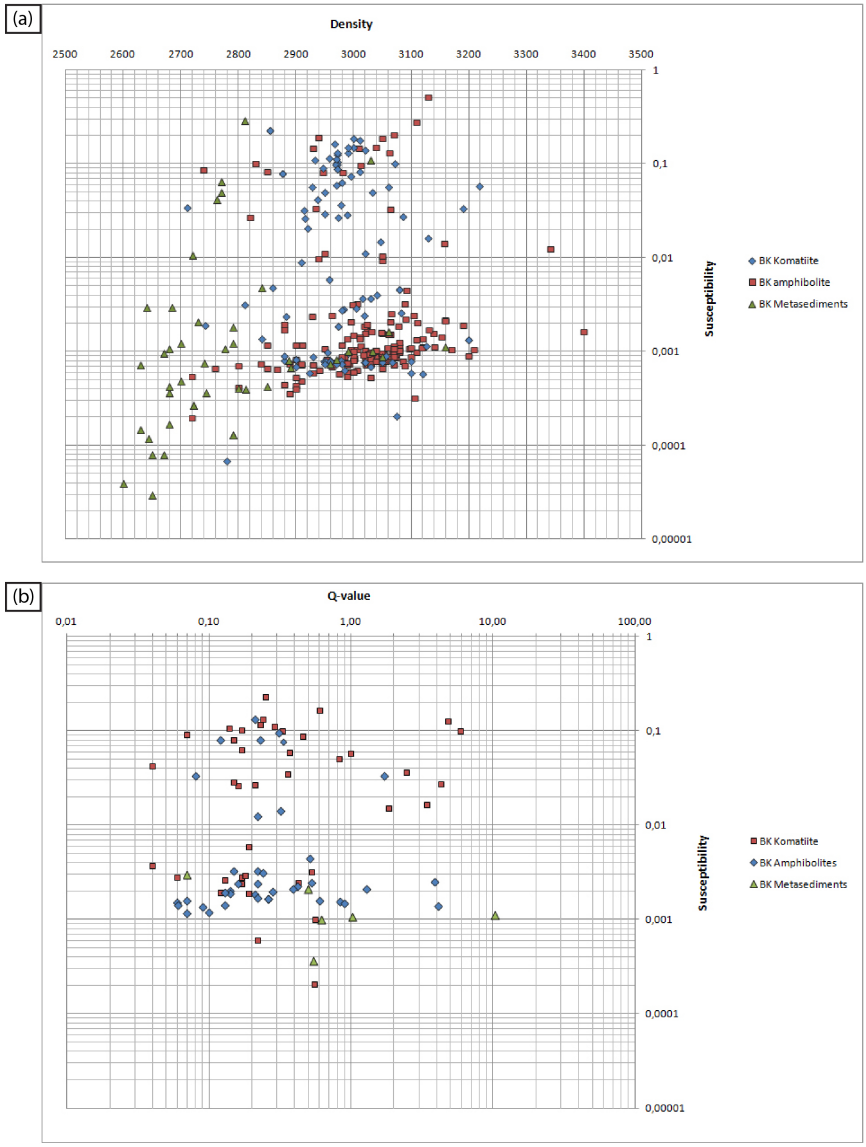

Figure 5.6: Petrophysical properties of the lithologies from the Bakkilvarri formation. (a) Susceptibility-density plot and (b) susceptibility - Q-ratio plot. In general, the komatiites are clustered with a much higher susceptibility than the amphibolites, but show similar density ranges.

Intrusive rocks

The mafic intrusions show susceptibility variation of several orders, and have a bimodal distribution ranging from 0.0005 to 0.43 SI, and an average of 0.0254 (Figure 5.7 (a), 5.4). The mafic intrusives have two main populations clustered around 0.001 and 0.1 SI. In general, the ultramafic rocks group around the 0.1 SI population, while the metagabbros have lower susceptibilities (Figure 5.7 (a)). More ultramfic intrusions, such as pyroxinites and peridotites, have an average susceptibility of 0.057 SI.

The large variation in susceptibility is mainly attributed to fluctuation in magnetic mineral contents (Clark, 1997; Grant, 1985a). Generally, the gabbroic intrusions have lower susceptibility than the more ultrmafic intrusions, due to the higher degree of differentiation and less Fe-content. In addition it has been shown that the oxygen fugacity controls the Fe-bearing mineral phases during crystallization. Field observations and petrographical investigations show that several of the intrusions have been altered by metasomatism, which can observed from the breakdown of pyroxene into biotite (Henriksen, 1991). The lateral variation in susceptibility is clear from Figure 5.1. For example, within the Sturro Gourpmet intrusion, the susceptibilities span from 0.0008-0.0564 SI, but are generally clustered around 0.001 SI. The felsic intrusions have low susceptibilities, similar to the JGC (Figure 5.7 (a)).

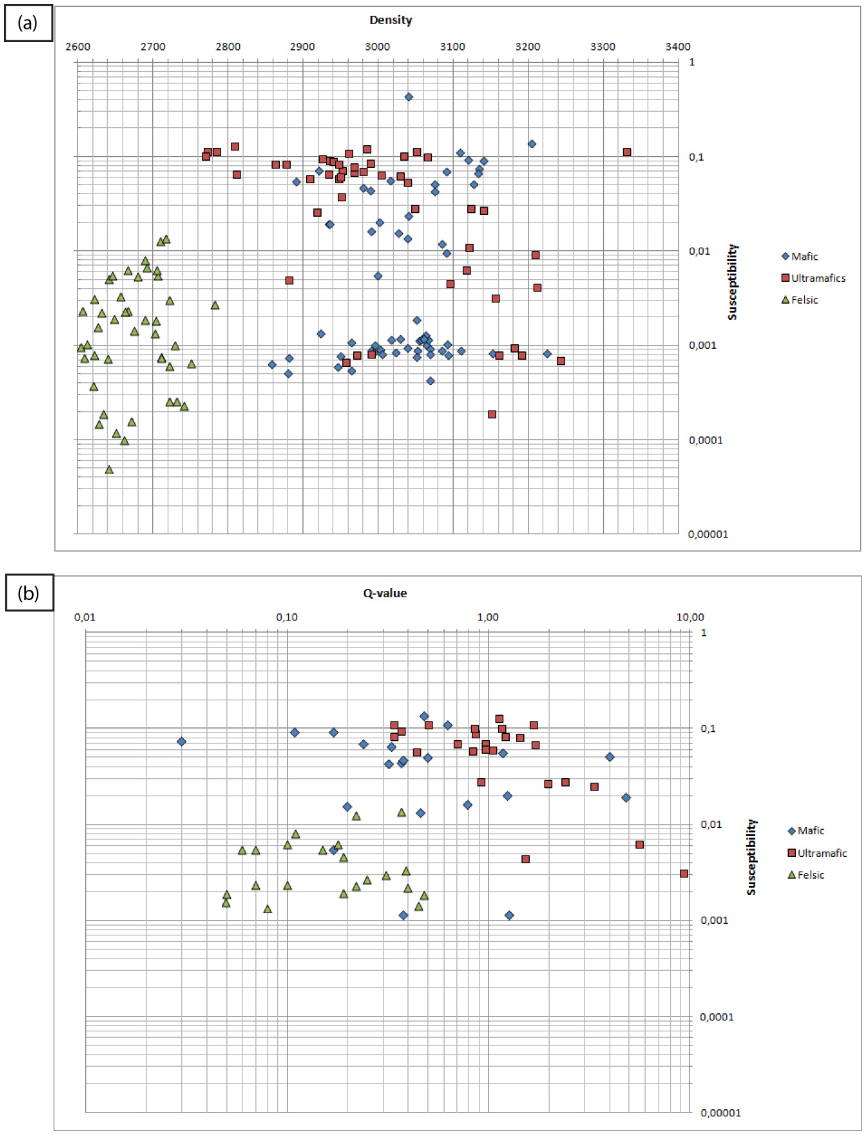

Figure 5.7: Petrophysical cross plot for the intrusive rocks. (a) Susceptibility-density plot and (b) susceptibility - Q-ratio plot.

Other units

The JGC is attributed to low susceptibilities (Figure 5.4). In general, the susceptibility population is concentration 0.005 SI. The maximum values reach up to 0.18 SI, indicating large variations in magnetite content in the gneisses. The in-

termediate gneisses are mostly related to the low susceptibilties, and only a small proportion of these units are related to any significant values. Several mafic dikes have been observed within the JGC (Often, 1985). In general, these are related relative low susceptibilities, but very high remanence. The remanent magnetization is often reversed relative to the present day field (Table 5.1, 5.8 (c))

The TMB shows a clear bimodal distribution of the susceptibility, but is generally recognized by low susceptibilities Figure 5.4). The more felsic, hornblende-plagiocalse gnessies appear to be more magnetic than the more mafic hornblende gneisses. The hornblende-plagioclase gneisses show a bimodal distribution, where the low magnetic parts correspond to suscetipibitlies less than 0.001 SI. The high magnetic variants are clustered around 0.05 SI. The hornblende gneisses are generally low magnetic, where the main popluation is concentrated around 0.003 SI.

5.1.2 Remanent magnetization

In order to derive the Q-ratios, the induced magnetization was calculated using the 2011 IGRF field at 150 m altitude. This yielded a total field strength (H) of 53 600 nT, with 78.3° inclination and 10.8° inclination. From the calculated Q-ratios, it is clear that there are large variations in the magnetization vector components, within the different lithologies. In general, all the formations within the KGB shows arithmetic mean Q-values below 1. However, maximum, minimum and standard deviations have larger variation, and indicate local variations at outcrop scale.

The komatiitic bodies have a large range of remanent magnetization intensity related to high susceptibilities. These observations indicate that the main magnetic mineralogy is dominated by magnetite.

The amphibolites with measured remanence tend to have high Q-ratios combined with low susceptibilities. Though there are few samples that have measured remanence, it indicates that the magnetization patterns can be influenced by remanence. Petrophysical investigations from Finland have shown that these amphibolites with high Q-values are related to monocline pyrrothtite (Airo, 2007).

The ultramafic intrusions have in general higher measured remanence, in addition to Q-values, which reaches up to 7.3. In contrary, mafic intrusions have lower remanence in addition to lower Q-values.

Some of the meta-sandstones and psammites show relative high remnant magnetization, and often high susceptibilities. This is consistent with field observations, where psammites may contain large amounts of magnetite. In the TMB, measured remnant magnetization is generally low, and Q-ratios rarely exceed 0.5. The JGC shows higher variations within the Q-ratios, but the arithmetic mean are below unity. The mafic intrusivs show a mean Q-ratio of 1, but peaks with a ratio of 7.5.

The NRM component has been measured on about 14 samples within the survey area, where all are from mafic to ultramafic intrusions (Table 5.1). In general, the orientation of the NRM component shows large variations. 11 of the samples have

Sample	*Inc*	*Dec*	*Rem (mAm/m)*	*Q-value*
Gabbros				
42091	- 6	131	4022.06	4.8
42092	74	237	1068.64	0.5
42093	56	57	49.3	0.9
42107	65	354	1079.16	1.2
42109	73	40	2770.13	0.5
42110	178	60	2822.74	1.2
42123	147	77	541.44	0.8
42125	346	2	8772.32	4
Sample	*Inc*	*Dec*	*Rem (mAm/m)*	*Q-value*
Komatiites and amohibolites				
312B1	42	88	46.33	0.2
623A	166	76	742.05	1.2
603B	137	58	1080.41	0.3
623B	315	53	460.43	3.7
652	328	47	630.78	0.2
312B2	6	47	122.93	0.1
603A	133	30	1401.14	0.3
612A	55	3	26187.5	4.8
612B	50	8	24715.84	5.8

Table 5.1: Overview of the measurements of the NRM components within the study area.

been collected from the Stourra Gourpmet Gabbro in the Karasjok area (Figure). The mean NRM vector shows a 30 °declination and 80 °inclination.

In the data set, two outliers of respectively declination of 131°and 346°and inclination of -6°and 2°, and are located on the northern most part of intrusive body.

The general low NRM within the KGB, suggests that remnant magnetization is not a general dominating factor. Yet, some lithologies and isolated bodies show signs of high NRM, with different magnetization vector than the present day field (PDF) (Figure 5.8). NRM can therefore explain some of the complex magnetization patterns that can be observed with in the Gållebaiki formation. The gabbro intrusion at Sturro Gorpme shows generally high susceptibility values, but the constitutes a magnetic low. Q-ratios for the intrusions are low, and the mean NRM vector is similar to the PDF.

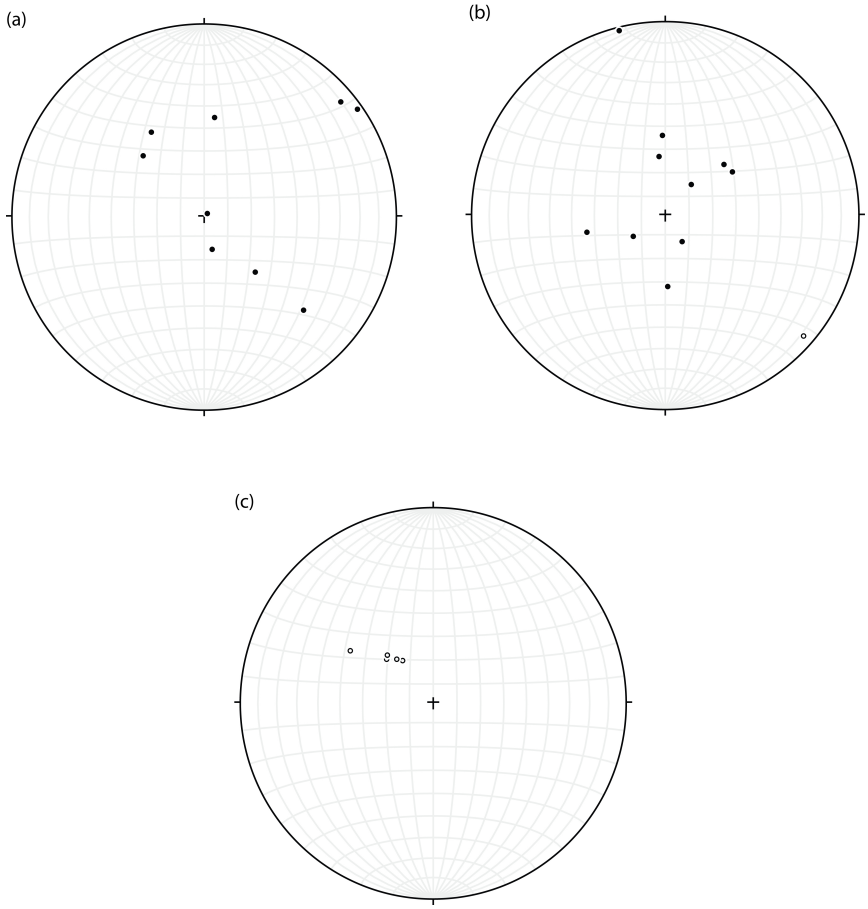

Figure 5.8: Stereonett projections of (a) amphibolites and komatiites, (b) gabbros and ultramafic intrusives and (c) diabase dikes within the Jergul Gneiss Complex. The amphibolites and komatiites show a generally large spread in NRM vectors, but can roughly be diveded into three groups. The gabbros and ultramafic intrusions have clustered NRM vectors, with inclinations around 60-70, i.e. close to the present day field. Note the tight clustering of direction of the NRM vectors in the diabase dikes, and negative inclination.

5.1.3 Density

The density distribution for each formation shows less variation, than susceptibility. In general, the volcanics from the Bakkilvarri and Gållebaike formation are recognized with high densities, with a average of about 3000 kg/m^3.

Gållebaike Fm.

The arithmetic mean of the Gållebaike Fm. lithologies is generally low, due to the high abundance of metapsammitic and metapelitic rocks. In general, the densities of the pelitic rocks are higher than the sandstones and conglomerates. The banded amphibolites appear to have slightly lower densities than the more massive amphibolites, which have been interpreted as metamorphosed lava flows (Often, 1985). Though the data collection is sparse, the banded amphibolites have a density contrast of about 50-100 kg/m^3 compared to the more massive amphibolites. As these rocks are interpreted as metamorphosed volcanoclastic sediments, they have generally lower content of mafic minerals and higher abundances of plagioclase.

The densities of the pelitic and clastic sediments within the KGB are lower than for the mafic volanic rocks. The mica schists show a large density span, and it would be natural to expect higher values than for the quartzite schists. The quarzites are marked by values of about 2670 kg/m^3. The quartzite schists are generally more dense, as they contain higher amounts of mica and are often related to thinner beds with abundant magnetite.

Bakkilvarri Fm.

The Bakkilvarri volcanics show slightly higher mean and maximum values. Both the amphibolites and komatites show similar density distributions. The variations can be a result of the larger variation of lithology with more siliclastic inputs. As reported from Airo and Mertanen (2008), the komatiites show higher densities with increasing amounts of hydrothermal alteration. Airo and Mertanen (2008) and Grant (1985b) suggest that increasing amounts of Mg and Fe-carbonates, on the expense of talc, increases the bulk density of the rock. Furthermore, increasing metamorphic grades can also cause higher densities, as secondary metamorphic minerals, e.g. amphibolites and garnet accumulate Fe in the crystal lattices, and increase the bulk density of the units (Clark, 1997).

Mafic intrusives

The mafic and ultramafic intrusions show the highest mean density in the area with a value of 3011 kg/m^3 (Figure 5.4). In general, the densities range from approximately 2740 to 3300 kg/m^3. The large fluctuation of the density can be attributed to the mafic mineral content, as a wide range of mafic lithologies have been merged into one category. However, it is worth noticing the larger density span within the ultramafic lithologies (Figure 5.7).

Other units

The lowest densities in the area are recognized seen from the JGC units, yielding a mean value of around 2686 kg/m^3 (Figure 5.4). This value is typical for Archean, felsic gneiss complexes within the Fennoscandian Shield (Olesen and Sandstad, 1993; Airo, 2005; Olesen et al., 2010). As a result, the JGC makes up a significant density contrast with the mafic volcanics and intrusions within the KGB.

The TMB shows some density variations, but in general the basic gneisses are denser than the more acidic gneisses, due to the higher content of mafic minerals. The average density values are lower than for the KGB amphibolites and komatites. The bimodal density distribution may therefore be a result of the lithology variation within the TMB.

5.2 Potential field data

The interpretations in this thesis were based on three newly acquired, high resolution geophysical data set, acquired in a time span from 2007 to 2011. From 2007 to 2009, GTK acquired a three-in-one survey, where the aeromagnetic and AEM data were available for this study. In 2011, Fugro acquired a new AGG and aeromagnetic data over a smaller area, just north of Karasjok.

5.2.1 Airborne Gravity Gradient Survey

The Airborne Gravity Gradient (AGG) data were acquired from 19th to 24th of August 2011 by Fugro. Figure 5.9 shows the regional outline of survey area, along with an overview of the topographic relief in the northern part of Norway. The data were acquired with line spacing and tie line spacing of respectively 200 and 4920 meters. The flight direction was E-W, with N-S tie lines. The survey was flown with a minimum drape height of 80 meters and a mean height of 117 meters. In total, 3291 new line km of measurements were flown.

The measured horizontal components were further transformed into five independent gradient components by using both the equivalent layer and Fourier transformation technique (Fugro, 2011; Lee, 2001). The vertical gravity was obtained transformation of the gravity gradients. To obtain both long and short wavelengths in the gravity data, the transformed gravity anomaly was conformed to the DNSC08 regional field (Dransfield, 2010; Fugro, 2011). As AGG systems measure the gradient of the gravity field, it does not require traditional gravity processing techniques. However, as the gradients are more dependent on the terrain features, it is important to select a correct terrain density for the correction. The lithologies within the Iddjajav'ri area show a large span in densities. Due to the very few outcrops in the area, the actual average density in the area is poorly constrained. Consequently,the terrain density was chosen to 2670 kg/m^3 for this

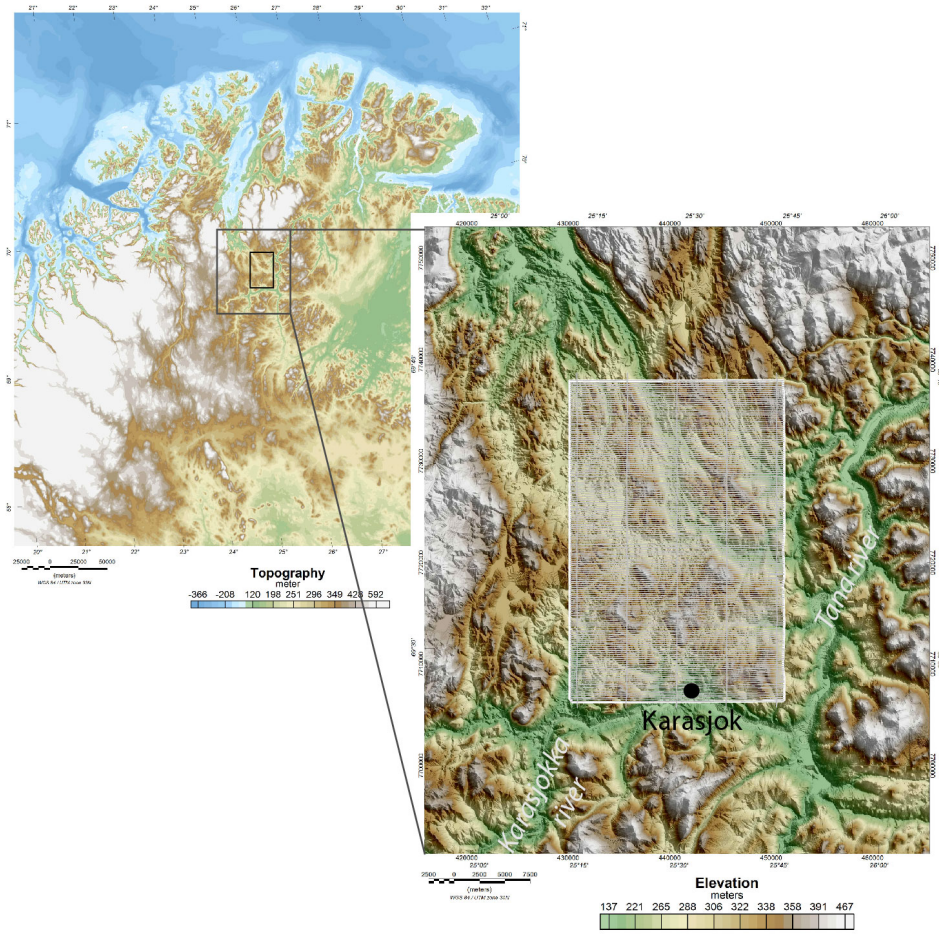

Figure 5.9: (a) Regional outline of the AGG survey. (b) Digital Terrain Model of the study area, with the outline of the AGG survey (white rectangle) and flight lines.

survey, as given by the contractor. This is also justified by the low relief in the area (Figure 5.9).

The system noise for the AGG system was calculated by the standard deviation of half of the difference between the A and B complementary measurements, for each of the UV and NE-components (Fugro, 2011; Lee, 2001). The average noise in the NE-gradient was 3.71 Eö and 3.58 for the UV-gradient. Following a Gaussian statistical distribution, the bulk population (95 %) lies between $\pm 2\sigma$ (Dransfield and Zeng, 2009). Consequently, the noise related to the curvature gradients are expected to have values between - 7.5 Eö and 7.5 Eö, while the transformed ver-

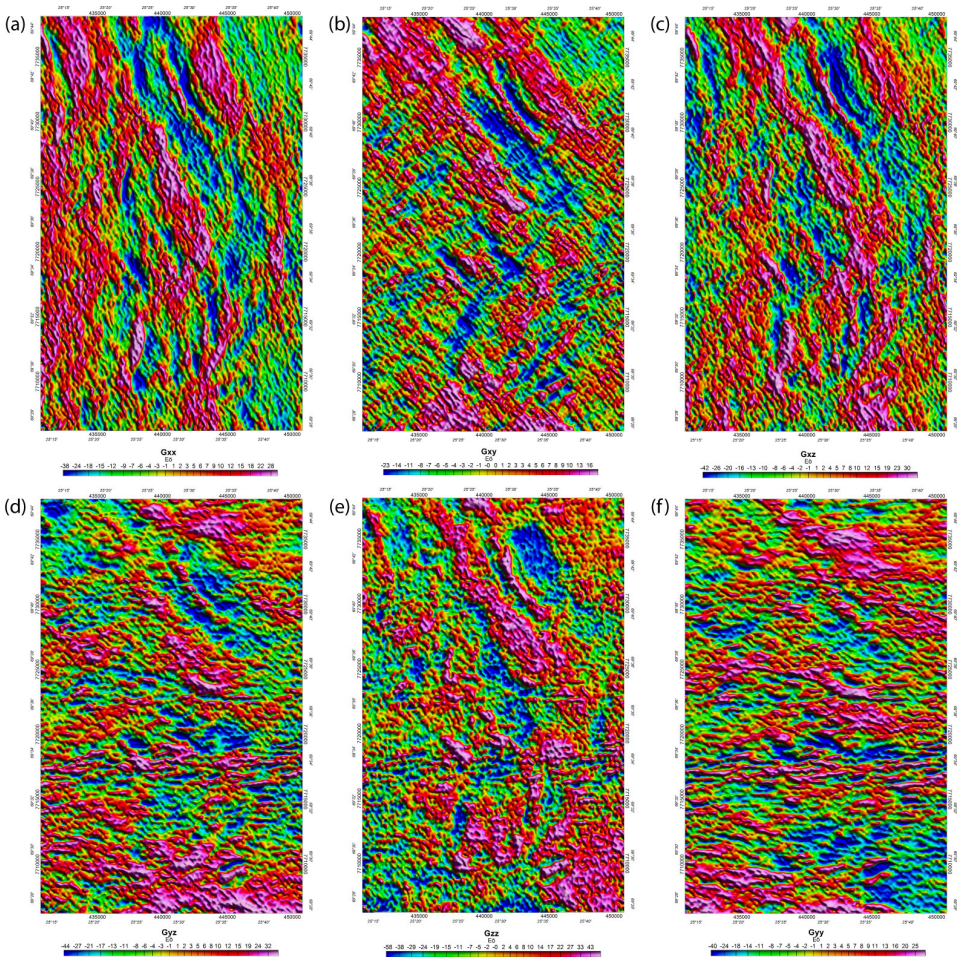

Figure 5.10: Terrain corrected gravity gradients from the AGG survey. (a) G_{xx}, (b) G_{xy}, (c) G_{xz}, (d) G_{yz}, (e) G_{zz}, (f) G_{yy}

tical gradient components are between -10 Eö and 10 Eö (Fugro, 2011). With a line spacing of 200 meters and 0.18 hz low pass filter, it should be expected that highest resolving power of the AGG data are sources 150 m apart. The Digital Terrain Model (DTM) used for the terrain correction was gridded with 10 meter cell spacing.

To quality control the AGG data set for any flight line parallel noise or poor leveling, the measured A_{NE}, A_{UV}, B_{NE} and B_{UV} components were plotted with linear stretched gray scale (Figure 5.11). Anomalies that are present only within single flight lines, are most likely due to artifacts and noise. At approximately UTM Y 771550, E-W elongated anomalies occur, and are recognized as high amplitude

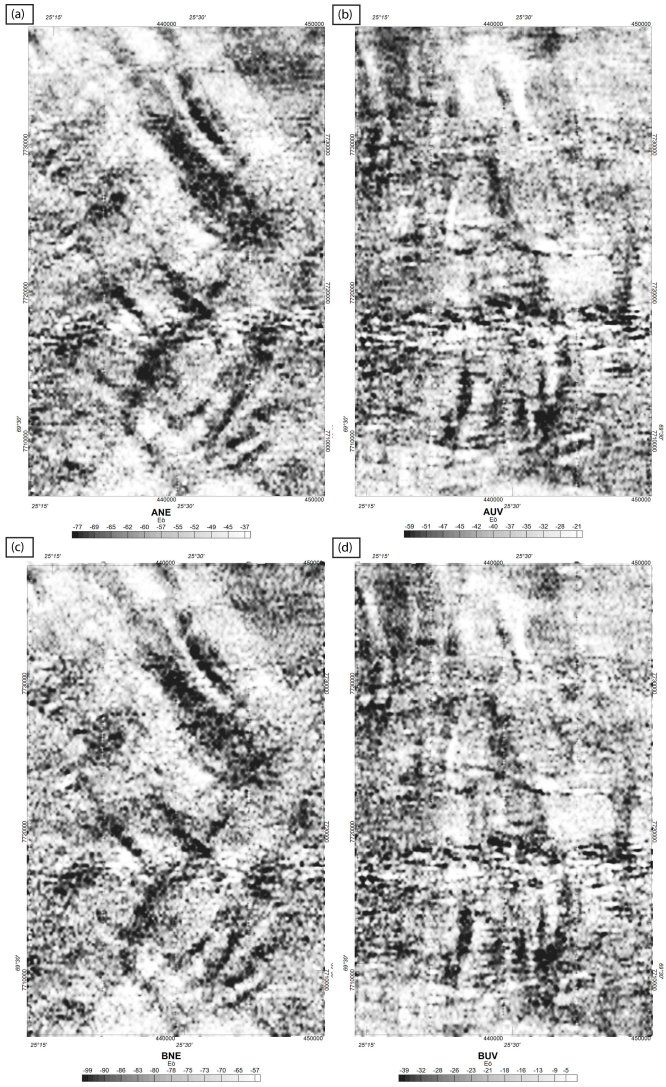

Figure 5.11: Greyscale versions of the measured horizontal tensor components (a) A_{ne}, (b) A_{uv}, (c) B_{ne}, (d) B_{uv}

short wavelengths features. The anomalies are present only at single flight lines, indicative to non-geological artifacts and noise. The artifacts are most evident in the UV-gradients (Figure 5.11 (b) and (d)). Some patchy gradient responses also exist in the same band, and should be interpreted with care, as they are most likely caused by non-geological noise. A similar, but thinner band of flight line parallel

artifacts also appears further north. In addition, small isolated anomalies tend to correlate well with the flight lines, and appear as single line anomalies.Their high amplitudes causes the spikes to remain after micro leveling. Consequently, these anomalies should be treated with care during the interpretation stages.

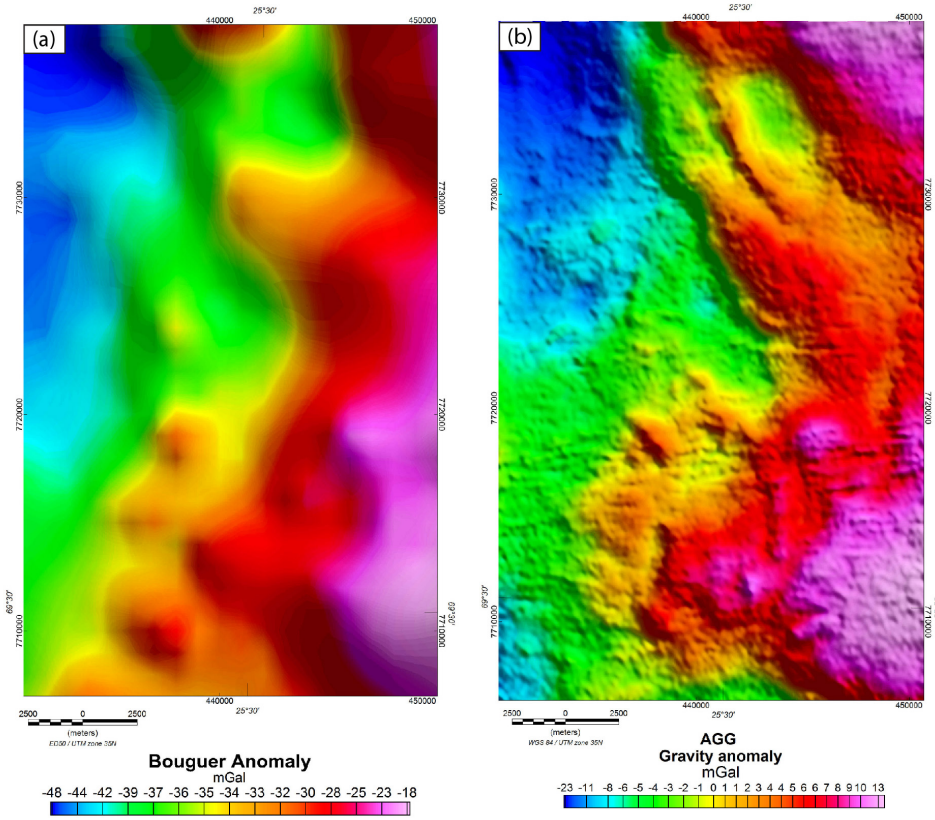

Figure 5.12: Comparison between the (a) gravity anomaly from ground measurements and (b) the AGG transformed vertical gravity conformed with the DNSC08 field. Both grids are taken from the ouline of the AGG survey area. Note the large difference between high frequency details, and significant higher resolution of the AGG data.

During the AGG survey, aeromagnetic data were simultaneously collected, with a Scintrex Caesium magnetometer attached in a tail stinger (See Figure 5.13 for position relative to other aeromagnetic surveys in the area). The data were processed by Fugro, using standard aeromagnetic processing techniques (Fugro, 2011; Luyendyk, 1997). For the quality control, about 200 km of tie lines were checked against diurnal variations, i.e. about 6 % of the survey. The recorded data never

exceeded 10 nT/10 min. Consequently the data are classified as high quality (Luyendyk, 1997). Finally, the International Geomagnetic Reference Field for August 2011(IGRF 2011), was subtracted to calculate the residual magnetic anomaly (RMI). The final grids were created using the minimum curvature techniques.

Figure 5.13: Overview of the different aeromagnetic surveys used in the compilation. The FRASE W, Karasjok GTK and FRASE were compiled as a part of the MINN project.

5.2.2 Regional aeromagnetic data

This study utilizes the aeromagnetic data collected during the MINN-project and from the regional aeromagnetic compilation from Finland. An overview of the compilation is shown in Figure 5.13. Most of the study area is covered by the

Karasjok-GTK survey, collected as a part of a collaboration between the NGU and Store Norske Gull. This survey was flown with an average drape height of 30 m drape, and 200 m line spacing, acquiring in total 16 207 new line km. The magnetic measurements were recorded with a Scintrex CS-2 Cesium magnetometer mounted at the nose stinger. The data was processed by GTK, using industry standard procedures (GTK, 2008). The parts that were not covered by the Karasjok-GTK survey, was acquired in 2012 as a part of the FRASE and FRASE W surveys (Figure 5.13).

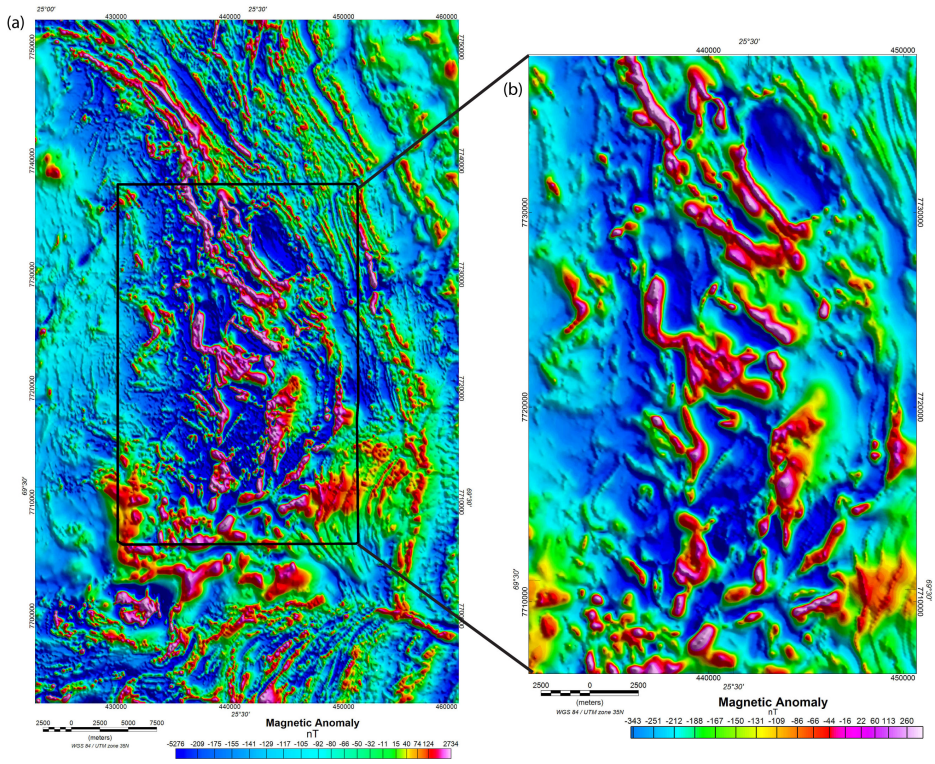

Figure 5.14: (a)Final merged grid of the aeromagnetic surveys, with an outline of the AGG survey. (b) Shows the aeromagnetic data acquired during the AGG survey. Note the difference in detials between the 30m and 110m surveys, as discussed in the text. Black outline corresponds to last figure.

In order to increase the data coverage towards the southeastern parts of the TMB and LGC, regional aeromagnetic data from the GTK were merged and compiled with the MINN dataset (Figure 5.13). The merge was completed using the GridKnit algorithm in Geosoft (Geosoft, 2005a). Final grids were produced using

the minimum curvature gridding technique, with a cell size of 50 m. Figure 5.14 (a) shows the final grid used for aeromagnetic interpretations.

Chapter 6

Potential field interpretation

The following chapter describes the results from lithological and structural interpretation of the potential data. Due to the lack of outcrops, the lithological distribution and structural understanding within the Iddjajav'ri area remains poorly constrained. In order to create a new 3D structural/density model of the area, it was necessary to improve the geological understanding and concept in the area. A first step was to map edges of the magnetic and gravity anomalies, and the interpret the distribution of lithological units and main structures in the Iddjajav'ri area. This process made it possible to establish the first-order regional structures of the area.

The results from chapter 4 suggests that the area is influenced by complex polyphased deformation, which makes the structural interpretation challenging. As mentioned earlier, there are few outcrops in the area. The sparse outcrops limit the constrains of the geophysical signatures from the different lithological packages. Consequently, constrains from outcrops have been correlated with geophysical signatures, in order to extrapolate and interpret unexposed areas. Careful integration of all available data allow for higher confidence when extrapolating interpretations in areas with few solid field observations or outcrops.

The results from this qualitative interpretations are presented in two main parts, reflecting the stepwise interpretation flow. The first part describes the geophysical signatures to major lithologies, and how these have been extrapolated into areas with few or none outcrops. The second part describes the main structural features observed and interpreted from potential field data, integrated with the results from Chapter 4. It is important to underline that the interpretations have been based all available data sets, using a range of different enhancement and filtering techniques (Section 2.3). However, only a few of the key data sets are presented.

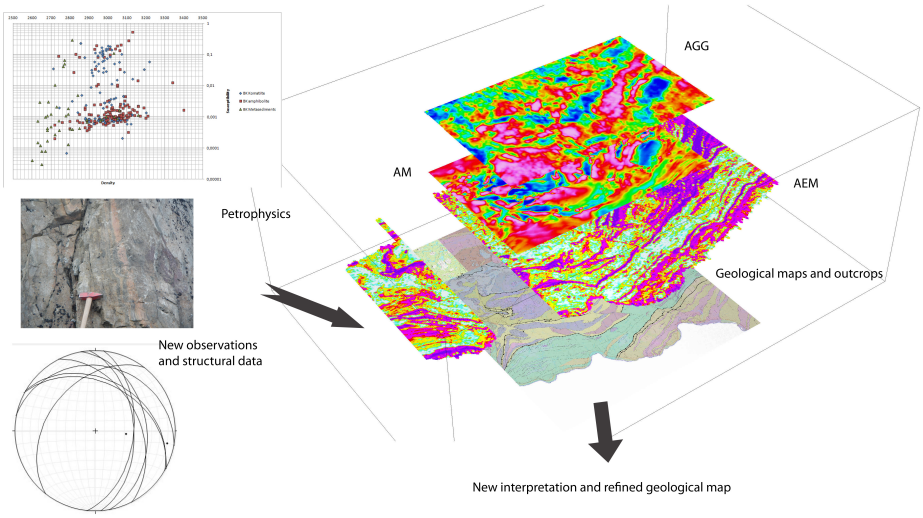

Figure 6.1: Diagram illustrating the integrated approach used to refine the geological map and structural interpretation within the Iddjajav'ri area.

6.1 Geophysical signatures and interpretation of major lithologies

The gravity and magnetic signatures of the KGB show large variations, both in wavelengths and amplitudes (Figure 6.2, 6.3). This reflects the large variations in density and susceptibility through out the area. Based on the correlation between known outcrops and interpretation of filtered magnetic and gravity gradient data, the KGB has been divided into two main domains; the Gållebaike and Bakkilvarri domain (Figure 6.2, 6.3). Further, these domains have been divided into zones that stand out with different gravity and magnetic signatures. These domains and zones are ascribed to variations in main lithologies and/or structural trends (Betts et al., 2003; Aitken et al., 2008). Though these zones approximately correspond to the tectonostratigraphical units, it is important to underline that they present changes in lithologies and structural styles recognized from their geophysical signature.

6.1.1 Bakkilvarri domain

The geophysical signature of the Bakkilvarri domain is dominated by high density metavolcanics, showing large variations in susceptibility (Figure 5.6 (a)). From a regional perspective, the Bakkilvarri domain can be outlined from its strong

positive gravity anomaly, reflecting the concentration of high density volcanics. The amphibolites are rarely exposed in the northern part of the Bakkilvarri domain. According to geological mapping, they have been considered as the most abundant lithology (Often, 1985; Henriksen, 1986).

Based on the magnetic and gravity data, the Bakkilvarri domain has been divided into three zones, reflecting changes in the bulk lithology and structural trends (Figure 6.2, 6.3). The Bakkilvarri Northwestern Zone (BNW) and Northeastern zone (BNE) are outlined on the basis of differences in the magnetization and dip of the main structures (Figure 6.2, 6.4). The division between the zones makes up a prominent linear NW-SE contact in the aeromagnetic data, and suggests a change in lithology and dominant structures (Figure 6.4).

The BNE zone is mainly recognized with moderate to low magnetic intensities, forming prominent NW-SE trending magnetic banding (Figure 6.4). The banding is mainly caused by the bimodal susceptibility distribution of the amphibolites (Figure 5.6). The linear, banded magnetic signature dominates the entire zone, and indicates that the zone is dominated by amphibolites and possibly graphite-bearing schists. Similar NW-SE trending gravity lineaments can also be observed from the HDT (Figure 6.7 (a)). The structures can be traced on the eastern side of a prominent negative gravity and magnetic anomaly. The geophysical data suggest that the structures within the BNE are mostly steeply dipping, linear features.

The BNW zone is mainly dominated by highly magnetized komatiites, interbedded with moderate to low magnetized amphibolites and thinner bodies of graphite bearing schists (Figure 6.4). The magnetic anomalies are dominated by alternating highs and lows, showing large spans in the amplitudes. In general, the high susceptibility komatiites correlate to the most intense positive anomalies wihtin the NW zone (LK in Figure 6.4, Table 6.1). The komatiites are recognized by a NW trending linear magnetic anomaly, with 500-600 m wavelength and amplitudes up to 1200 nT. Correlations between gravity and magnetic data indicate that most of the outcropping amphibolites coincide with weak to negative anomalies, with a patchy magnetization pattern (Table 6.1, Figure 6.4). The lack of strong magnetic signals are mainly explained by their main magnetic mineralogy. Pyrrothite appears to be the main magnetic phase. The amphibolites within the BNW show a less banded magnetic pattern, compared to the BNE. Additionally, the banding appear to be stronger towards the northern prolongations of the KGB.

The zero contour of the gravity tilt proposes that the main bulk of the volcanic units within the BNW is concentrated in a NW-SE trending structure, Bakkilvarri Volcanic Complex (BVC) (Figure 6.8 (b)). The outline of the high density volcanics is also marked by significant terracing effects in the horizontal directive tendency (HDT) (Figure 6.7 (a)), indicating the main concentration of the volcanic lithologies. The response from the third order invariant and HDT suggests that the main volcanic belt is recognized by an internal NW-SE trending structural grain,

	Metapsammites	**Metapelites**	**Komatiites**	**Amphibolites**	**Mafic intrusions**
G_{zz} response	Strong negative domains	Moderate amplitude features	High amplitude, linear feature	High amplitude linear features	High amplitude isolated bodies
	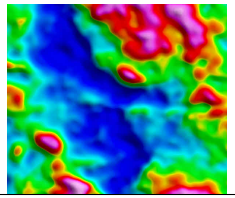	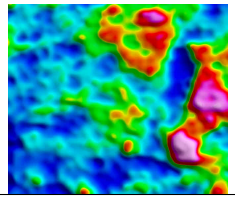	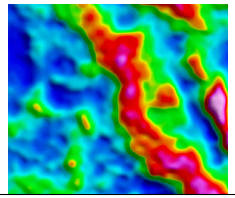	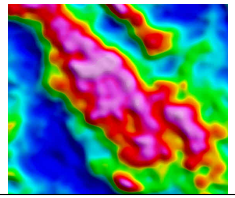	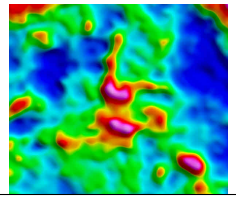
Mag response	Smooth, low intensity feature	Moderate intensity domains	Very high intensity, strike enduring	Low to moderate intensity layers	High to very low intensity domains
	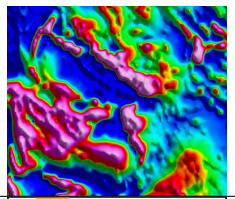	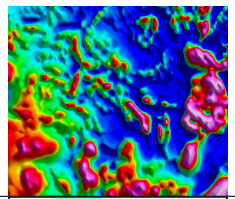	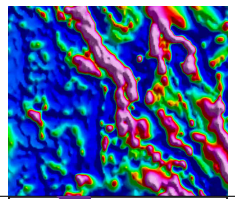	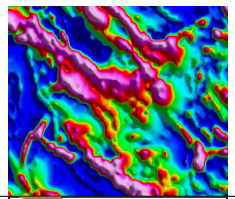	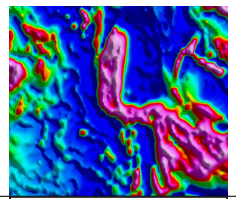
Map	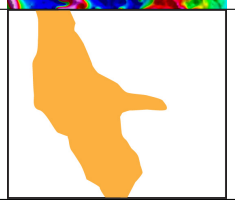				

Table 6.1: Summery of the main lithological units and their respective geophysical signatures. G_{zz} and magnetic responses are taken from the same outline. Note that the G_{zz} is upward continued with 150 m.

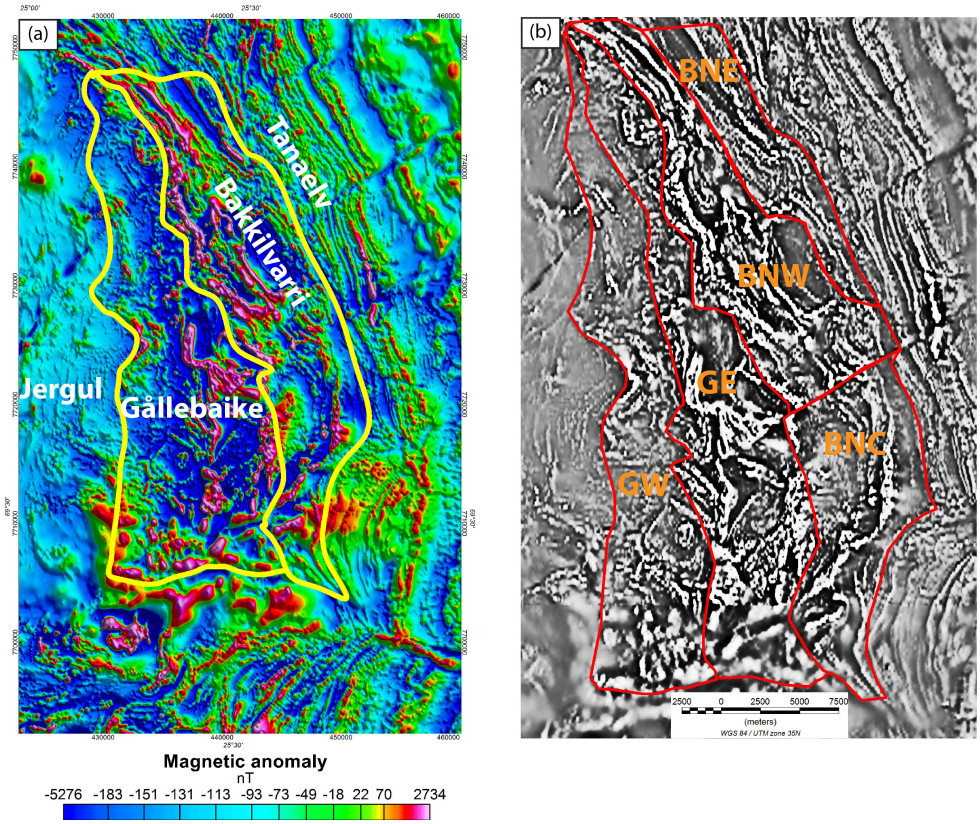

Figure 6.2: Overview of the interpreted geophysical domains and zones within the study area. (a) The main domains within the KGB, overlying the magnetic anomaly. (b) Presentation of the zones within the main domains, overlaying the first vertical derivative. Note that the outline of the domains are similar to shown in (a); Abbreviations: BNE: Bakkilvarri Northeastern Zone; BNW: Bakkilvarri Northwestern Zone; BNC: Bakkilvarri Central Zone; GE: Gållebaike Eastern Zone; GW: Gållebaike Western Zone.

and outline the 3D shape of the body (Figure 6.3 (b), 6.7 (b)).

The most prominent mafic intrusion within the BNW correlates to a high amplitude, 6 km long NW-SE trending magnetic and gravity high, located just northeast of the BVC (Figure 6.3 (a), 6.4). The gabbro and the BVC is separated by a NW-SE trending, linear gravity low. In the magnetic data, the structure correlates to moderate to high intensity anomalies. Midtun (1988) interpreted this structure, based on the magnetic data, as the eastern limb of the Lassevarri Komatiite (LK) (Figure 6.4), forming a recumbent antiform. However, the NW-SE elongated shape,

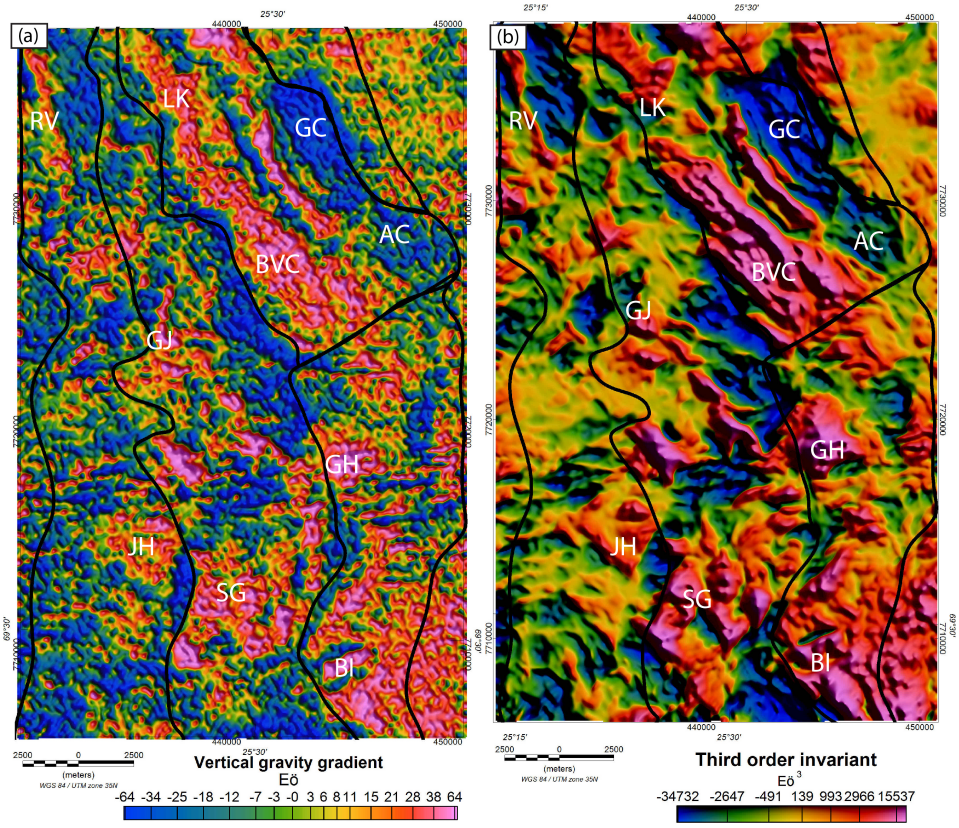

Figure 6.3: (a) The vertical gravity gradient with interpreted geophysical zones. (b) The third order invariant. Note the complex third order invariant response from the Bakkilvarri Volcanic Complex. Abbreviations: AC: Adjatskaidi Complex; BI:Biipovarri Intrusion; BVC: Bakkilvarri Volcanic Complex; JH:Jalgesvadda Hill; GC: Geassacopma Complex; GH: Gimesvarri High; GI:Gallujavri Intrusion; LK: Lassevarri Komatiite RV:Rivdnjesvada; SG:Stuorra Guorpmet Intrusion

in addition to its steep gravity gradients, suggests that the anomaly is related to a low density source, juxtaposed to the BVC. This structure may reflect a more felsic unit, corresponding to lower densities.

The banded magnetic anomalies within the BNW and BNE wrap around an outcropping tonalite, informally named the Geassacopma Complex (GC), recognized as a prominent circular negative magnetic and gravity anomaly (Figure 6.3, 6.4). Due to the significant wavelength of the anomaly and its smooth HDT, it appears that the source makes a regional, deep seated feature (Figure 6.7 (a)). Similar negative anomalies are located just south, correlating to outcropping tonalites. This structure forms a NW-SE trending belt, outlined by its elongated oblong geometry,

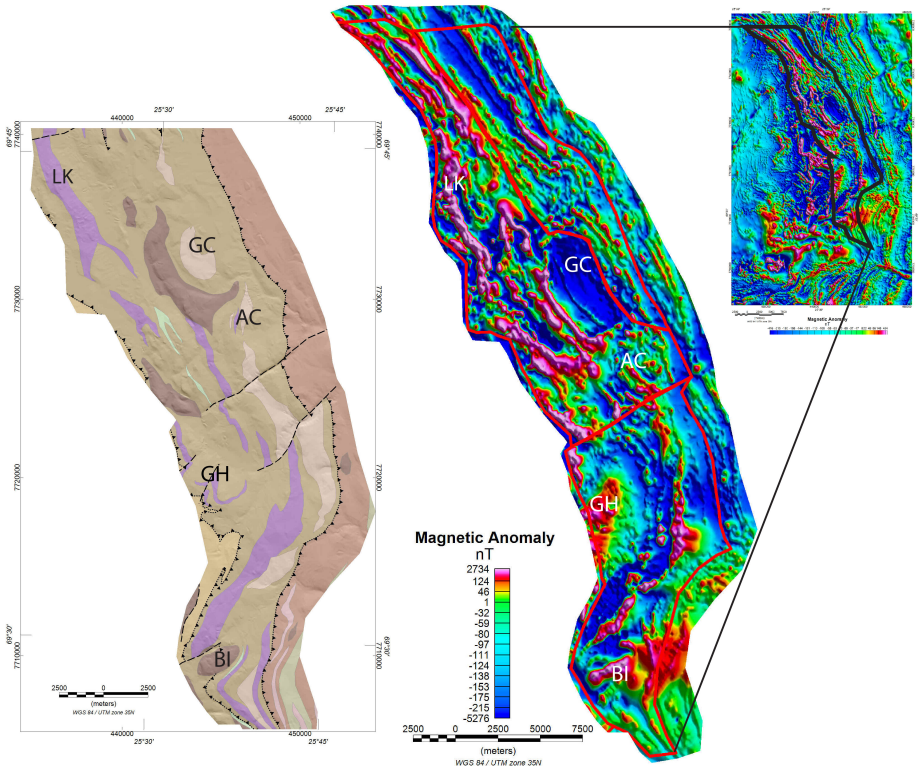

Figure 6.4: Overview of the Bakkilvarri domain, with the geological map on the left, and magnetic anomaly grid on the right. Both the geological map and magnetic grid have been masked to only show the Bakkilvarri domain. Legend for the geological map as Figure 3.1. See text for description of different features. Abbreviations: AC: Adjatskaidi Complex; BI: Biipovarri Intrusion; BV: Bakkilvarri Volcanics; GC: Geassacopma Complex; GH: Gimesvarri High GI: Gallujavri Intrusion; LK: Lassevarri Komatiite

termed the Adjatskaidi Complex (Figure 6.3). The NW-SE structural grain of this complex is particularly well imaged from the HDT (Figure 6.7 (a)). The body appears to rotate the magnetic patterns clockwise in the north, and anti-clockwise in the south, making up a complex structural feature. It is also noteworthy to observe how the magnetic lineaments within the Adjatskaidi Complex appear to swing towards the SE, and terminate against a trending NE-SW break further south (Figure 6.4, 6.8 (b)). It is also noteworthy to observe how the Geassacopma complex appears to be influenced by NE-SW trending breaks towards the southern parts (Figure 6.7 (b)).

The AGG data reveals that the transition from the northern domains toward

the Bakkilvarri Central Zone (BNC) is related to a change in structural styles (Figure 6.3, 6.4). The high amplitude NW-SE trending gravity lineaments within the BNW and BNE end abruptly along a NE-SW trending lineament. South of this lineament, the high amplitude gravity anomalies are recognized by discontinuous sub-circular features within the BNC (Figure 6.3). The most prominent high amplitude gravity anomaly is related to the Gimesvarri High (GH) (Figure 5.6, 6.3). The Gimesvarri High correlates to outcropping mafic to ultramafic volcanics. From the cylindrical shape, and low amplitude HDT signatures, it appears as a deep seated concentration of metavolcanic lithologies (Figure 6.7 (a)). The lack of any structural consistencies between the gravity highs suggest that the volcanics occur as discrete packages, rather than linear structures. Additionally, the komatiites stand out as thinner, linear units within the BNC, and are recognized by less prominent magnetic intensities. It is also noteworthy to observe the N-S striking, linear negative gravity anomaly, located just east of the Gimesvarri High. This feature appears to be the southern prolongation of Geassacopma and Adjatskaidi complexes (Figure 6.3).

The southern part of the BNC is recognized by a change in structural grain, from N-S to NE-SW trending structures (Figure 6.3, 6.4, 6.8). The changing anomaly pattern is readily visible from the magnetic tilt map (Figure 6.8 (a)). The volcanic package appears to be concentrated in a NE-SW trending linear body. The magnetic anomalies correlating to the komatiites can be traced up to 12 km, and make up the most prominent magnetic feature in the southern part of the Bakkilvarri domain. The Biipovarri intrusion appears to terminate magnetic and gravity lineaments, suggesting a break in the structural pattern.

6.1.2 Gållebaike domain

The metasedimentary rocks in the Gållebaike formation are mainly dominated by more discontinuous linear trends and features, compared to the Bakkilvarri Fm. (Figure 6.3, 6.5). The dominant magnetic and gravity anomalies are mostly correlated to mafic and ultramafic intrusions. The metapelitic lithologies appear as subtle and weakly magnetized domains, seen as curvilinear anomalies (Table 6.1). Areas dominated by quartzites and quartzitic gneisses are recognized as domains with a general smooth, negative magnetic signal. Outcropping magnetite-rich quartzite schists correlate to discrete magnetic highs (Table 6.1). However, the high magnetic quartzite structures are consistent with negative gravity anomalies.

Mainly based on the aeromagnetic signature, the Gållebaike Fm is divided into two main zones, western (GW) and eastern (GE) zone, delineated by a break in the lineament orientation, and termination of the high amplitude magnetic anomalies (Figure 6.2 (b)). This is suggestive to a change in dominant lithologies, and appear to be structurally controlled.

The eastern zone is recognized by negative anomalies related to quartzites and

quartzite schists, juxtaposed to high amplitude anomalies created by mafic to ultramafic intrusions (Figure 6.5). The mafic to ultramafic intrusions are recognized as small, isolated features. Most of the outcropping ultramafic intrusions correlate to both magnetic and gravity highs (Table 6.1). From the AGG data, the mafic and ultramafic intrusions appear to be concentrated in the eastern parts of the easter zone within the Gållebaike domain (Figure 6.3 (a), 6.5). The metasedimentary rocks stand out as prominent low density feature (Figure 6.3, Table 6.1). Based on the AGG data, the metapsammites appear to be concentrated along a NW-SE trending structure just east of the BVC, recognized from the prominent negative vertical gravity gradient anomaly (Figure 6.3 (a)).

The Gållebaike domain is recognized by two larger mafic/ultramafic intrusion complexes; The Stourra Gourpme and Gallujav'ri intrusion (Figure 5.5, 6.3). The geophysical data suggest that the intrusions follow the general structural grain of the host lithologies, and make up a NW swinging trend. In addition, neither the magnetic nor the gravity anomalies are suggest that amphibolites are located within the eastern zone within the Gållebaike domain. The Stuorra Gourpmet intrusion is located 3-4 km north of Karasjok, where parts are exposed around the Stuorra Guorpmet hill (Figure 6.5). The body stands out both as a prominent magnetic and gravity anomaly. The zero contour of the gravity tilt, as well as the third order invariant (Figure 6.3 (b), 6.8), outlines well the edges of the body. The gravity gradient components suggest that the intrusions are attributed to several isolated structures, rather than one homogeneous structure. From the HDT, it appears that the northeastern parts of the intrusion are the largest, indicated by a more spherical equipotential field. The easternmost parts displays a clear arcuate structural trend, linking up with an outcropping gabbros further north.

The gravity gradient components show that the Gallujavri intrusion makes up a significant mafic to ultramafic complex, incorporating the mafic intrusion located to the east and possible to the north (Figure 6.3, 6.7). The most prominent magnetic anomaly is caused by the ultramafic part of the intrusion, while the outcropping gabbro is recognized as a negative magnetic anomaly. The third order invariant indicates that intrusion is made up by two main high-density concentrations. Similar results are also shown from the third order invariant and the shape index (Figure 6.3 (b), 6.7 (b)). Consequently, it appears that the main bulk of the Gallujav'ri intrusion is located within these two units, forming a complex shaped structure. The most prominent magnetic anomaly is caused by the ultramafic part of the intrusion, while the gabbro is recognized as a negative magnetic anomaly. The magnetization contrast between the southern and northern part of the complex is conspicuous, and show structural changes along the strike of the body.

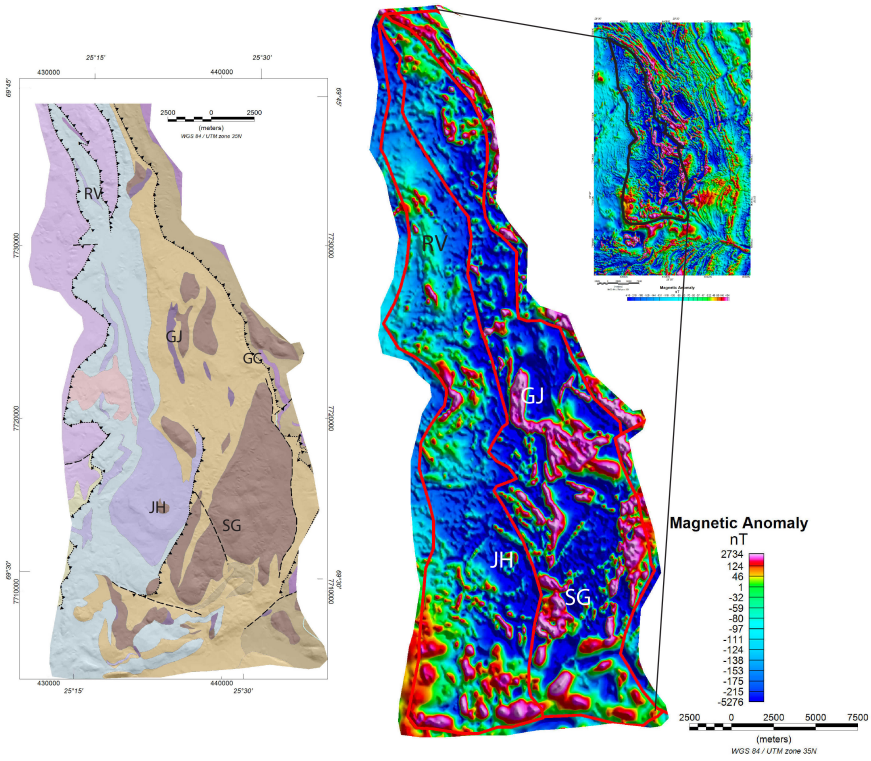

Figure 6.5: Overview of the Gållebaike domain, with the geological map on the left, and magnetic anomaly grid on the right. Legend for the geological map is shown in Figure 3.1. Both the geological and magnetic grid have been masked in order to only show the Gållebaike domain. See text for description of different features. Abbreviations: JH: Jalgesvadda Hill; GI: Gallujavri Intrusion; SG: Stuorra Guorpmet Intrusion

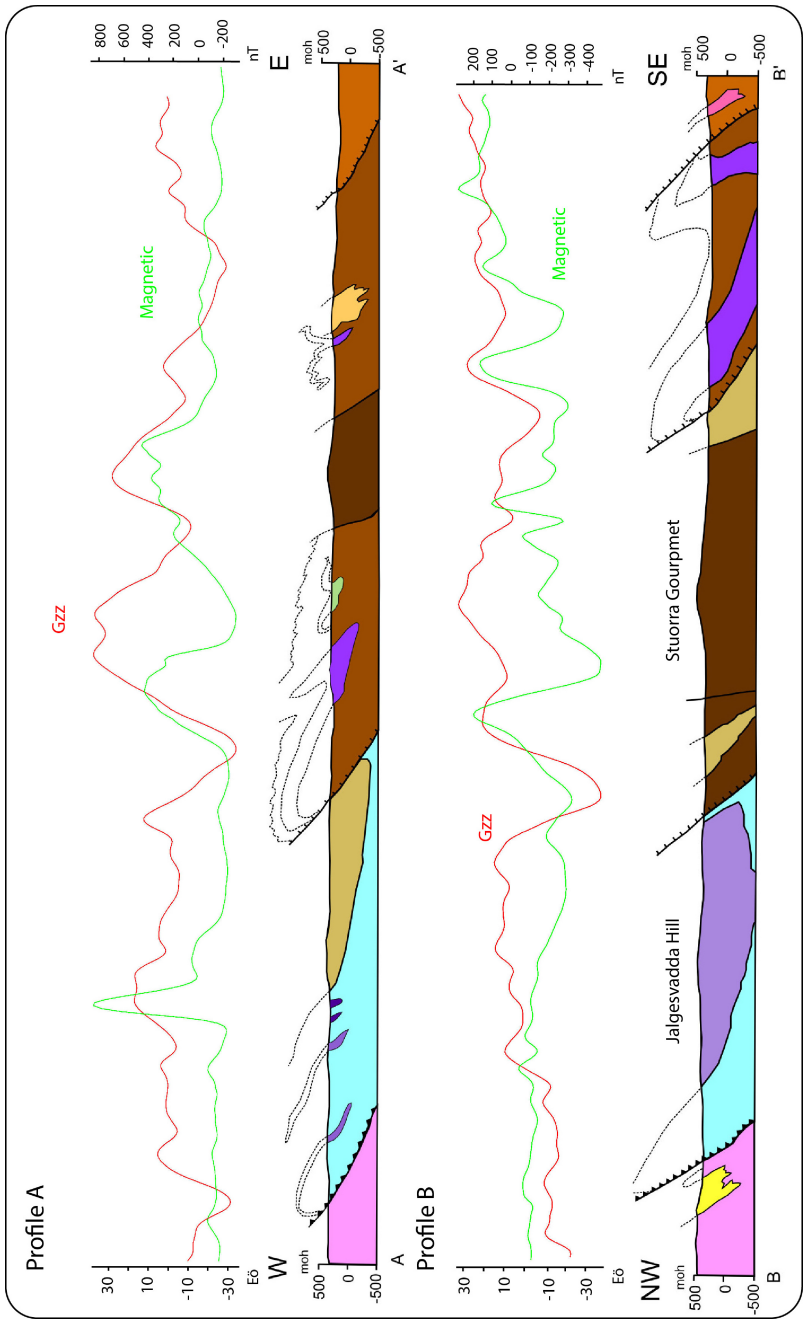

Figure 6.6: Geological profiles from Henriksen (1986), with corresponding vertical gravity gradient and magnetic anomaly. Location of the profiles are given by Figure 3.1.

The mica schists and amphibolites within the western zone of the Gållebaike domain are recognized by smoother and more moderate gravity anomalies (Figure 6.3, 6.5). In the magnetic data, they stand out as curvilinear, weak to moderately anomalies (Table 6.1). In the western parts of the Gållebaike domain, exposures of the mica schists and amphibolites are limited. This makes it challenging to evaluate their geophysical signature and lateral distribution. However, in general, the mica schists correspond to negative to moderate, patchy amplitudes (Table 6.1). Their large span in susceptibility suggests that the magnetite content is controlled by later stage metamorphism. The amphibolites stand out as short wavelength positive anomalies. The mica schists and amphibolites appear mainly steeply to moderately dipping linear features, and with their main concentration the western zone of the Gållebaike domain. In the central parts of the GW, the contact to the JGC is marked by a high amplitude, linear magnetic anomaly, correlating to outcropping granodioritic gneisses, where the magnetic grain corresponding to the contact shows an undulating trend (Figure 6.5).

A thin, linear NE-SW trending magnetic anomaly, correlating to an outcropping diabase dike, appears to cross-cut both the anomalies related to the KGB and JGC, in the Rivdnjesvada area (Figure 6.5, 6.9). The strong, negative magnetic anomaly appears to be caused by reversed remanent magnetization of the dike. It is noteworthy to observe that the dike cross-cuts both the supracrustal rocks within the KGB and the thrusted basement sliver.

The Jalgesvadda Hill stands out as the most prominent amphibolite feature within the western zone (Figure 6.3, 6.5, 6.6). The deformed gabbro within the central parts of the hill is observed as a sub-circular gravity and magnetic high, while the amphibolites appear to be wrapped around this feature, and constitute patchy, curvilinear magnetic lineaments (Figure 6.11). In particular, the amphibolites show large spans in magnetic intensities. The variations in gravity signature suggest that the structure decreases in thickness towards the northern prolongation. Its eastern boundary is marked by a steep gravity gradient, most likely caused by the juxtaposed quartzite schists. According to earlier interpretations, this has been interpreted as an elongated, N-S striking feature of amphibolites, extending towards the northern part of the area (Figure 6.5). However, the new potential field data indicate that the structure is more limited in its N-S extension, and appears rather to be sub-circular concentration of high amphibolites.

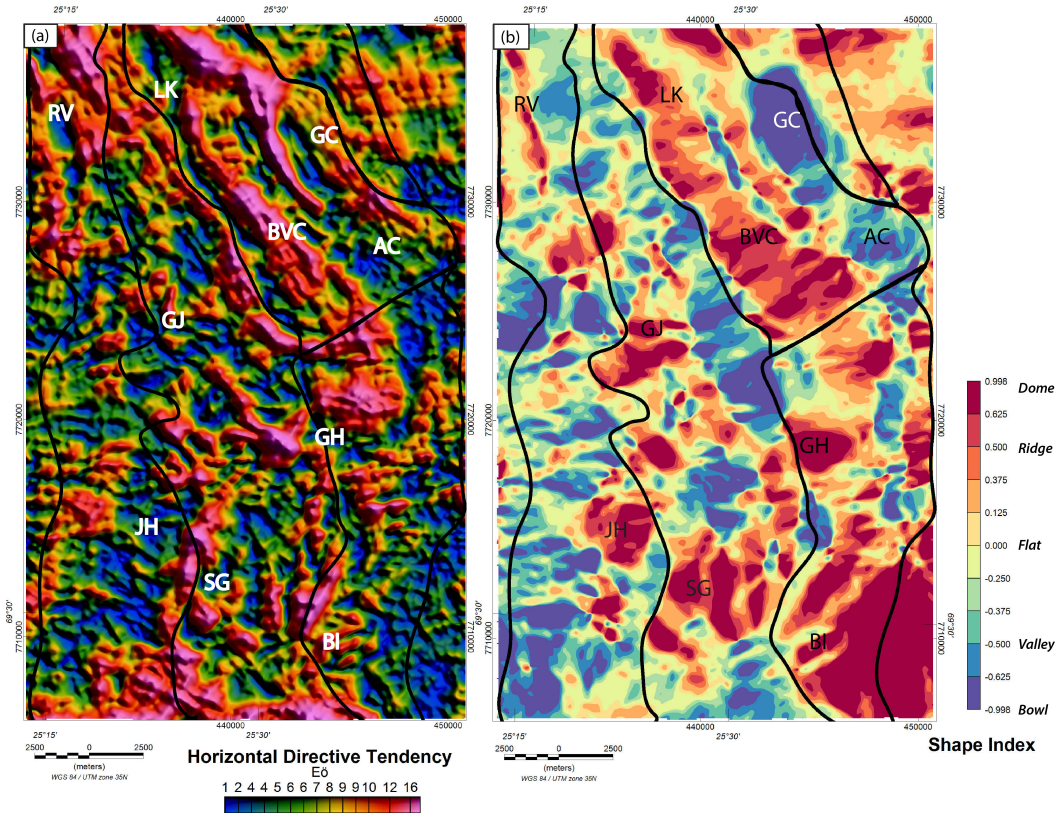

Figure 6.7: Curvature analysis of the gravity gradients. (a) The horizontal directive tendency and (b) the shape index of the equipotential field. Abbreviations: AC: Adjatskaidi Complex; BI:Biipovarri Intrusion; BVC: Bakkilvarri Volcanic Complex; JH:Jalgesvadda Hill; GC: Geassacopma Complex; GH: Gimesvarri High; GI:Gallujavri Intrusion; LK: Lassevarri Komatiite RV: Rivdnjesvada; SG: Stuorra Guorpmet Intrusion

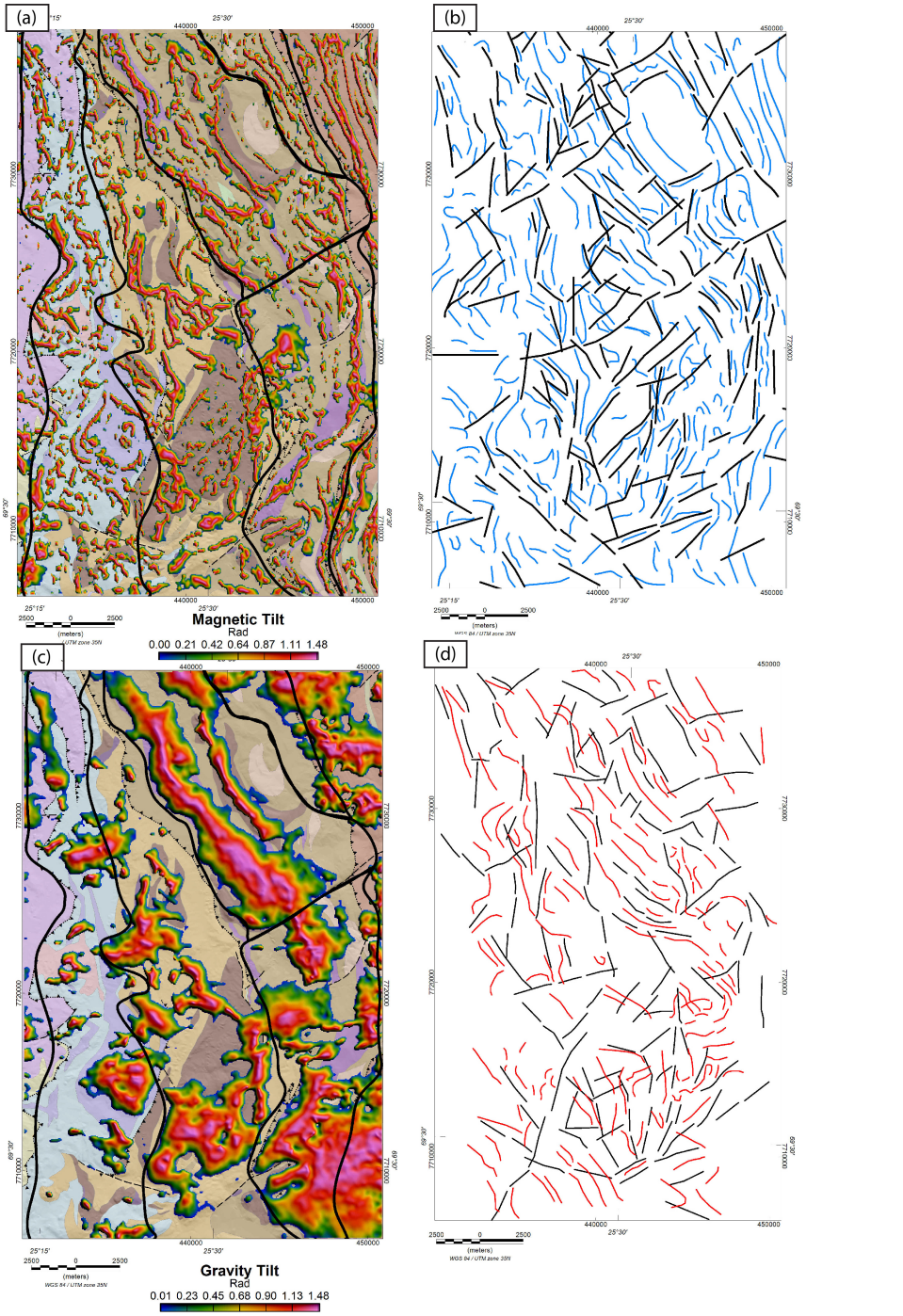
(a)
(b)
(c)
(d)
Magnetic Tilt
Rad
0.00 0.21 0.42 0.64 0.87 1.11 1.48
Gravity Tilt
Rad
0.01 0.23 0.45 0.68 0.90 1.13 1.48
Magnetic TDR lineaments
Gravity gradient lineaments
Magnetic/grav break

Figure 6.8 *(previous page)*: Gravity and magnetic interpretations from the Iddjajav'ri area, together with the geophysical zones. Breaks in the magntic and gravity pattern are defined as unspecified faults, fractures and unconformable contacts. (a) Positive magnetic tilt values, overlying the geological map by Henriksen (1986) (b) Interpretated magentic breaks of anomaly patterns and magnetic lineaments in the area. (c) Positive gravity tilt, overlying the geological map by Henriksen (1986) (d) Interpreted gravity breaks anomaly patterns and lineaments from the gravity gradients.

6.2 Structural interpretations

The available high resolution datasets have allowed for a detailed structural analysis of the study area. It has been possible to map out several first and second order faults, folds and shear zones, not readily observed from earlier field mapping. Due to the limited amount of outcrops, it is challenging to interpret the structural features only based on outcrop information. The structural analysis is therefore based on interpretation of magnetic and AGG lineaments and breaks, correlated with available field observations obtained during the field work (Figure 6.8, Chapter 4).

Figure 6.9 shows the interpreted main 1st and 2nd order structures within the study area. The analysis of the magnetic and AGG data reveals that the area is dominated by several regional fault and fold structures. From overprinting relations, it has been possible to identify structures related to four deformation phases. These have different characteristics and main structural grain, and are therefore indicative to a polyphase deformation history of the area (Table 6.2).

The earliest structures within the area are observed mainly to be related to a NW-SE trending structural grain, correlating to the S_1 foliation. From the magnetic data, this phase are particularly well imaged within the northern parts of the Bakkilvarri domain (Figure 6.9). In general, these structures are related to isoclinal recumbent F_1 folds and layer parallel D_1 thrust zones, forming repetitions and discordances in the observed tectonic layering and fabric. The D_1 structures are recognized by a consistency in NW-SE trending magnetic and gravity lineaments (Figure 6.9, 6.10).

The D_1 structures appear most evident within the Bakkilvarri domain. Here, magnetic and AGG lineaments make up pervasive, NW-SE trending linear features (Figure 6.8 (a), (c)). These structures are in particular well imaged from the third order invariant and the HDT (Figure 6.3 (b), 6.7 (a)). Within the Bakkilvarri domain, several local thrust zones are developed. These layer parallel thrusts extend along the entire length of the belt, forming prominent linear structures (Figure 6.8, 6.9). For example, the NW and NE zones within the Bakkilvarri domain are

interpreted to be separated by a such NW-SE trending thrust fault, separating two blocks with different bulk lithology. Based on the magnetic and AGG lineaments, these thrusts faults appear mainly to be moderately NE-dipping. Towards the southern part of the study area, the D_1 structures to be influenced by later deformation, observed by changes to N-S and NE-SW oriented structures. It is also noteworthy to observe how the structural grain of the D_1 thrusts varies between the western and eastern contacts of the Bakkilvarri domain (Figure 6.9).

The transition between the KGB and the TMB is recognized by smoothly NW-SE trending, linear 1 km wavelength magnetic low (Figure 6.9). Magnetic lineaments on either side of the linear low show a discordant relationship. Though the field appearance of the TMB mafic gneisses is similar to the upper most part of the Bakkilvarri domain (Marker, pers.com, 2014), they stand out as different crustal domains in the geophysical data (Figure 6.2 (a)).

Overprinting relations mainly shown in the magnetic data, support field observations that the contact to the JGC is tectonic (Figure 4.9, 6.9), and represent a D_1 thrust. The magnetic lineaments related to the contact have an undulating signature, and suggest that the contact was folded and faulted by later deformation phases(Figure 6.9). These results correlate well with the observed fold trends from field observations (Figure 4.6).

Field mapping (section 4.1) and analysis of the AGG and magnetic data suggest that the boundary between the Gållebaike and Bakkilvarri domain is tectonic, separated by a NW-SE trending thrust zone (Figure 6.9). From the gravity anomaly, the thrust zone is clearly recognized by the termination of the NW trending Bakkilvarri Volcanic Complex (BVC), forming a steep gradient (Figure 6.3 (a), 6.6). Additionally, magnetic lineaments within the Bakkilvarri domain appear to truncate fold structures developed within the Gållebaike metapsammites. The magnetic data reveal several smaller, second-order thrusts, suggesting imbricate structures (Figure 6.9). Its regional character, and influence on the lithological distribution in the area, suggests a D_1 origin.

As observed within the Bakkilvarri domain, several local D_1 thrust zones are developed internally within the Gållebaike domain, forming N-S to NW-SE trending thrust zones (Figure 6.9, 6.11). These thrusts are mainly outlined from changes in the magnetic grain, and are often related to the development of isoclinal folding. Linear structures observed in the Ravdojavri area represent a such thrust fault. However, from overprinting relations, the shear zones are displaced by later NE-SW trending faults (Figure 6.11).

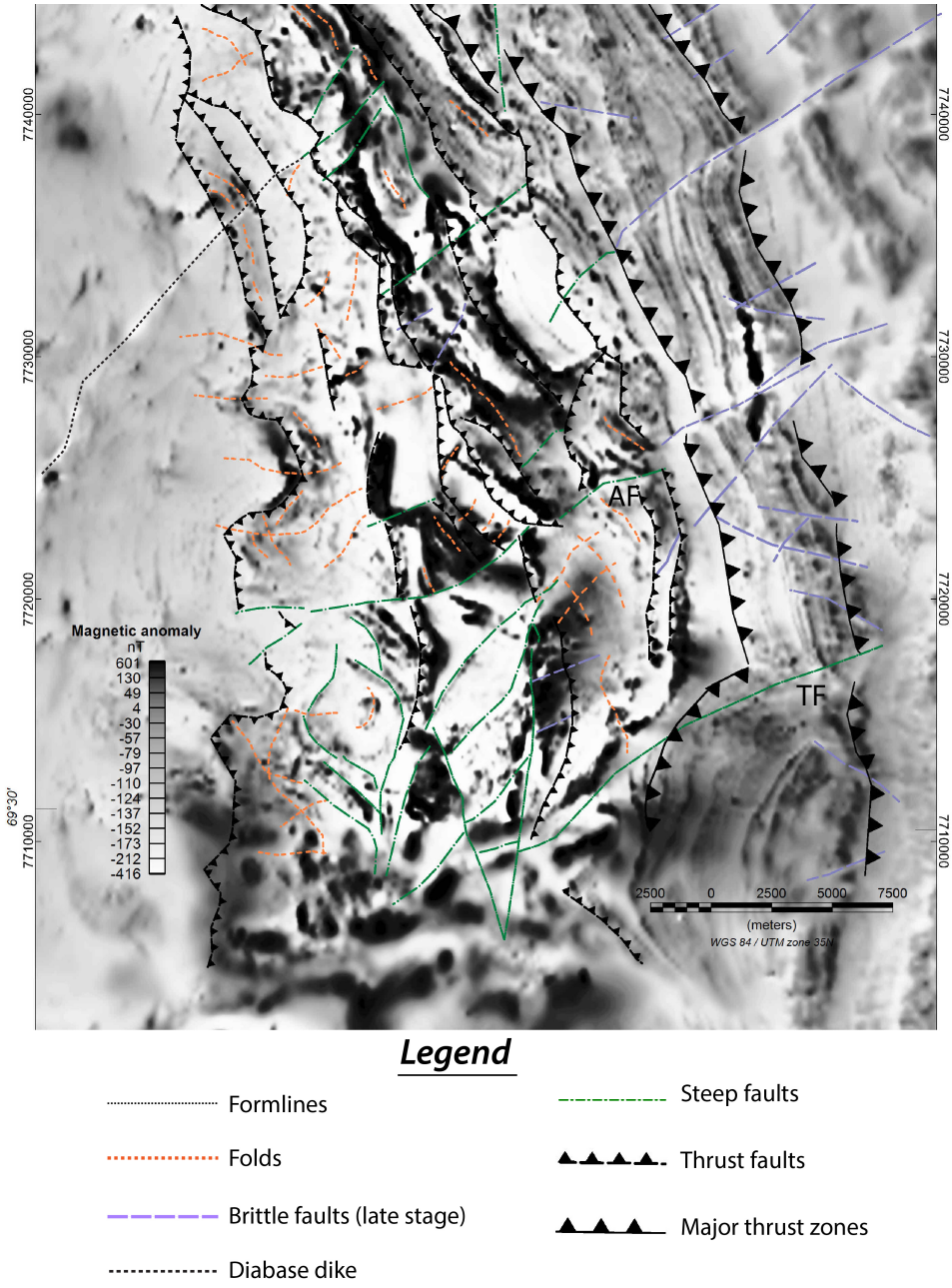

Figure 6.9: Overview of the main interpreted structural elements within the study area. Shown on top of magnetic anomaly. Interpretation is inferred from the gravity gradients and magnetic data. The NE-SW faults discussed in the text, the Adjatavzi Fault (AF) and Tanaelv Faults (TF), are marked on the map.

It is noteworthy to observe how local D_1 thrusts are related to occurrences of komatiites and graphite bearing schists (Figure 6.4, 6.10). These observations are supported by field observations in the Lakselv and Karasjokka area, where the contacts of the komatiites often are related to alterations and shear movement (Davidsen, 1994; Henriksen, 1991; Airo and Mertanen, 2008). These observations are consistent with the expected competence contrast between the quartzite schists and volcanics, particularly related to komatiites. In these situations, the komatiites make up low competence gliding planes, where strain easily can be accommodate, which then forms basal thrust zones.

From the magnetic and gravity lineaments within the NW zone of the Bakkilvarri domain, it is clear that the outcropping tonalite at the Geassacopma complex indicate a complex structural influence on the adjacent supracrustal rocks (Figure 6.10). Magnetic lineaments appear to truncate against the body, both in the northern and southern prolongation, indicative that the along strike influence is larger than inferred from the surface observations (Henriksen, 1986, 1991). Both the third order invariant and HDT indicate a NW-SE trending structural grain internally within the tonalite complex (Figure 6.3 (b), 6.10 (b)). Accordingly, from its apparent regional trend, it appears to be related to the D_1 thrusting within the KGB.

The outcropping, isolated JGC structure within the northwestern part of the survey area, near the Rivdnjesvadda area, is well imaged both in the aeromagnetic and gravity gradient data (Figure 6.3, 6.5). The outcropping basement sliver is separated from the main basement complex by a thin structure of associated mica schists, metasandstone and layers of komatiites, identified by NW-SE trending magnetic lineaments. From the apparent cross-cutting relation between the basement sliver and supracrustal rocks, the structure appears to reflect a NW-trending thrust system, emplaced during the D_1 phase. This interpretation is supported by reports further north, where thrusted basement slivers have been identified based repetitions of the lower most sequence of the KGB (Krill, 1985; Pharaoh and Walsh, 1987).

Field observation and analysis of aeromagnetic data suggest a second deformation phase within the Iddjajav'ri area. The best evidence for these structures is indicated km-scale F_2 folding, around an approximately N-S trending axial traces (Figure 6.9). From the aeromagnetic and AGG data, these folds stand out as form lines caused by tight to open folding of the metapelites and metapsammites (Figure 6.8, 6.9). The orientation and trends of these geophysical observations correlate well with the assumed F_2 folds observed from field observations, e.g. in the Olagevarri and Nieiddaidvarri area (Figure 4.6). The F_2 folds are best recorded within the Gållebaike domain, where they stand out as discrete, curvilinear shaped lineaments (Figure 6.9, Table 6.2). F_2 folds are superimposed on the D_1 thrust contact to the underlying JGC. This fold trend explains the undulating structural

Domains	Field observations	AGG	Magnetic	Interpretation
BNW	Not-visited	Moderate to weak anomalies, aligned along a NW-SE trend	Moderate to weak magnetic lineaments, with a dominant NW-SE trend grain. Lineaments offset by NE-SW faults	Mainly D_1 structures, related to isoclinal folding and local NE-dipping thrust zones. Offsets of D_1 structures due NE-SW trending faults
BNE	Not-visited	Volcanics situated in a NW-SE trending belt. Small scale arcuate trends shows variations in the structural style along strike	NW-SE to N-S oriented linear anomalies, related to steeply dipping lineaments. Lineaments reassemble N-S striking axial planes	Linear structures related to the D_1 thrusting of the TMB. Arcuate trends and local rotated thrusting most likely caused by emplacement of the tonalite within the Geassacopma Complex
BC	Penetrative SE-dipping foliation. Map-scale, ENE-plunging open folds	Arcuate gravity lineaments change orientation from N-S to NE-SW, related both to F_1 and F_2 folding, along with D_1 thrusting	Rotated structural grain from N-S in the north to NE-SW towards the south. Lineaments offset by NE-SW trending, penetrative faults. High density bodies occur as subcircular features.	Possibly F_2 and F_3 of D_1 thrusts and F_1 isoclinal folds, causing circular bodies of amphibolite. NE-SW trending faults have caused dextral, oblique movement, offsetting the entire sequence to the west.
GE	SE to NW-dipping foliation, folded by gentle to steep E to NE plunging folds	NW-SE pervasive structural grain in the north, swinging to NE-SW in the- south. Local arcuate E-W trends towards the central parts.	Discrete magnetic lineaments, dominated by N-S to NW-SE to structural grain. Rock packages defined by local thrusts. Lineaments indicate eastward plunging folds. Magnetic anomalies offset by NE-SW trending breaks	NW-SE trending D_1 structures folded by F_2 folds causing reorientation of the earlier structural grain. Area influenced by local thrusting and possibly transpression.
GW	SE-dipping foliation, with NW vergence, along with NE plunging fold axes	Chaotic patterns, with partly developed NE-SW and NW-SE oriented structural grain.	Arcuate discrete lineaments, with moderate to low intensities. Curved trends show E-W and N-S plunging fold axes. Prominent lineaments marked by NE-SW breaks	E-W trending F_2 and N-S trending F_3 folding of D_1 structures causing reorientation of the structural grain. NE-SW trending faults offsets D_1 ductile structures, with an apparent dextral movement.

Table 6.2: Overview of the observed structural trends observed from the geophysical data, along with a summary of the interpretation.

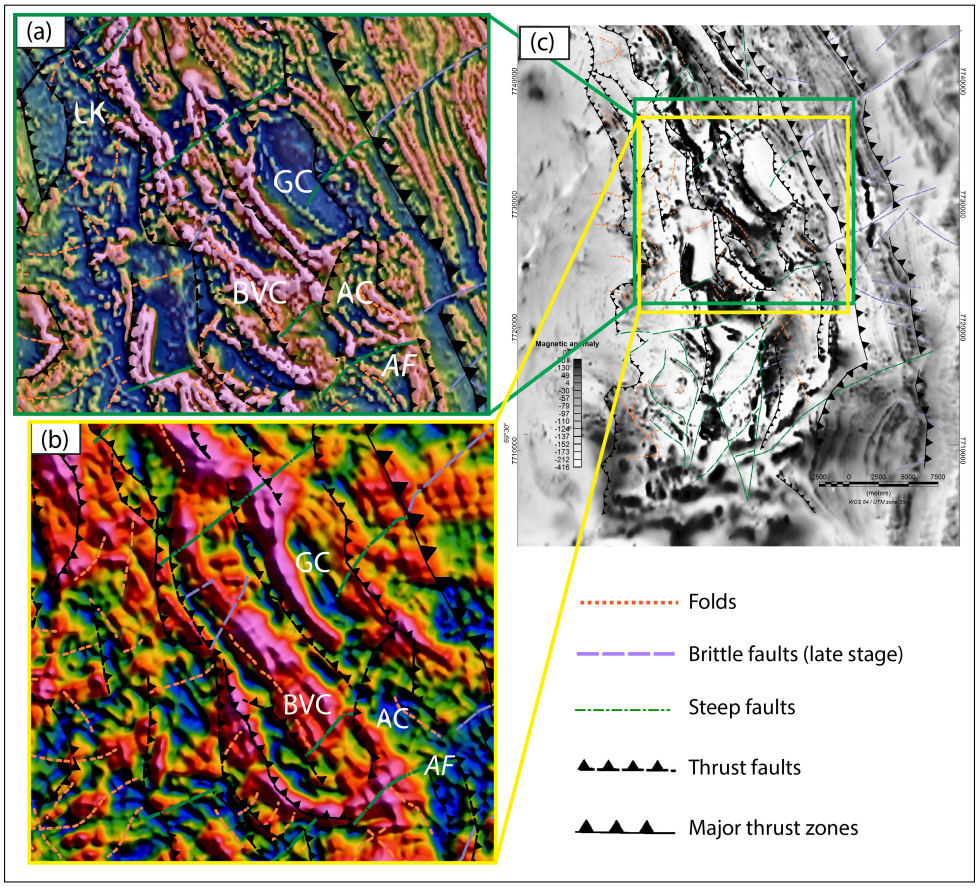

Figure 6.10: Geophysical signature of the tonalite units from the Bakkilvarri domain. (c) illustrates the regional outline. Note the influence of the NE-SW fault, termed the AF fault. (a) shows the magnetic response and (b) Horizontal directional tendency response from the NE part of the study area. The magnetic data show steeply dipping banded anomalies, indicative to supracrustal lithologies. Abbreviations: AC: Adjatskaidi Complex; BVC: Bakkilvarri Volcanic Complex; GC: Geassacopma Complex; LK: Lassevarri Komatiite

trend of the thrust contact (Figure 6.9). As similar structural trends are observed within both the JGC and KGB, it suggests that the basement was folded together with the supracrustal rocks during the same deformation phase. Furthermore, it is noteworthy to observe that F_2 folds are most evident within the Gållebaike domain, and do not appear to influence the NW-SE trending lineaments within the northeastern parts of the Bakkilvarri domain.

Several of the developed D_1 thrust zones appear to have been reactivated dur-

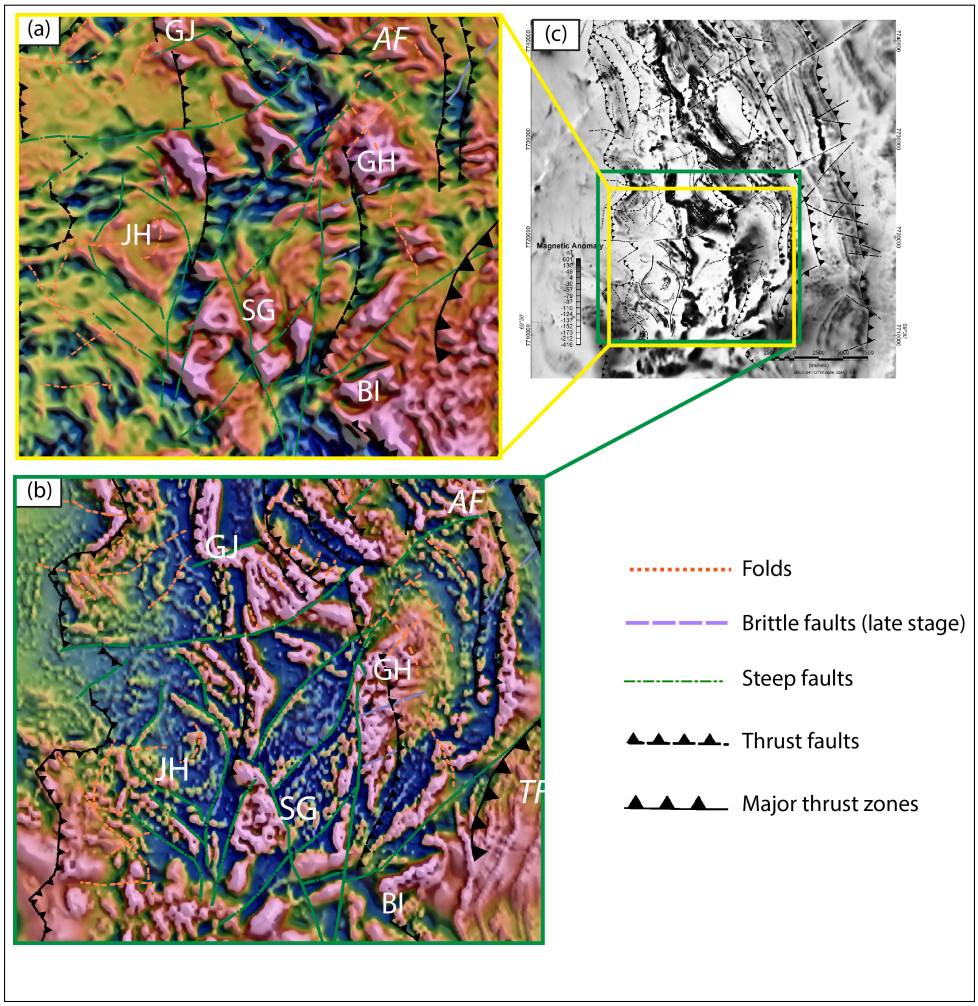

Figure 6.11: Structures observed within the central and southern part of the study area. (a) The third order invariant, with overlay of the structural interpretation. The invariant indicate that the SG intrusion is a complex body, consisting of several, isolated highs. Also note the GH, which stands out as an anomlous high within the BC. (b) Structural interpretation showed overlaid a composite image of the magnetic anomaly and first vertical anomaly. Abbreviations: AF: Adjatavzi Fault; BI: Bippovarri Intrusion; GH: Gimesvarri High; JH: Jalgesvadda Complex; GJ: Gallujavri Intrusion; SG: Stuorra Gourpmet Intrusion; TF: Tanaelv Fault.

ing the D_2 phase. The analysis of the magnetic data suggests that the structures have caused displacement along N-S striking shear zones, which seem to be reactivated D_1 thrust zones, forming E-W striking strike-slip faults (Figure 6.11). Field

observations of steeply dipping, NW-SE striking mylonitic foliation from the Ravdojavri area support these results, indicating a non-coaxial component, as well as west-vergent thrusting (Figure 4.7 (c)). The magnetic lineaments in the vicinity of the Jalgesvadda hill curve around the central gabbro, and may reflect a km-scale porphyroblast structures (Figure 6.9, 6.11). These observations indicate that the thrust fault just east of the Jalgesvadda hill, is related to an additional strike slip component. Breaks in several prominent anomalies along similar strike direction underline this interpretations, reflecting the regional scale of the structure (Figure 6.8 (b), (d)). Thus, the Jalgesvadda hill may represent a complex fault-fold related structure, inherent to complex reactivation during several deformation phases.

The potential field analysis has identified several NE-SW trending faults (Figure 6.9). The most significant NE-SW trending fault marks the transition between the northern and central zones within the Bakkilvarri domain, and is informally termed the Adjatavzi Fault (AF) (Figure 6.4, 6.9). From the AGG data, the Adjatavzi Fault appears to truncate the NW-SE trending BVC, and marks the termination of the main volcanic belt. This is related a an curvilinear, eastward rotating trend of the belt. This appears to be related to the reorientation of magnetic lineaments from NW-SE to N-S (Figure 6.11). The NE-SW trending structures are recognized from the marked signatures of the breaks in magnetic and gravity lineaments (Figure 6.8 (b) and (d)). From the magnetic data, the Adjatavzi Fault stands out as a complex structural feature, and appears to have offset several of the magnetic lineaments with at least 1 km (Figure 6.9, 6.11). From structural analysis, the fault appears to be related to a high strain zone, where first and second order features have caused magnetic complex structures (Figure 6.11). Magnetic lineaments appear to be rotated inwards to the main fault zone, indicating a dextral component. Towards the south, several 2nd order faults appear to link up with the main structures, creating a splay fault system. In terms of the magnetic signature, the southern splay of the Adjatavzi Fault stands out with a quite magnetic signature, compared to the adjacent structures.

Further south, a similar trending fault zone can be observed to offset the TMB and LGC several km towards the SW. The fault zone, informally named the Tanaelv Fault (TF) occurs with a similar structural trend as the Adjatavzi Fault (Figure 6.3, 6.9). The structures within the Bakkilvarri domain, just north of the Tanaelv Fault, appear to be influenced by NW plunging folds, possibly related to this structure. Furthermore, the Tanaelv Fault is related to a significant high amplitude gravity anomaly, together with strong, SW curving magnetic lineaments (Figure 6.3 (a), 6.11). The magnetic lineaments undergo a northwesterly rotation, and the thickness of the Bakkilvarri domain thins out. This is interpreted to a result of E-W trending fault movement along the Tanaelv Fault, causing the SW displacement of the TMB, and juxtaposition against the lower density parts of the KGB. The curved horizons mark the fault's offset, indicating dextral kinematics (Figure 6.11). The

long wavelength of the gravity anomaly indicates that the Tanaelv Fault is related to a significant displacement of crustal architecture. Within the LGB, the faults are mostly recognized from linear magnetic lows, indicating destruction of magnetite (Henkel, 1991; Grant, 1985a).

Where overprinting relationship can be observed, N-S trending axial traces seem to refold the E-W striking F_2 folds, indicating a D_3 deformation phase. The F_3 folds appear to refold F_2 folds around an N-S axial trace. These F_3 folds can in particularly be observed in the SW parts of the Gållebaike domain, and are well developed within the mica schists and amphibolites (Figure 6.9, Table 6.2). These observations correspond well to field observations, indicating a third fold phase. As expect for the F_3, it is difficult to assess the structures related to the D_3 phase. Additionaly, NE-SW trending shear zones that appeared to be active during the D_2 event, show indications of being reactivated during D_3, overprinting F_2 folds (Figure 6.11). However, it is challenging to evaluate the influence of the D_3 structures on the NE-SW trending faults. As the folds are mostly related to N-S trending axial traces, they broadly correspond to N-S shortening. However, from variations in observed kinematic indicators related to the N-S and NW-SE trending shear zones, it appears that they reactivated during the D_3 phase.

The most obvious and recent generation of structures are interpreted to be NE-SW and NW-SE trending faults and fractures that truncate several marker horizons (Figure 6.9). These breaks are particularly clear from the magnetic data and topographic depressions. Due to the brittle signature of these structures, they are interpreted to be related to a brittle D_4 phase. The D_4 phase is appears to be influenced by cross-cutting NE-SW and NW-SE trending, conjugate brittle faults (Figure 6.9). In the magnetic data, they stand out as linear trending magnetic lows, suggesting destruction of magnetite. The D_4 structures appear to be well developed within the LGC and TMB, throughout the region (Figure 6.9). It is however noteworthy that the conjugate sets are not developed within the KGB.

6.3 Summary and implications

The qualitative interpretation of the geophysical data sets have revealed a more complex lithological distribution. Based on the geophysical data, it is clear that the Bakkilvarri domain are a more complex structural domain than earlier interpreted.

In addition, it has been possible to delineate faults, shear zone and folds that have not been readily observed during field mapping. The new data sets have allowed to bride the gap between outcrop-scale structures and larger regional features. The potential field analysis has revealed several new NW-SE trending thrust faults, within both the Gållebaike and Bakkilvarri domain. The qualitative interpretation indicate the complex structural geometries caused by NE-SW and NW-SE trending ductile to semi-britte faults and fractures in the area. It is apparent that these

fault trends are responsible for the most prominent terminations and breaks in large scale structures. From the analysis of the magnetic data, these grids appear to have a vertical component, causing a oblique movement along the fault plane (Figure 6.11 (b))

In addition, it appear that the km-scale folds have influenced the belt, both during the primary deformation phase and in later stages. These findings are supported by outcrop scale observations made through out the belt. The most prominent structures are the changing style from the northern to the central parts of the belt, that are associated to a drastic change in the orientation of magnetic and gravimetric lineaments.

Chapter 7

3D Density Modelling

The integration of surface observation, petrophysical data and the new high resolution AGG data allows for the possibility to construct a new 3D density/structural model of the KGB, within the Iddjajav'ri area. A such quantiative approach makes it possible to test different concepts and ideas developed during the qualitative interpretation of the potential field data, in order to create an coherent crustal model of the KGB.

Several important questions regarding the tectonic and structural evolution of the KGB still persist. The development of a 3D crustal model provides more insight into the tectonic setting and structural architecture of the KGB. Furthermore, by creating a 3D model of the KGB increases the insight in how shallow structures link to deeper and more regional features.

The outline of the model was constrained by the AGG survey, and makes up a 20 x 30 km rectangular block, just north of Karasjok. (Figure 7.2 (b)).

7.1 Model constrains and input

The structural architecture of the KGB remains poorly constrained, and has not been investigated since the late 80's. The study area lacks depth information from deep drilling, audio-magnetotellurics (AMT) or reflection/refraction seismic. Furthermore, the overall exposure degree is lower than 5 % in the area, which makes surface mapping challenging.

The starting point of the 3D density model was therefore mainly based on the refined interpretation and geological concepts developed in the previous chapters (see Chapter 4 and 6), in addition to previous mapping efforts and collected surface data (Often, 1985; Henriksen, 1986, 1991). The current tectonostratigraphic interpretations from Often (1985) and Siedlecka et al. (1985) (Figure 3.3), were used to constrain the modelled lithologies and rock units. From the present geological map

Geological units	Lithologies	Modeled densities (kg/m^3)
Gållebaike	Metapelites	2750
	Metapsammites	2650-2700
	Volcanics	2940
Bakkilvarri	Volcanics	2950-2960
	Metaschists	2750
	Tonalite	2700-2770
Tanaelv Migmatite belt	Acidic and mafic gneisses	2800
Archean Basment	Jergul Gneiss Complex	2675
	Thrusted basement	2700
	Intermediate gneiss	2800
intrusions	Granite	2640
	Mafic/ultramafics	2980-3150

Table 7.1: Overview of the densities used in the 3D density modelling.

and field work, nearly ten main lithologies are recognized within the area. In order to create a 3D model that represents the large structures within the Iddjajav'ri area, several of the lithologies were simplified into single rock units (Table 7.1).

The petrophysical properties of the modelled bodies were constrained by measurements from the Iddjajavri area, as presented in Section 5.1.3. As the petrophysical properties from the area may be biased due to the lack of outcrops, petrophysical properties and studies from analoges further south in the CLGB were also used to constrain the modelling procedure (Figure 5.4; Elo et al. (1989); Glaznev et al. (1989); Airo (2005, 2007)).

Gravity data do not implicitly contain depth information. Therefore, the deeper architecture of the model was based and constrained by an integration and interpretation of:

- Previous geological work and models (Chapter 3)
- Recovered density model from VOXI inversion of the AGG data (See section 1.4)
- Updated and refined geological interpretations (Chapter 6)
- Petrophysical data (Section 5.1)

In particular, the recovered density model from the VOXI inversion by Ellis and Ebbing (2013) was helpful, in order to constrain some of the main density features within the area. In cases with well defined density contrasts and surface structures, the inverted model can be used in order to evaluate the possible structures.

Observations from structurally similar areas further south were also used to infer possible structural settings and concepts (Lehtonen et al., 1998; Luosto et al., 1989; Airo and Mertanen, 2008). The results from the POLAR and FIRE profiles were particularly investigated to infer the structural and compositional variations in the basement and deeper crust (See e.g.Moisio and Kaikkonen (2012), Janik et al. (2009) and Glaznev et al. (1989)).

7.2 Model set-up and approach

In order to develop the 3D density model, an integration of both GeoModeller and IGMAS+ was utilized. These softwares have different strengths and application. IGMAS+ has the disadvantage that it is quite cumbersome to create 3D models only based on field surface data, and no continuous horizons, e.g. as given by seismic profiles. On the other hand, GeoModeller has a significantly less interactive 3D forward modelling capacity of gravity gradients, and requires large amount of surface data in order to create a coherent 3D model. In addition, GeoModeller does not support interactive forward modelling of the gravity gradients and invariants. The fact that the 3D structures within the area are not well constrained makes the use of gravity gradients necessary in order to develop a coherent 3D model.

The initial 3D model of the KGB was built using the GeoModeller software package (Figure 7.1). In order to include the topography in the modelling, the DTM acquired during the AGG survey was used. This first model was constructed based on current surface information, i.e geological contacts and structural data, discussed in previous section. As the available surface information is limited, the first model was constructed as an initial low resolution geological model, resolving only the regional features in the area.

The initial model was based on a six layer model, with the JGC as the western boundary and the TMB as the eastern boundary, all dipping approximately 30-40°towards the east (Figure 7.1). The intrusions were introduced as isolated bodies, as suggested from the qualitative interpretation (Chapter 6). The deeper parts of the thrust contact to the JGC were assumed to follow the structural trend observed at the surface, and inferred from the geological concept proposed by Henriksen (1986) (Figure 3.4).

Following geological maps, the Gållebaike Fm. was modelled as two main layers. The metapelites within the Gållebaike were modelled to be an east-dipping feature extending below the metapsammites, as interpreted by both Henriksen (1991) and Often (1985). The mica schist unit was introduced as a homogeneous layer, where the average density of the mica schists were used as the main density (Table 7.1). This assumption was based on the observation that most amphibolites within the Gållebaike Fm. occur as less than 5 meters layers within the mica schists (Often, 1985; Henriksen, 1986). The Gållebaike metapsammites were first included as a

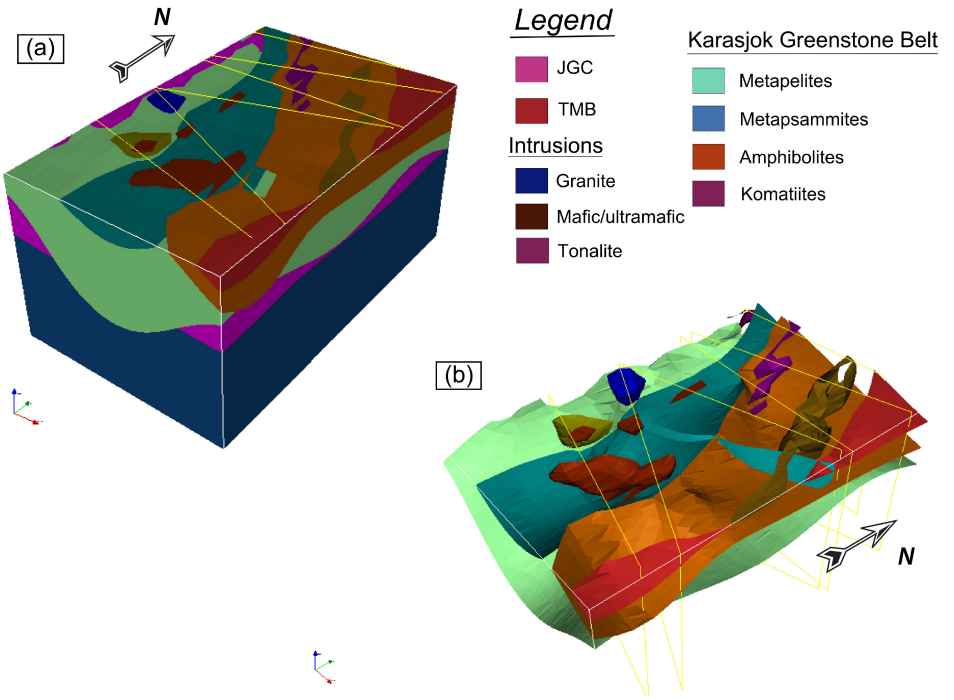

Figure 7.1: The geological start model built in GeoModeller, based on available surface and structural data. (a) shows the filled block model of the area, while (b) visualize the model only with the interfaces between different units.

low density layer, forming the contact to the Bakkilvarri units.

The Bakkilvarri domain was first model as a homogeneous unit of metavolcanics, following the observations and interpretations by Often (1985) and Henriksen (1986). The layer was assigned the high densities seen from the amphibolites in the petrophysical data (Section 5.1.3). The amphibolites and chlorite-actinolite rocks were not discriminated from each other in the density modelling, as the petrophysical data indicate nearly equal densities (Figure 5.6). The outcropping tonalites within the eastern part of the survey area were first introduced as a relative shallow intrusion, as inferred by Henriksen (1986) (Figure 3.4).

The initial density model was further refined using gravity forward modelling in GeoModeller. The modelling was a highly iterative process, where the new interpretation from the structural and potential field interpretation was added to further refine the 3D model. Throughout the modelling procedure, it was clear that a sufficient fit was not achieved using the GeoModeller approach. Consequently, the defined model was exported to IGMAS+, as IGMAS+ is better suited for interactive 3D forward modeling. The 3D model in IGMAS+ was constructed

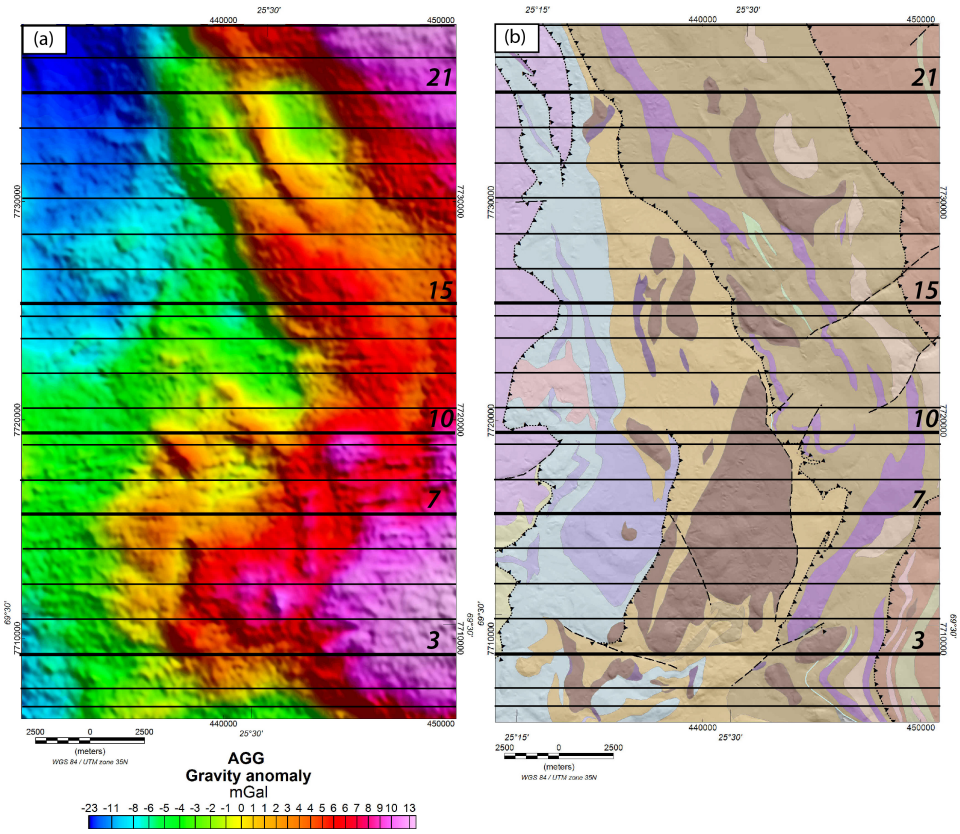

Figure 7.2: Overview of the modelled sections, shown by the solid black lines, over (a) the gravity anomaly and (b) the geological map after Henriksen (1986). See Figure 3.1 for legend. Thick black lines with numbers show locations of the profiles presented in the text.

by a using 24 vertical cross-sections, oriented almost perpendicular to the main orientations of the structures in the area (Figure 7.2). The distance between the cross-section varied between 1.5 km to 500 m, based on the complexity of the geological structures.

In order to use absolute densities in the model, a reference density was defined. In this case, a reference density of 2670 kg/m^3 was used. This was the value used for terrain correction of the AGG data (See section 5.2.1). The 3D model was extended with approximately 60 km in each direction in order to avoid edge effects.

The 3D model was further refined and developed by forward modelling of the gravity anomaly, gravity gradients, invariants and the horizontal directive tendency (HDT) (Section 2.1.2). An advantage of using the gradients and invariants during modelling, are their higher sensitivity to shallower structures and their 3D shapes

and orientations (Pedersen and Rasmussen, 1990; Murphy and Brewster, 2007). The main structures were modelled using the g_z and g_{zz}. After the main features were resolved, the gravity gradients and invariants were used to constrain and refine the shallow geological and structural features, as the different gradient components contain higher frequencies in the spectral density. As described in section 2.1.2, the invariants contain more information about the 3D structures of anomalies, than the different gradient components alone. Accordingly, the second and third order invariants were used to improve and constrain the 3D shape of the modelled bodies. The HDT was in particular useful to model the edges of bodies. In order to refine the density model, different structural concepts from the qualitative interpretation were tested. Early in the modelling procedure, it was clear that several new structures had to be introduced in order to fit the calculated data.

7.3 Modelling results

In general the modelled gravity anomalies fit with the observed field. The gravity anomaly misfit ranges between +8 to -6 mGal, and shows a standard deviation of 1.06 mGal (Figure 7.3). The modelled g_{zz} component has a standard deviation of 13.1 Eö. The survey errors were approximated to be 5 Eö for the transformed vertical gradient components, 0.1 mGal for the vertical gravity component (Section 5.2.1). The vertical gradient residual map shows that most of the mis-fits in the model are due to short wavelength features, occurring either on or between modelled sections. Most of the misfits seen from the g_{zz} component are attributed to the section spacing, as the complexity of 3D bodies is not resolved with the regional modelling set-up (Figure 7.2). However, most of the regional trends from the vertical gravity gradient have been matched (Figure 7.4). From correlation between the gravity components and observed lihtologies, it is clear that most of the high density bodies within the Gållebaike domain are related to mafic and ultramafic intrusions. As the average section spacing is approximately 1.5 km, several of these bodies have been modelled as single units in order to include them in the 3D model. The large misfits in the second and third order invariants are in most cases related to challenges to fully model complex 3D shaped bodies. Furthermore, the edges of the model are related to amplitude mis-fits, and are in most cases edge effects.

7.3.1 Regional field

It is important to evaluate and model the observed regional field, as it has large influence on the observed gravity anomaly. The modelling of the regional field shows that the eastward increasing gradient is generally caused by the emplacement of supracrustal rocks of the KGB, in addition to the TMB and LGB, creating a significant density contrast compared to the lower JGC.

The DNSC08 gravity field (Dransfield, 2010) indicates that long wavelength components of the gravity field show more complex lateral variations within the model area. The regional Bouguer anomaly (Figure 5.12 (a)) confirms these observations, and a prominent negative gravity anomaly dominates the field towards the northwestern corner of the study area. In addition, the south-central parts of the study area show a positive sub-circular long wavelength bulge in gravity field. The long wavelength components suggest a deeper source. These regional features are interpreted to be caused by a higher density intermediate gneiss, most likely located structurally lower than the JGC (Figure 7.11). The fluctuating regional field within the model area indicates that the basement reflects more complex compositional variations. The intermediate gneiss was modelled with an average density of 2800 kg/m^3, supporting earlier modelling results from the Finnmarkvidda area (Midtun, 1988; Olesen and Solli, 1985; Olesen and Sandstad, 1993). The bulging of the regional field is therefore attributed to local doming of the intermediate gneiss (Figure 7.11).

As observed from the northern and southwestern corners, the final model is not able to explain the marked low wavelength of the regional field. In order to fit the model, undulating topography had to be attributed to the intermediate gneiss (Figure 7.11). In particular, the southern parts of the model area are attributed to an up-doming of the intermediate basement, explaining the general upward shift of the regional field.

Based on the crustal investigations by Janik et al. (2009) and Moisio and Kaikkonen (2012), a higher density basement variant was modelled beneath the eastern parts of the belt, as their results indicate a 2700 kg/m^3 basement underlying the CLGB. The final modelled results indicate that this body do not influence the regional field in the area in any significant way.

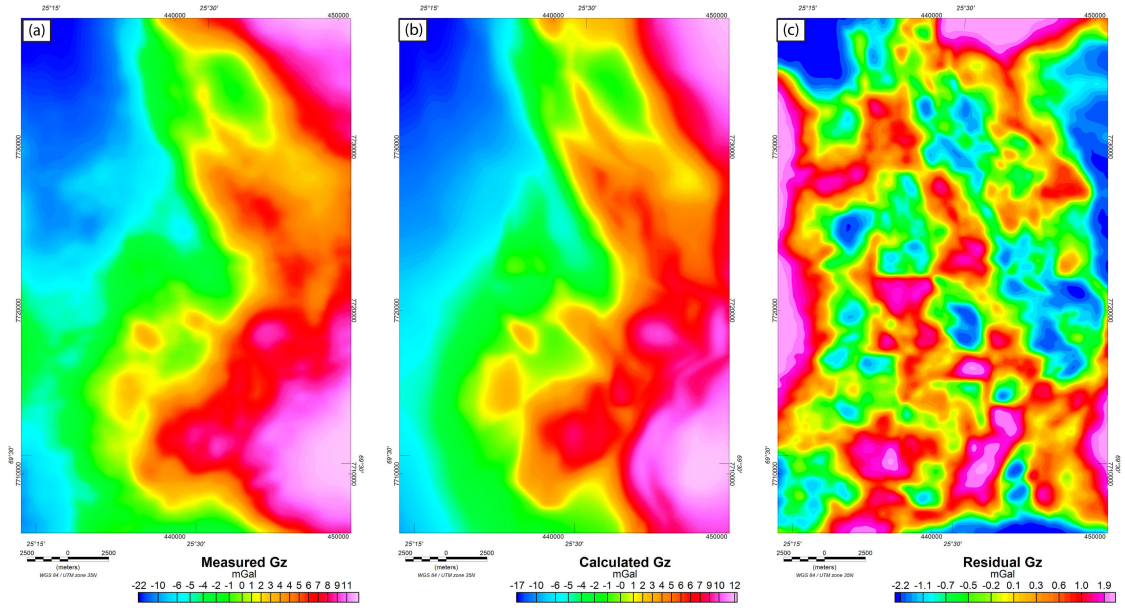

Figure 7.3: (a) Observed vertical gravity anomaly from the study area. (b) Calculated vertical gravity anomaly from the 3D model. (c) Residual gravity anomaly, representing the difference between observed and calculated gravity anomaly.

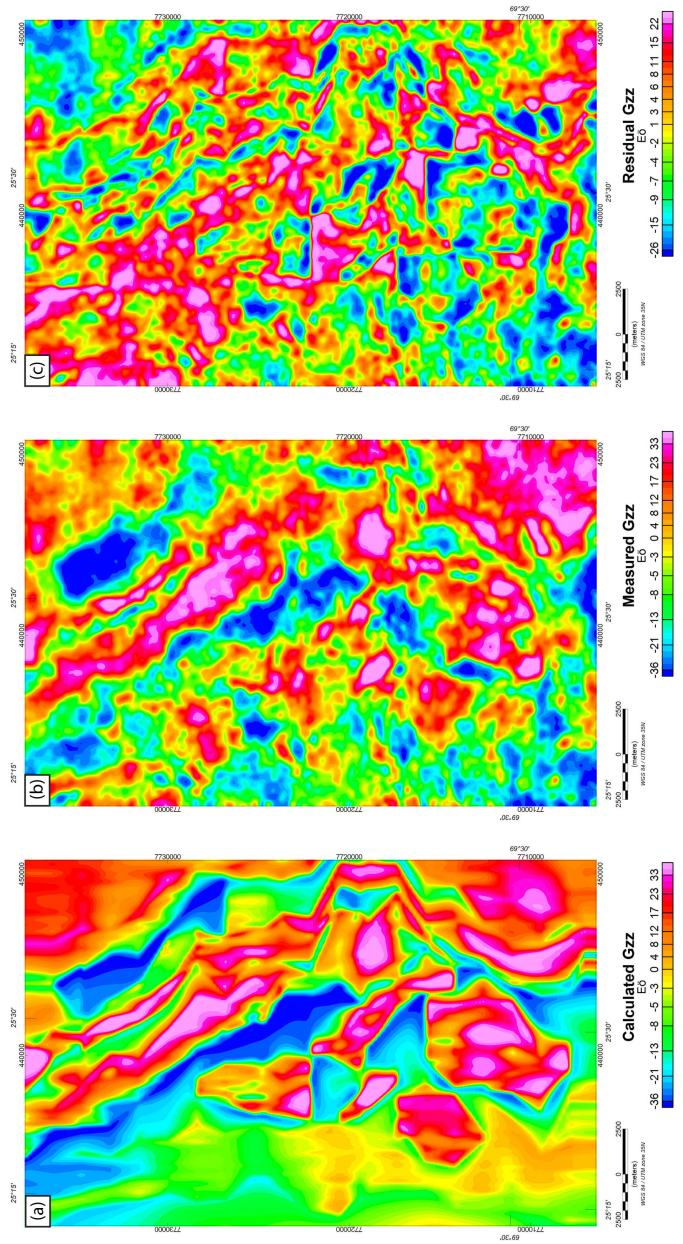

Figure 7.4: (a) Observed vertical gravity gradient from the study area. (b) Calculated vertical gravity gradient from the 3D model. (c) Residual gravity gradient, representing the difference between observed and calculated gravity gradient.

7.3.2 Main structures of the KGB

The final 3D density model explains the KGB as a shallow crustal feature, dipping towards the east sandwiched between the Archean JGC and high-grade metamorphic TMB. The model shows that the large variations of the gradients are mainly attributed to the complex distribution of metasedimentary, volcanic and intrusive units. In general, the results show that the supracrustal units make up an east-dipping structure supporting the east-dipping trends from surface mapping and regional interpretations (Henriksen, 1986; Often, 1985; Krill, 1985).

The base of the KGB is modelled as an eastward-dipping contact to the JGC, extending to a maximum depth of approximately 3 km (Figure 7.11). Towards the depths, the dip decreases and develops into a flat-lying structure (Figure 7.5, 7.6, 7.11). The western contact towards the TMB has been modelled to dip moderately towards the east throughout the entire belt, and supports earlier tectonic interpretations that the TMB has been thrusted on top of the KGB (Krill, 1985; Gaàl et al., 1989). In general, the TMB consists of a mixture of high-grade metamorphosed rocks, and shows large variations in density (Figure 5.4). As observed from outcrops in the Iddjajav'ri area, the felsic gneisses and migmatites appear to be intermingled with the more mafic gneisses. However, the TMB has been modelled to as single layer, and assigned an intermediate value of 2800 kg/m^3. The contact between the KGB and TMB is recognized by a slightly decrease in the observed gravity gradients. This appears to be caused by the higher densities observed from the upper parts of the Bakkilvarri domain. The Bakkilvarri doma has been modelled with a density of 2950 kg/m^3. The contact to the Levajok Granulite Belt is situated outside the model area, but is inferred to be an east-dipping feature, thrusted on top of the TMB (Midtun, 1988; Gaàl et al., 1989; Cagnard et al., 2011). This feature has not been included in the modelling, as the Levajok Granulite Belt reflects similar density distribution as the TMB (Elo et al., 1989).

A key part of the 3D modelling has been to determine the depth of the supracrustal units. However, the low density contrast between the metasediments and the JGC, in addition to the lack of other depth constrains, limits the accuracy of the depth estimations. The supracrustals have been modelled to a maximum depth of about 3 km, indicating shallow crustal feature. The horizontal thickness of the belt increases towards the south, but the modelled depths do not increase accordingly.

The Gållebaike domain is mainly dominated by low to intermediate density metapelites and metapsammites. The metapsammites make up a density contrast of approximately 80 kg/m^3 to the metapelites (Figure 5.4), which is sufficient to create a response in the modelled gravity gradients. The high amplitude features within the Gållebaike Fm. are mostly explained by to the lateral distribution of high density gabbros and ultramafic rocks (Figure 7.6, 7.7). Most of the short-wavelength, positive anomalies are related to discrete high density, amphibolite bodies. These appear to be mainly attributed to the western parts of the Gållbaike

domain.

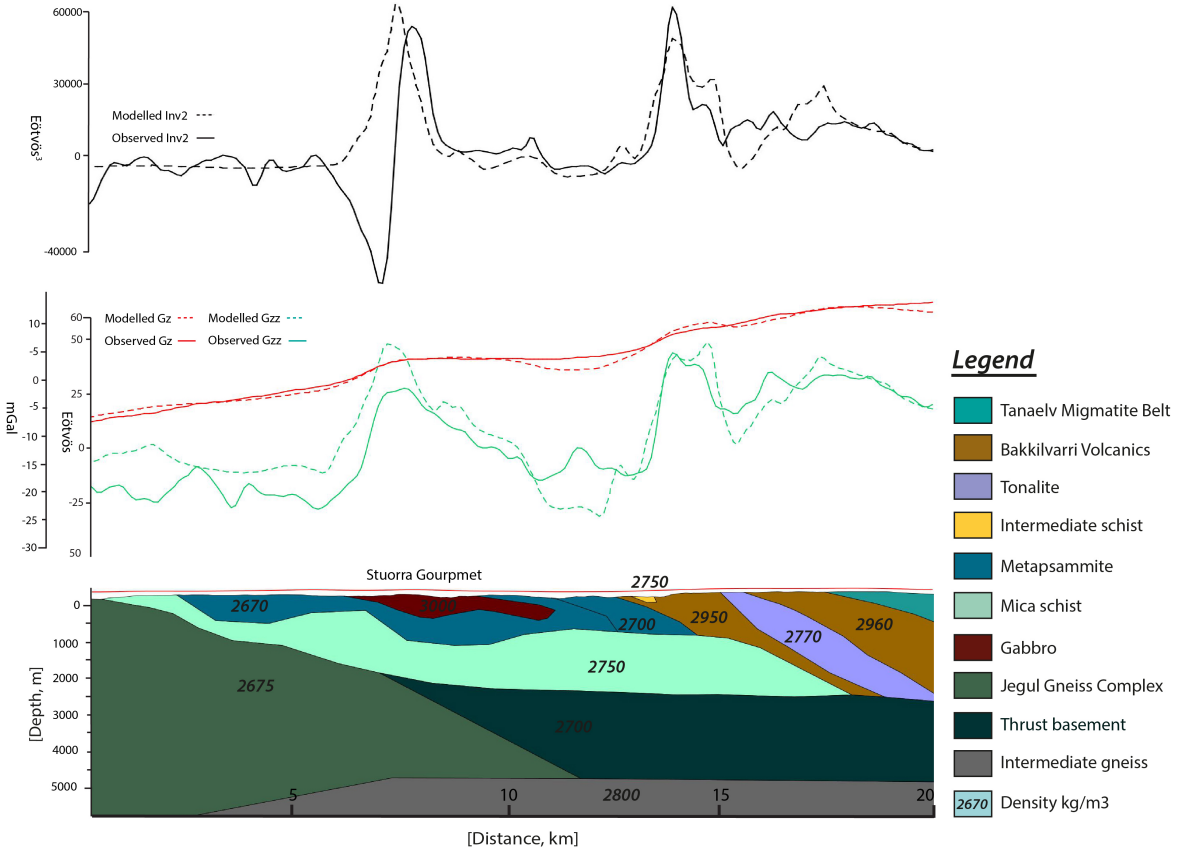

Figure 7.5: Profile 3 shows vertical cross section through the southern parts of the 3D model. The profile indicates the complex structures within KGB. The mafic intrusion stands out as the most prominent density feature within the Gållebaike domain, and is clearly limited in the west by low density metapsammites. The Bakkilvarri domain is interpreted to be divided in to by the tonalite body.

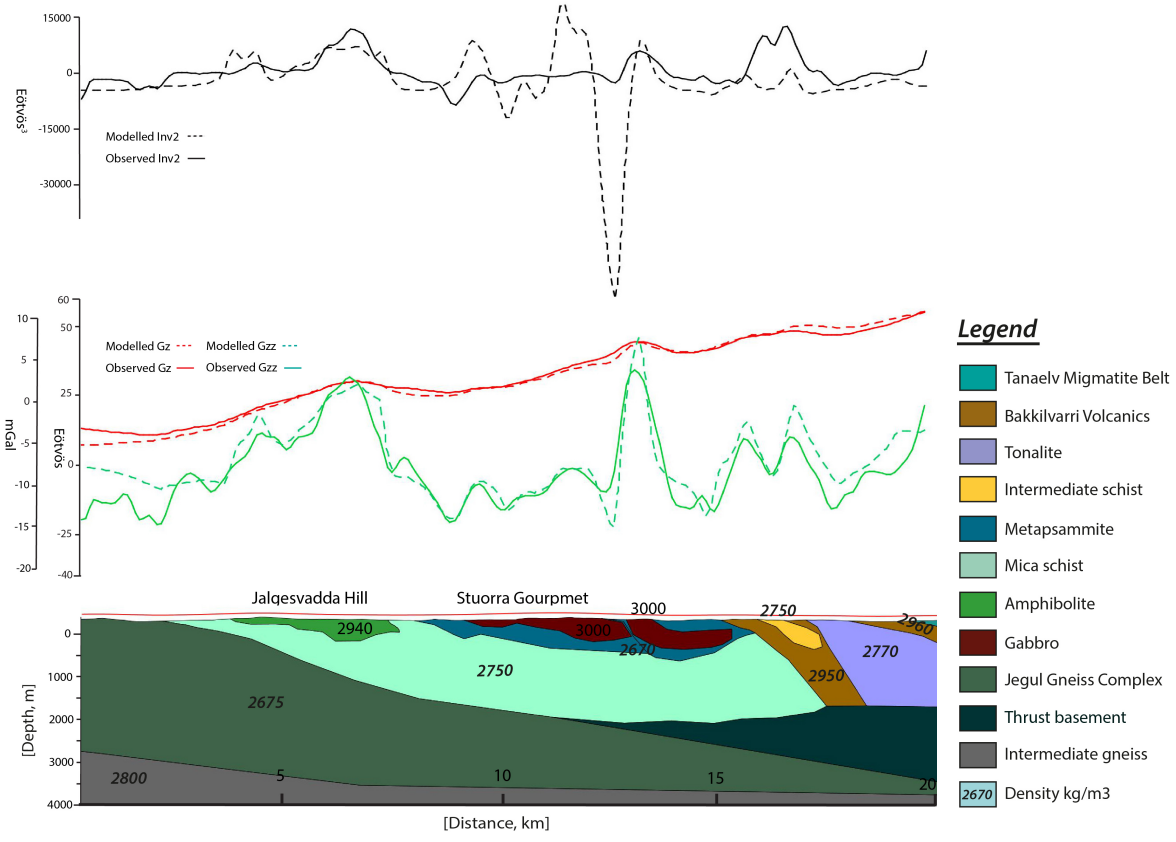

Figure 7.6: Profile 7. The profile crosscuts both the Jalgesvadda Hill and the Stuorra Gourpmet intrusion. The Stuorra Gourpmet gabbro stands out as a complex feature, interpreted to be caused by several smaller intrusions. The modelling indicates that the mafic and ultramafic intrusions follow the structural grain of the host rocks. The strong gradient related to the metagabbros suggests a significant density contrasts, and are explained by the juxtaposed low density Gållebaike metapsammites.

The final modelled thickness of the Gållebaike metasediments varies in both vertical and horizontal thickness along strike of the KGB. In the northern parts, the Gållebaike units are at their thinnest. Here, the lateral thickness is modelled to be 4 km, while the vertical thickness is approximately 1 km. Further south, the lateral thickness of the Gållebaike domain increases to over 13 km (Figure 7.5, 7.10). The final model also indicates that the depth to the Archean basement is shallower in the southern parts, compared to the northern prolongation (Figure 7.11). The thinnest part of the Gållebaike domain appears to be in close relation to the outcropping basement sliver in the Rivdnjesvada area (Figure 6.5, 7.10), where the metasedimentary units form a steeply dipping structure. However, the 3D modelling suggests that the supracrustal rocks become more shallow-dipping towards the southern prolongation of the belt (Figure 7.5, 7.6).

The modelling of the Rivdnjesvada structure shows that the low density feature related to the outcropping sliver of the JGC must be attributed to a significant deep seated source, in order to match the negative vertical gravity gradient anomaly (Figure 7.10). The modelling results suggest that the sliver is a part of the main Archean basement complex. From the geometry and size of the sliver, it reassembles a local thrust repetition within the belt. Consequently, the supracrustal wedge observed in the west appears to be an isolated feature, separated from the main part of the belt. The thrust sliver is modelled to be a local feature. There are no indications that the structure extends as a deeper towards the south.

In order to fit the model, the thickness of the metapsammites within the Gållebaike domain had to be increased from the starting model to match the observed gravity gradients. Compared to the interpretations by Henriksen (1986) (Figure 3.4), the modelled metapsammites reach depths of approximately 1-1.5 km, forming a complex NW-SE trending structure (Figure 7.4). Throughout the length of the belt, the metapsammites form the contact to the Bakkilvarri domain, explaining the prominent gravity gradient response (Figure 7.8, 7.10). The contact to the underlying mica schists appear to be gradual, due to their in-folded structures (Figure 7.5, 7.7).

The modelling indicates that most of the amphibolites are attributed to short wavelength anomalies within the Gållebaike domain. However, as pointed out from field mapping and earlier investigations, the Jalgesvadda hill reflects a high concentration of high density amphibolites (Henriksen, 1986). The modelling results show that the amphibolites and mafic intrusion appear as a demarcated, oblong structure, concentrated around the Jalgesvadda hill (Figure 7.6). In order to fit the model, the Jalgesvadda structures are restricted in its northern prolongation, compared to earlier interpretations (Figure 7.2 (b)). The model results indicate shallow depths, and the maximum thickness does not appear to exceed 500 m. Compared to the modelled structures within the Gållebaike domain, the Jalgesvadda amphibolites stand out as an anomalous feature in terms of lateral extension and depth.

The contact between the Bakkilvarri and Gållebaike domains is defined by a marked density contrast between the low density quartzite schists from the Gållebaike Fm., and the high density amphibolites within the Bakkilvarri domain (Figure 7.10). Due to the high density contrast between the lithologies, the contact between the domains has been modelled with relatively high confidence. However, due to the lack depth constrains, it is difficult to accurately determine the depth of the metapsammites beneath the volcanic bodies in the eastern parts of the model (Figure 7.8).

The volcanic units within the Bakkilvarri domain stand out as the most prominent high density unit within the study area, and are modelled with densities ranging between 2950-2960 kg/m^3. From the gravity gradient response, the main volcanic units appear to be homogeneous structures, with little internal variations in terms of density. The volcanic units account for the most prominent gradient anomaly in the northeastern parts of the study area (Figure 7.4). The final model shows that the volcanic units extend as a linear belt throughout the region, generally dipping towards the east (Figure 7.12). The base of the volcanics is poorly constrained, but in general, the volcanics are modelled to reach no deeper than 3 km (Figure 7.10).

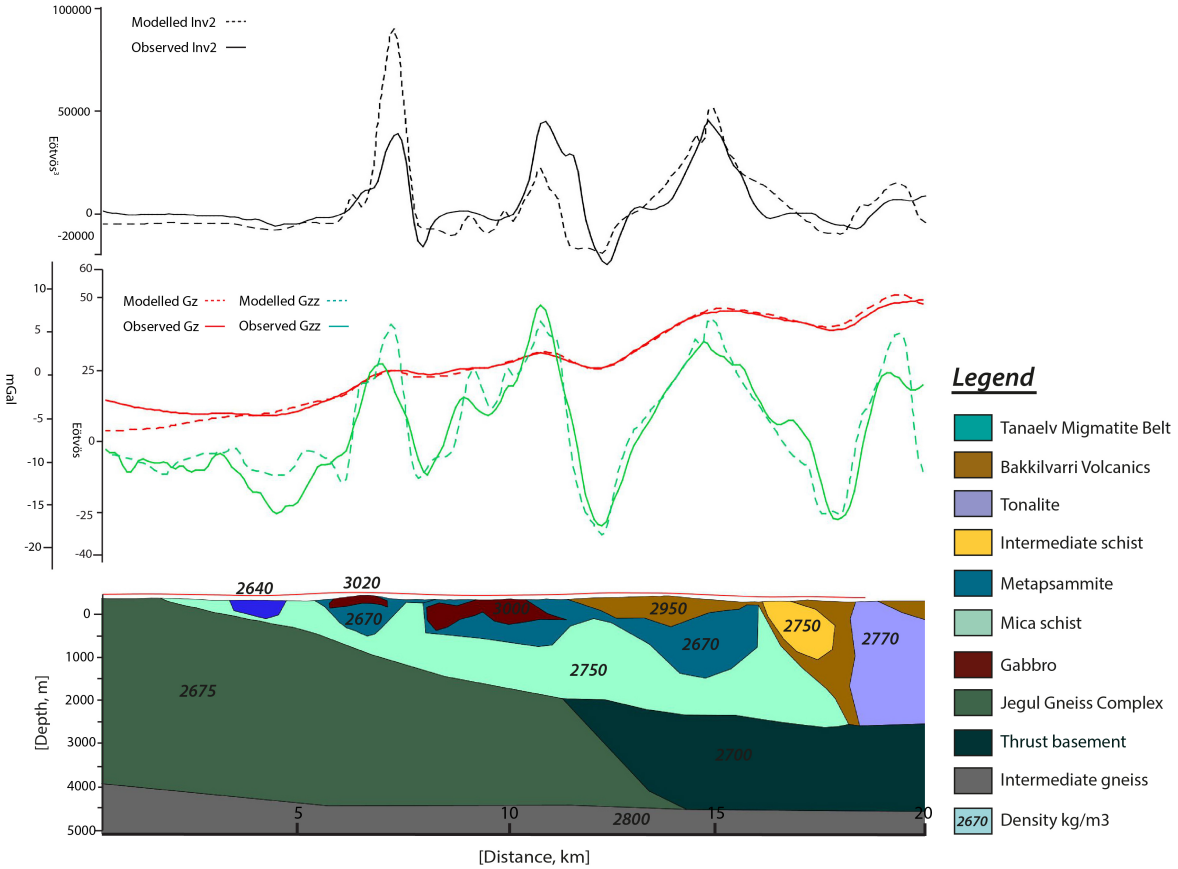

Figure 7.7: Profile 10 illustrates the structures from the central parts of the model. The profiles crosses the eastern prolongations of the structurally complex Stuorra Gourpmet gabbro. Note the strong third order invariant anomaly related to the easternmost intrusion. In the central parts, the Bakkilvarri Fm. are dipping gently towards the east.

The final 3D model proposes a significant change in the structural geometry within the northern parts of the Bakkilvarri domain. The modelling of the negative gravity anomaly at the Geassacopma complex (Figure 6.3) revealed that the outcropping tonalites correspond to larger and more complex structure than earlier inferred. The initial geometries, where the outcropping tonalites were modelled as smaller intrusions (See Figure 3.4), showed a significant mass excess. In order to the fit the observed negative gravity gradient anomaly, the outcropping tonalites within the Geassacopma complex had to be modelled as a regional dome shaped feature, where its maximum depth reached the base of the KGB (Figure 7.10). The modelled tonalite dips moderatly towards the WNW and ESE, and supports geological field observations. The modelled structure extends as far as the Karasjokka river, and forms a consistent feature throughout the length of the Iddjajav'ri area. In order to fit the model, the tonalite had to be attributed higher densities towards the southern prolongations, with modelled values of 2770 kg/m^3. The northern parts outcropping at the Geassacopma complex were modelled with 2700 kg/m^3.

Compared to the earlier geological mapping, it was clear that the initial model geometry (Figure 3.4, 6.6), where the Bakkilvarri volcanics made up a main part of the Bakkilvarri domain, contributed to a significant mass excess in NW zones of the Bakkilvarri domain (Figure 7.9; Section 6.1). The combined response from the invariants and magnetic field are suggestive to changes in bulk lithology (Figure 7.10). The vertical slices shown in Figure 7.9, indicates that the calculated gravity anomaly yields twice as the observed (1.5 mGal difference). In order to match the modelled and calculated response, it was necessary to introduce an intermediate lithology with a density of 2750 kg/m^3. The assigned density was mainly based on the measured petrophysical properties of metasediments within the Bakkilvarri Fm (Figure 5.4). The model results show that the intermediate body are related to complex structures, changing along strike of the belt. Towards the north, the body had to be modelled as a large scale feature (Figure 7.10) in order to fit the gravity gradients. Further south, towards the central zone of the Bakkilvarri domain, the modelled geometries are smaller and becomes more shallow (Figure 7.8, 7.10). This indicates a complex relationship with the volcanic units.

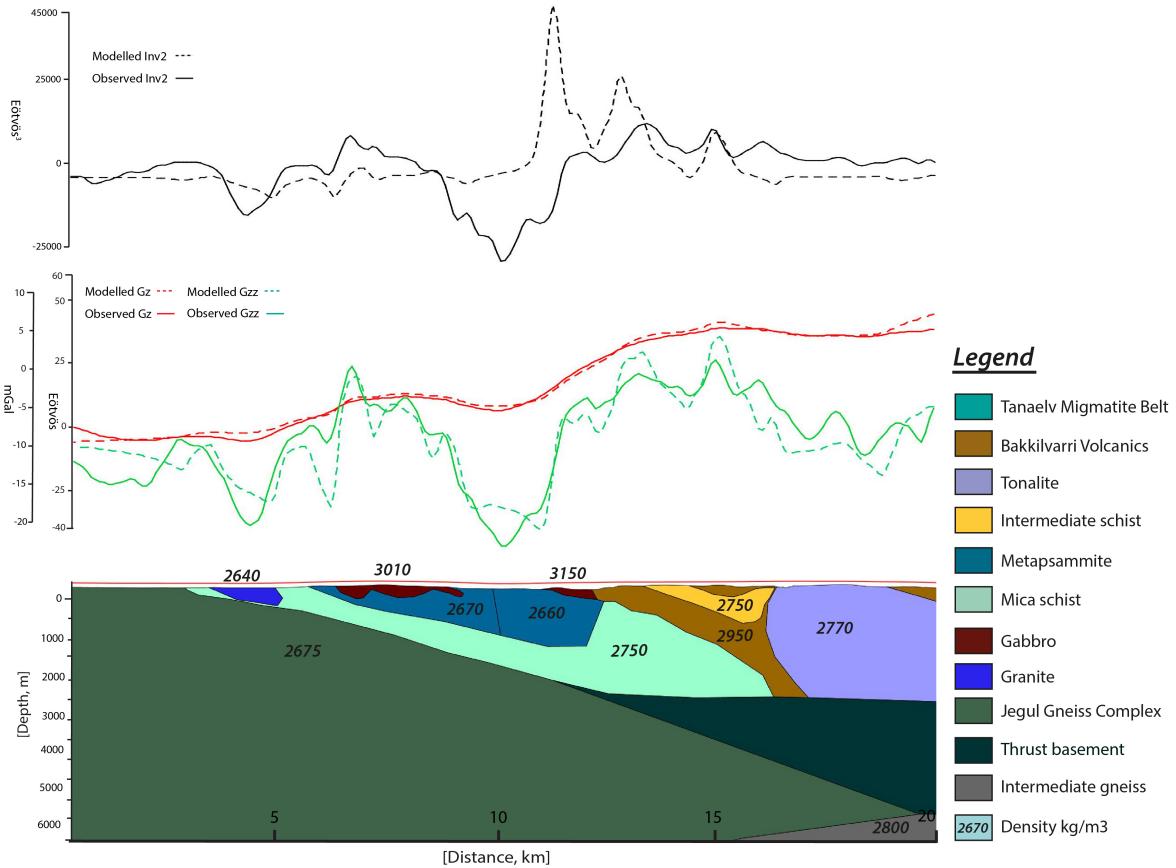

Figure 7.8: Profile 15. The profile show the structures located in the north central parts of the model. The eastern gabbro are related to the Gallujav'ri intrusion. Note the complex structures related to the intermediate schist body.

The introduction of the new structural features within the Bakkilvarri show that the volcanic units within the northern parts of the Bakkilvarri domain, are concentrated in a NW-SE trending wedge shaped structure. The final modelled structure was modelled with a considerable reduced thickness compared to the starting model (Figure 7.1, 7.10). The final model suggests that the thickest parts of the Bakkilvarri volcanics are located to the southern parts of the NW zone, explaining the marked third order invariant signal in this area (Figure 6.3 (b)). This main belt can be traced further north, following NW striking trend (Figure 7.12, 6.4). Further north, the volcanic belt becomes a thinner structure, juxtaposed in the east by the intermediate density body.

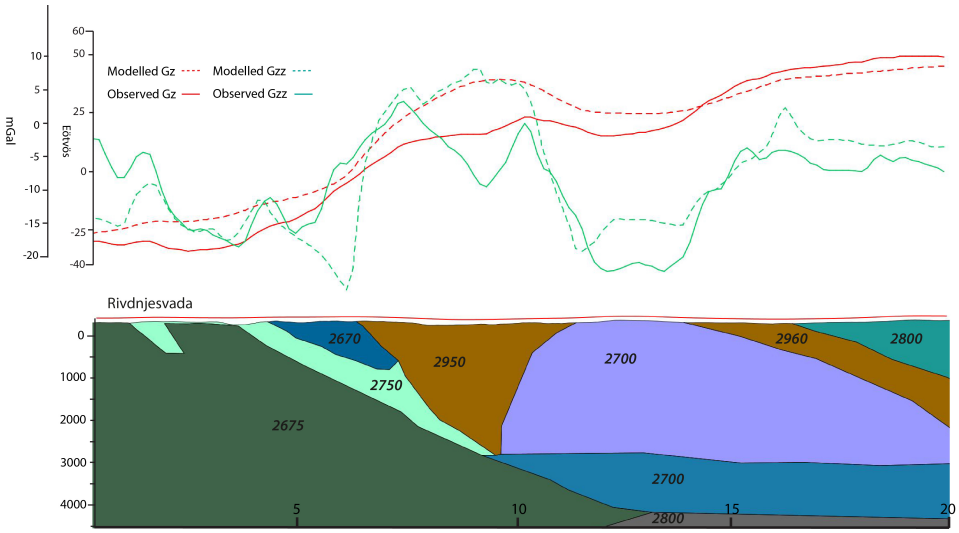

Figure 7.9: Profile 21 of the 3D model, before the intermediate body was included. Note the large misfit between the observed and calculated anomaly in the Bakkilvarri domain. See Figure 7.10 for legend.

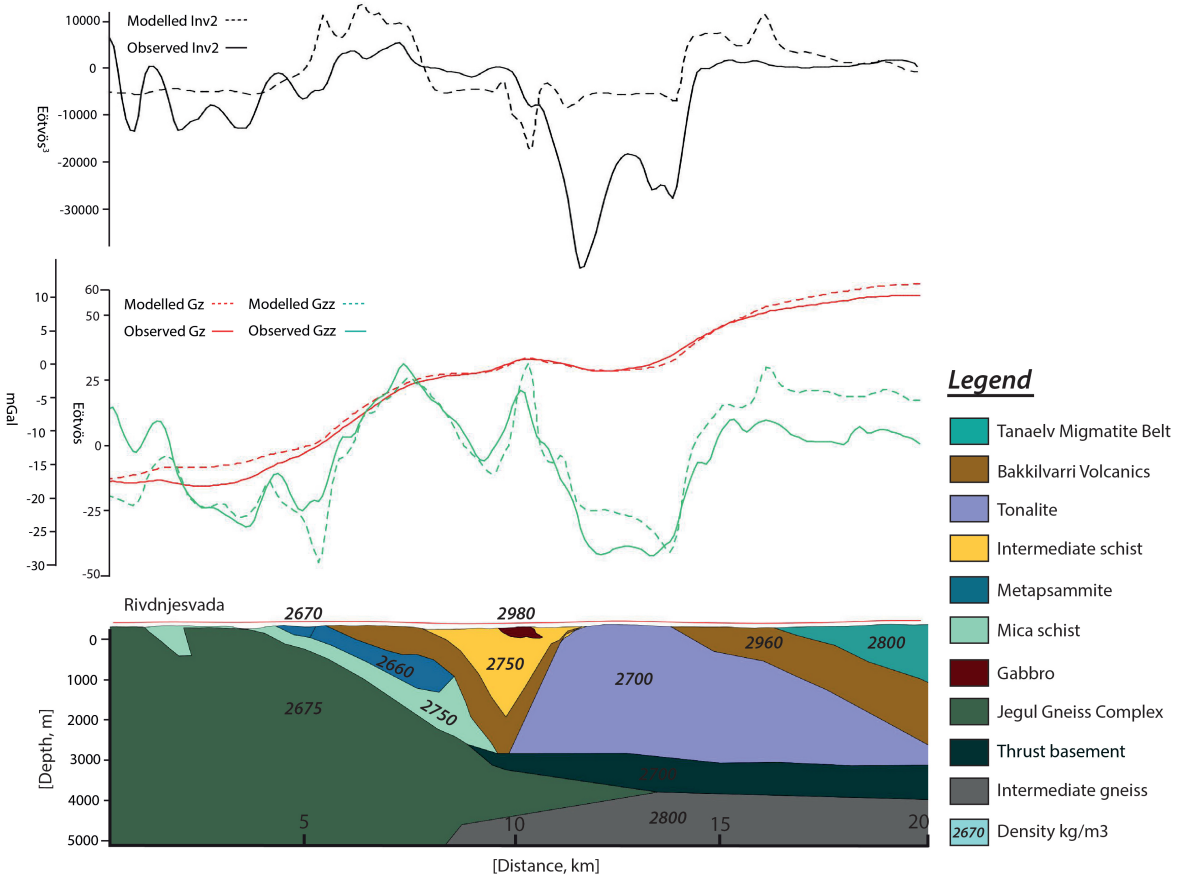

Figure 7.10: Profile 21 shows a running through the northern part of the 3D model. The profile shows the proposed geometry of the JGC basement sliver in the Rievdnjesvarri area, in the western part of the profile.

The transition from the northern to central zones of the Bakkilvarri domain is marked by changes in modelled structural trends. In order to fit the model, the volcanics in the western parts of the central zone within the Bakkilvarri domain were modelled as more flat-lying and gently dipping structures, compared to the structures observed within the northeastern parts (Figure 7.7). In this part of the model, the amphibolites are overlying the Gållebaike units, making up a flat-based, approximately 300 m deep structure. The circular gravity anomaly related to the Gimesvarri High is modelled as a circular body of high density metavolcanics, reaching depths of approximately 3 km (Figure 7.12). The modelling indicates that the amphibolites within the northern parts of the central zones make up an antiform structure. The Gimesvarri High stands out as an enigmatic structure within the central parts of the Bakkilvarri domain.

Further south, the volcanic structures make a change in geometry, and the modelling results indicate that the volcanics extend further south as east-dipping structure, juxtaposed to the outcropping tonalites (Figure 7.5, 7.6). As a consequence, the final 3D model indicates that the supracrustal package becomes more flat-lying towards the central parts, where the volcanic units reach its thinnest part.

7.3.3 Intrusions

The potential field analysis reveals that the lower parts of the KGB are intruded by several intrusions, ranging from felsic to ultramafic composition. In the Gållebaike Fm., the first order gravity gradient anomalies are caused by several high density mafic to ultramafic bodies (figure 7.4). As seen from the qualitative interpretation (see Figure 6.3 (b)), the mafic to ultramafic bodies stand out as highly 3D features, with complex internal structures. In many cases, intrusions terminate or occur as less then 1 km in the strike direction. Consequently, it has been necessary to simplify some of these complex structures, in order to build the 3D model. However, the resulting 3D model clearly outlines the main trends and geometries related to these bodies.

The petrophysical properties of the mafic and ultramafic bodies are relatively well constrained from surface measurements (Figure 5.7 (a)). Consequently, the structures have been modelled using density values measured from each intrusion, constraining the petrophysical properties of the structures. Where such measurements were not available, an average density was selected (Table 7.1).

The Stourro Gourpmet intrusion is modelled as the largest intrusion in the Gållebaike domain. The body is responsible for a significant anomaly, observed both from the gravity anomaly and the gravity gradient (Figure 7.3, 7.5). The intrusion appears to reach its maximum depth at approximately 700 m in the southern prolongation. The largest structures of the intrusion appear to be located in its southern prolongations. In order to fit the model, the intrusion was divided into two main structures. The eastern part of the intrusion can be traced as NW

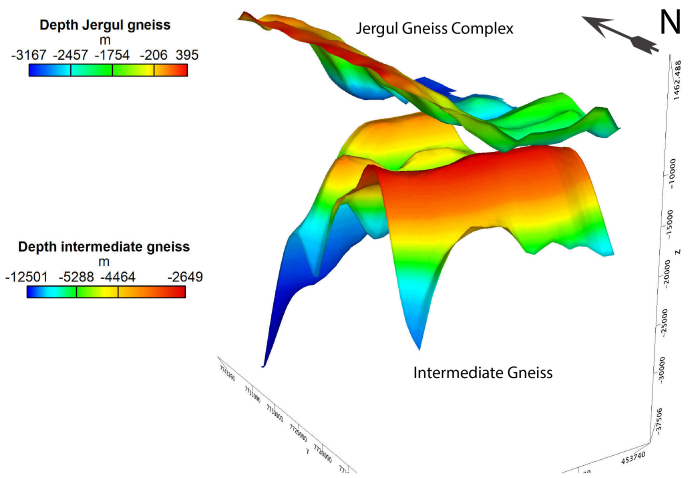

Figure 7.11: 3D perspective view of the modelled topography of the intermediate gneiss and the JGC. Vertical scale exaggerated three times

trending body, towards the southern end of the Gallujav'ri intrusion. From the modelling results, the two modelled bodies are not connected at deeper crustal levels (Figure 7.6). The central part of the intrusion is mainly located around the Gallovaras hill.

The Gallujavvri intrusion has been modelled with a relative high density of 3010 kg/m^3, reflecting the average measured density of both the mafic and ultramafic parts of the intrusion. From the modelling, most of the outcropping metagabbros are connected to a large deep seated source, but its surface geometry is variable from north to south (Figure 7.8). The depth of the body is only moderate, and reaches approximately 1 km in its southern parts. The northern parts of the intrusion differ in both geometry and thickness. The structure becomes a more shallow feature, with an apparent total thickness of approximately 300 m. Furthermore, the intrusion appears to be separated into two N-S elongated structures, separating the ultramafic from the mafic parts (Nilsson and Often, 2005). The ultramafic parts stand out as a deeper, bowl shaped structure, while the metagabbro appears to have a more flat lying keel (Figure 7.8). It has been challenging to accurately

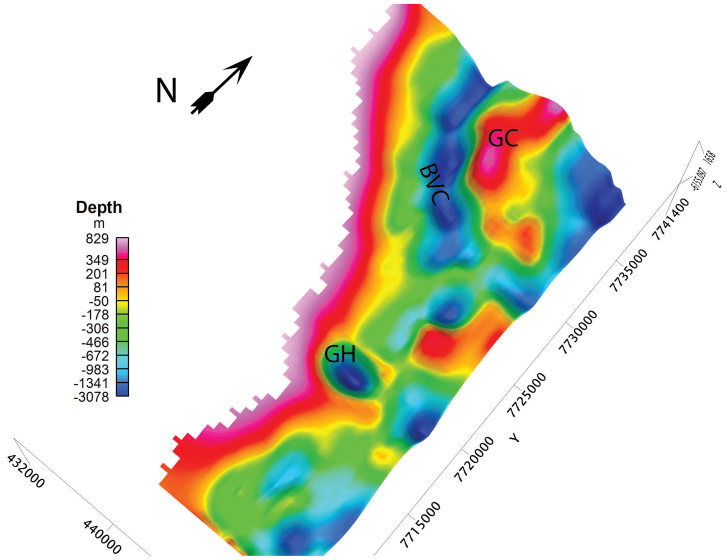

Figure 7.12: Modelled topography of the Bakkilvarri volcanics. Abbreviations: BVC: Bakkilvarri Volcanic Complex; GH: Gimesvarri High; Geassacopma Complex. The abbreviations are the same used in Chapter 6.

determine the depths and geometric shapes of the mafic intrusions. From their gradients, they appear mainly as east and west dipping structures. The final 3D model clearly indicates that the mafic and ultramafic intrusions follow the general structural grain of the hosting metasedimentary rocks.

Due to the high densities of the Bakkilvarri volcanic units, mafic and ultramafic intrusions make a less pronounced gravity anomalies within the Bakkilvarri domain. The most prominent anomaly appears to be related to the NW-striking gabbro, juxtaposed to the Geassacopma Complex (Figure 7.10). In order to fit the model, the gabbro had to assigned a density of 2980 kg/m^3. The modelling results of the third order invariant suggest that the 12 km, linear gabbro is hosted in the intermediate schist unit.

The granite located towards the thrust zone against the JGC (Figure 7.2 (b)), correlates to an array of N-S neagtive vertical gravity gradient anomalies. In order to explain the 2-3 km wavelength anomaly, the granite body was assigned a density of 2640 kg/m^3, and modelled as a N-S structural feature, following contact to

the JGC (Figure 7.8). In order to fit the model, the granite was modelled as significantly larger body than inferred from the starting model. The final modelled granite body extends to the base of the KGB, indicating that the structure is possibly rooted in the basement complex.

Chapter 8

Discussion

By integration of structural observations, petrophysical data and high resolution potential field data, this study has developed a new 3D model of the northern part of the KGB. This has allowed to gain better insight in the structural setting of the KGB within the northern part of the KGB. The large amount of data available for this study have helped to overcome the lack of outcrops and seismic profiles in the Iddjajav'ri. The integrated interpretation of AGG and aeromagnetic data has also allowed to refine the structural interpretation in the area. The combined interpretation of both the new 3D model and structural analysis allows to link shallow to the more deep seated structures within the KGB.

The details regarding the structural evolution of the KGB supracrustals remain somewhat unclear. The results from the qualitative interpretations and 3D modelling allow for a more detailed interpretation of the tectonic evolution of the supracrustal rocks within the Iddjajav'ri area.

8.1 3D interpretation of the Karasjok Greenstone Belt

The results from 3D modelling and structural interpretations place the KGB as an east-dipping, sequence of supracrustal rocks, sandwiched between the JGC and TMB. The final 3D crustal model indicates that the KGB makes up a 10-20 km wide belt, where the supracrustal rocks do not reach any deeper than 3 km. Field investigations, the qualitative interpretations and the 3D model suggest that the contact to the adjacent JGC and TMB are tectonic throughout the study area (Figure 4.9 (a),(b), 6.9). Based on the geophysical interpretations and 3D density modelling, the TMB and KGB are interpreted as two different structural units, both geophysically and structurally. The two structures are separated by a regional NW-SE trending thrust zone. Due to the marked aeromagnetic signature related to the

thrust zones, it is interpreted to be regional scale, deep seated feature (Figure 6.9). This interpretation is also supported by the observed steep gradient in metamorphic temperatures and the change in mineral assemblage, observed across this thrust zone (Krill, 1985; Cagnard et al., 2011). Based on the structures the base and top of the KGB, this study prefers an interpretation that the KGB was emplaced on top of the JGC during the main colliasional phase of the Lapland-Kola orogeny, defining the D_1 deformation phase (Figure 8.2 (a)), supporting earlier regional investigations (Krill, 1985; Cagnard et al., 2011).

The modelling results indicate that the underlying basement complex is not made up by a homogeneous unit. The main component of the regional field is interpreted to be caused by lateral undulation of a high density intermediate gneiss complex, underlying the Archean JGC (Figure 7.11). The lateral bulges of the regional field within the study area can therefore be explained by a local up-doming of the intermediate gneiss. The presence of an layered basement complex was also proposed by Olesen and Solli (1985) and Midtun (1988), in order to explain the regional field in the Finnmarksvidda area.

The pronounced negative gradient of the regional field in the NW part of the study area cannot be explained by a heterogeneous crust, as modelled here. The wavelengths of this trend shows larger bandwidth than what can be observed from the south central parts of regional field. Olesen et al. (1990) showed that the southern parts of the Finnmarksvidda area were related to a significant long wavelength negative anomaly, caused by an increase of the Moho depth. These results appear to correlate with the findings in this study, and are therefore interpreted to be caused by the same source as interpreted by Olesen et al. (1990).

The development of the new 3D model of the KGB allows for a refined interpretation of the internal structures within the KGB. The identification of several internal NNW-SSE thrust faults (Figure 6.9), in addition to an apparent structural control on the stratigraphic distribution, suggests that structures internally within the KGB originate from the main D_1 thrusting (Figure 8.1). The contact between the Bakkilvarri and Gållebaike domain is interpreted reflect a such D_1 thrust zone (Figure 6.9). This interpretation is supported by kinematic indicators at the base of the Bakkilvarri domain, showing west-vergent thrusting (Figure 4.11 (c)). The interpretation of the 3D model suggests that the thrust zone is rooted at lower crustal levels. However, due to the lack of depth constrains, it is difficult to determine if units from the Gållebaike Fm. are located within the Bakkilvarri domain at a lower crustal level. This interpretation is clearly in contrast to structural observations further south in the KGB, where the entire stratigraphic sequence has been interpreted to sit in a km-scale, isoclinal fold (Braathen and Davidsen, 2000; Often, 1985) (See their Figure 13).

The 3D modelling indicates a significant variation in horizontal thickness between the northern and southern parts of the Gållebaike domain (See Figure 7.5

compared to 7.10). It is noteworthy to observe that the thinnest parts of the Gållebaike supracrustals are related to thrusted sliver of the JGC, in the Rivdnjesvada area (Figure 7.10, 6.9). Based on these findings, it is apparent that the thickening of the Gållebaike domain appears to be structurally controlled throughout the study area. A possible interpretation of the thickness variations, may be that the southern parts of the belt are more influenced by internal thrusting and folding, thicknening the metasedimentary sequence (Figure 8.1). This explanation is favored by the fact that the outcropping mica schists are not observed in the eastern part of the belt, hence excluding large scale stratigraphic repetition within the Gållebaike domain. As the Bakkilvarri domain do not reflect the similar thickening, it further supports the idea that the Bakkilvarri domain was thrusted on top of the Gållebaike domain (Figure 8.1). Consequently, imbricate stacking and folding appear as a more viable interpretation, than km-scale basement folding as proposed by (Midtun, 1988).

The potential field analysis and 3D modelling suggest that the Bakkilvarri domain makes up a complex feature, both in terms of structural setting and lithologies. The interpretation of the qualitative analysis and the modelling results imply that: (a) the Bakkilvarri domain cannot be explained as a monotonous volcanic sequence as earlier suggested (Often, 1985; Henriksen, 1991), and (b), that the outcropping tonalites in the Geassacopma complex are a significantly larger crustal structure than inferred from the surface data.

The strong negative gravity anomalies from the NW-parts Bakkilvarri domain (Figure 6.3) are interpreted as east-dipping package of graphite bearing, quartz-mica schists, juxtaposed in the west by the Bakkilvarri Volcanic Complex (BVC) (Figure 7.10). The Bakkilvarri volcanics are generally related to thoeliitic composition, and are measured with density values clustered around 3000 kg/m^3 (Figure 5.6). Similar results have been proposed for other amphibolite units within the CLGB (Elo et al., 1989; Airo, 2007). Therefore, it is unlikely that thoelitiic lithologies within the BVC are attributed to such low density values. As this area is one of the least exposed parts in the Iddjajav'ri area, it cannot be ruled out that intermediate density body represents other lithologies, as e.g. intermediate volcanics or felsic intrusions. Such lithologies have not been observed within the northern parts of the KGB, and are therefore less likely to be present (Nilsen, 1986; Davidsen, 1994). Consequently, these findings clearly suggest that the stratigraphy of the Bakkilvarri Fm. must be attributed to larger lithological variations, than defined by Often (1985).

The interpretation of the 3D model proposes that the outcropping tonalites within the Bakkilvarri domain, make up a larger complex that can be traced along strike of the KGB. The tonalite complex shows large variations in size and structural trends, from north to south. In the northern part, it makes up significant crustal features, indicated by the modelled depth of at least 3 km (Figure 7.10).

Here, the tonalite complex dominates the Bakkilvarri domain, and allow for a reinterpretation of the crustal setting of the KGB. However, as the structural trends and the modelled, density changes towards the southern parts of the belt (Figure 7.6, 7.10), it is possible that there are variations in composition and structural history.

Midtun (1988) interpreted the negative gravity anomaly related to tonalites at the Geassacopma complex as a crustal scale antiform, folding the entire stratigraphical sequence (showed in his Profile E). However, the interpretations from this study suggest that the main early ductile structures within the Iddjajav'ri area, are dominated by NNW-SSE striking thrusts, rather than thick-skinned folding, as interpreted by Midtun (1988) (Figure 8.1). For the existence of a steeply reclined, isoclinal basement fold within the NW part of the Bakkilvarri domain, it should be possible to delineate either geophysical or surface observations of the lower stratigraphies. As neither of this can be observed within the area, the outcropping tonalite appears rather to represent an intrusive unit, or an thrust emplaced part of the basement. Field observaions show that the tonalite is foliated (Figure 4.11 (d)). Hence, if the tonalite represents an intermediate intrusion, it appears that it was emplaced before the main deformation event. If the tonalite represents a basement complex, the structural observations and 3D modelling suggests that the complex represents a thrusted basement sliver, rather than the core of a thick-skinned antiform. It is not unlikely that a part of the underlying basement was detached during the main compressional phase, as this is a common feature in collisional orogenies. Age datings by Marker et al. (2000), showed ages of 1974 $\pm$ 8 Ma for a meta-granodioritic body, south of Karasjok. Even though this age is not acquired from the Iddjajav'ri area, it indicates that younger, granodioritic intrusions exist within the KGB, and opens the possibility for an interpretation that the modelled tonalites within the study area represents intrusions from the Lapland-Kola orogen. However, the lack of any radiometric datings of the tonalites within the Iddjajv'ri makes it difficult to conclude if the tonalite complex represents a part of an Archean basement feature, or Paleoproterozoic intrusion. Field observations in the lower stratigraphical units of the CLGB, i.e. the Savukoski and Sondakylä Groups, have shown that these units were structurally emplaced on top of the Archean basement complex, forming a thrust duplex systems, during the collisional phase of the Svecofennian Orogeny (Väisänen, 2002; Ward et al., 1989). Evins and Laajoki (2002) interpreted these lower groups as a fold and thrust belt-system, structurally emplaced during the overthrusting of the Tanaelv Migmatite Belt and Lapland Granulite Belt (See their Figure 15). These thrust structures fit the structures that are observed within the Iddjajav'ri area. However, investigations from the KtGB have shown that several dome shaped, negative gravity anomalies correlate to tonalites and granodiorites (Olesen and Solli, 1985; Olesen and Sandstad, 1993). These are clearly of magnetic origin, and have been dated to

post-date the greenstones (B. Bingen, pers.comm. May, 2014).

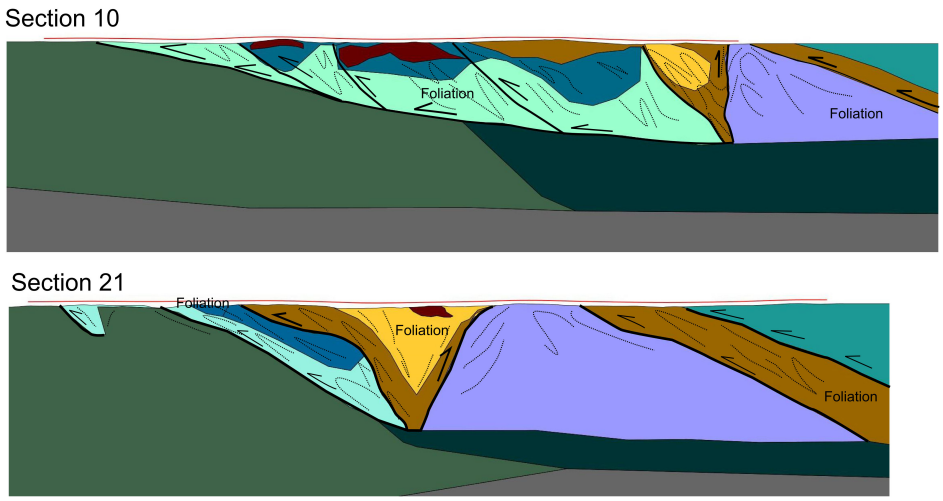

Figure 8.1: Geological interpretation of two of the modelled profiles. The profiles illustrate the NNW-SSE trending thrusting interpreted as imbricate stacked features. This stacking is interpreted as the thickness N-S variations of thickness of the Gållebaike lihtology.

Following interpretations of the 3D modelling and potential field analysis above, this study suggests a refined interpretations of the structural setting of the Bakkilvarri domain. This results from this study propose that the main parts of the volcanic units within the Bakkilvarri domain are concentrated within the NW zone, forming a NW-SE trending linear belt (BVC in Figure 7.12, 7.7). In the light of the new proposed 3D model, it appears that the large scale tonalite and inferred intermediate density schist appear to be the largest influence on the reduction in the size of the volcanic body. This interpretation is in contrary to earlier suggestions that the eastern parts of the Iddjajav'ri area were recognized by mainly volcanics (Henriksen, 1991) (Figure 6.6).

As the gravity data contain no inherent depth information, and the deeper structures in the area are poorly constrained, it is challenging to accurately determine the exact depth of the supracrustal rocks within the KGB. The 3D model has been modelled with a flat-lying base towards the JGC. However, based on the present knowledge and data, these structures cannot be constrained sufficiently. In particular, the depth to the Archean basement towards the southern prolongation of the KGB are rather suggestive. It cannot be ruled out that the basement topography may reach shallower depths, than what is inferred from the final 3D model. This could replace the large volumes of mica schists in the deeper parts of

the model, and indicate that the Archean basement topography is more undulating than obtained from this study (Figure 7.11). The results from the 3D modelling indicate that the outcropping granite at the thrust contact to the JGC, extends to the base of the KGB (Figure 7.8). Due to the highly strained and recrystlized texture of this granite (Figure 4.10 (b)), it opens for the possibility that the intrusion represents parts of the JGC. This could also explain several of the negative gravity anomalies near the base of the KGB (Figure 6.3 (a)).

Based on the observed orientation of D_2 from field observations and the aeromagnetic data, this study proposes a gradual, anticlockwise rotation of the main stress orientation, after the main thrusting episode (Figure 8.2). The orientation of axial traces of ENE plunging F_2 folds observed in the field, kinematics from outcropping shear zones and geophysical signature from F_2 folds, propose that the D_2 was related to a NNW-SSE oriented shortening (Figure 8.2). Braathen and Davidsen (2000) defined the D_2 phase as the NE-SW shortening, and a general dextral transpression. As the D_2 structures were refolded and possibly reactivated by D_3 phase, and there is a general lack of clear overprinting relationships of these phases, it is difficult to accurately determine the main compressional direction.

The overprinting relations of thrust contact to the JGC show that the supracrustal rocks within the KGB emplaced on top of the JGC before the initiation of the F_2 folding. This signature cannot be observed at the contact to the TMB, as the thrust zone appears as a more or less linear segment throughout the area. One reason for these differences could either be attributed to a more prolonged (re)activation of the thrust zones separating the KGB and TMB. Another possibility is that the thrusting of the TMB occurred after the refolding of the basal thrust contact of the KGB. However, based on the observed structural relations and 3D modelling results, this study prefers an explanation where the eastern parts of the KGB underwent a more complex structural evolution, and possibly one or more reactivation of the thrust zone. The later fold phase could also explain the enigmatic structures observed in the central zones within the Bakkilvarri domain. Here, folding may have caused deep synforms, due to refolding of the D_1 structures. However, this study has not been able to accurately confirm or reject these possibilities. However, Midtun (1988) concluded that 4-5 km deep synforms further south had been formed due two overprinting fold phases. This opens for the possibility that the intermediate body modelled in the vicinity of the Gimesvarri High (Figure 6.3 (a)) may actually represent mica schists from the Gållebaike Fm. (Figure 7.7).

The 3D modelling and structural interpretation indicate that the observed NE-SW trending faults (Figure 6.9) have a more prolonged and important deformation history, than interpreted by Henriksen (1991) and Midtun (1988). The 3D modelling and potential field analysis suggest that the NW-SE trending BVC terminates against the Adjatavzi Fault (Figure 7.12, 6.9, 6.3). The subtle magnetic signature related to the Adjatavzi Fault, in addition to the rotation of both magnetic gravity

lineaments towards the fault zone (Figure 6.3, 6.9, 6.10), suggest that the fault has been active at some point as a ductile structure, possibly at some point during D_2 and D_3 (Figure 8.2). However, based on its structural control on large scale structures within the Bakkilvarri domain, it is possible that the Adjatavzi Fault was active already during the D_1 phase.

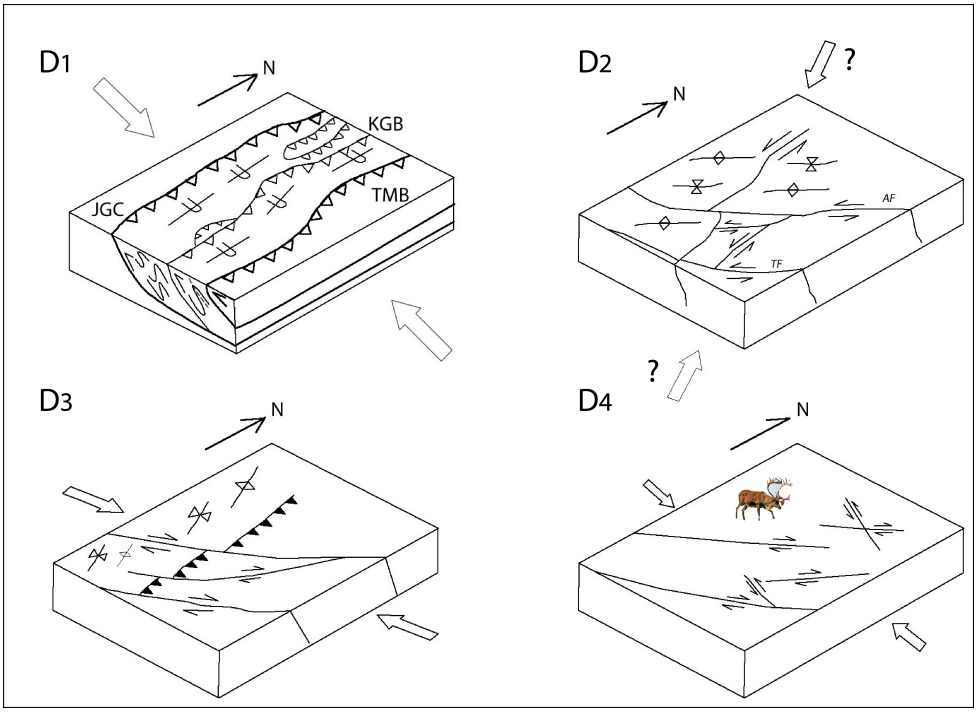

Figure 8.2: Block models indicating the main structures formed during the different deformation phases. (a) Shows the D_1 thrusting and imbrication. (b) D_2 caused ENE plunging folding, in addition to transpresional kinematics on previous active D_1 thrust zones.

The structural trends related to the Tanalv Fault suggest a complex evolution for the steep NE-SW trending fault (Figure 6.9, 6.11). However, the Tanaelv Fault differs somewhat from the Adjatavzi Fault in terms of the length and influence on the TMB. The rotation of magnetic and gravity lineaments within the southern parts of the Bakkilvarri domain is interpreted to be caused by at least on generation of dextral kinematics (Figure 6.11). This is interpreted to be the cause of the arcuate trend of the structural grain within the southern part of the central zone within the Bakkilvarri domain. The marked gravity anomaly related to the Tanalv Fault is interpreted to be caused by the juxtaposed TMB against the denser Bakkilvarri volcanics, causing a significant N-S density contrast. Due to the displacement

and total length of the Tanalv Fault, it is interpreted to be of a significant depth. As the NE-SW trending faults are not exposed within the Iddjajav'ri area, the interpretation described here is mainly based on geophysical data. However, steep fault zones, with high angle to the main thrusting direction have observed throughout the CLGB (Väisänen, 2002; Patison, 2007; Niiranen et al., 2014). Combined with the results from this study, the existence of such faults appears as a viable hypothesis. Ward et al. (1989) indicated that such steep shear zone forming at high angle to the main thrusting during the Svecofennian Orogeny, could represent ancient transfer faults formed during rifting and opening of the intracratonic basin. Following the general tectonic model for the KGB, the observed NE-SW trending faults could be related to such ancient transform faults, later reactivated during basin inversion. However, due to the arcuate trend of thrust fronts, it is not uncommon that transform faults occur during large scale thrusting and nappe emplacement (Macedo and Marshak, 1999).

Similar NE-SW trending shear zones have been reported throughout the Paleproterozoic domains of the Finnmarksvidda (Olesen et al., 1990; Olesen and Sandstad, 1993). Olesen et al. (1990) interpreted the Mierujavri-Sværholt Faults (See their Figure 8) as a Proterozoic fault, active during or just after the emplacement of the Levajok Granulite Complex. The results from the magnetic analysis from this study are of striking resemblance to these findings. Furthermore, the observation of a reversed magnetized diabase dike in the NW part of the Iddjajav'ri appears to correlate well with a NE-SW striking fault zone, causing dextral rotation and SW bulging of the Bakkilvarri Volcanics (Figure 6.9). Hence, it appears that the dike intruded into the fault, causing the reversed magnetic pattern observable today. This interpretation correlates well with similar structures by Olesen et al. (1990). Both the fault movement and dike emplacement suggests post-thrusting movement. However, from the lack of overprinting relationships, it is difficult to evaluate if the fault was active during the D_3 or D_4 phase. Furthermore, due to the orientation of the modelled sections of the 3D model, it has been challenging to quantify the cumulative displacement, and assess the possible dip-slip component of the NE-SW trending faults. This is particuarly evident for the Adjatavzi Fault.

Both field observations and overprinting relations from the aeromagnetic data indicate that the internal D_1 thrusts within the KGB may have been reactivated as steeper, transpressional or strike-slip shear zones, one or several times during D_2 and D_3 (Figure 8.2). A such interpretation could explain the enigmatic structures observed at Jalgesvadda Hill (Figure 4.8, 6.11). The steep eastern boundary of these 3D modelled structures and truncation of magnetic lineaments, suggest that structure was possibly first developed as an east-dipping D_1 thrust fault, where the metapsammites were thrusted on top of the amphibolites (Figure 6.11, 7.6). The rotation of the main paleostress field during D_2 may have reactivated these early D_1 structures, forming approximately N-S trending shear zones. This expla-

nation is supported by the observation of steeply dipping N-S trending mylonitic metapsammites at the eastern contact of the Jalgesvadda Hill (Figure 4.8 (c)). From the magnetic data, the magnetic lineaments related to the Jalgesvadda hill could reassemble a flower structure, or km-scale sigma clast (Figure 6.11). Due to the complex shape of the structures Ravdojavri area, it is difficult to attributed to a specific deformation phase. As the area is so poorly exposed and lacks 3D constrains, these interpretations remain speculative.

8.1.1 Distribution of mafic and ultramafic intrusions

The use of gravity gradients have allowed to model the distribution of mafic and ultramafic intrusions. The mafic and ultramafic units observed within the Gållebaike domain appear to follow the same structural trends as the hosting supracrustal units. Compared to the interpretations by Henriksen (1986), the qualitative analysis and 3D modelling suggest that the intrusions make up complex structures, influenced by thrusting, folding and later stage faulting (Figure 6.11, 7.5,7.6). Within the eastern zone in the Gållebaike domain, the magmatic bodies appear to follow an arcuate, along the strike of the belt. As described by Midtun (1988), the mafic to ultramafic intrusions show large variations in magnetization intensity.

The 3D density modelling indicates that the largest intrusions in the area are made up by the Stuorra Gourpmet and Gallujavri (Figure 7.5, 7.6). From the vertical gravity component, they stand out as relative large scale anomalies. From their shape and structural relations with the hosting metapsammites, the intrusions are seemingly influenced by both folding and faulting (Figure7.5).

The Stuorra Gourpmet intrusion is interpreted as the largest intrusions within the modelled area. From the modelling results, the Stuorra Gourpmet intrusion is interpreted to be made up of at least two separate units (Figure 6.3, 7.6). From the structural intepretations (Figure 6.9, 6.11), it appears that the intrusion has been influenced by N-S and NE-SW trending faults. The new 3D model clearly supports the qualitative interpretations, that the lateral distribution of the intrusion is significantly less than interpreted by Henriksen (1986). The NW part of the intrusion follows a NW-SE, arcuate trends, where it seemingly terminates just southeast of the Gallujavri intrusion. The central part of the intrusion is main located around the Gallovaras hill, and its northern prolongation is less then earlier interpreted. The modelling show that the Stuorra Gourpmet intrusion is not connected to the outcropping gabbros at the Oalgevarri hill.

The Gallujav'ri intrusions stands out as a structurally complex feature. From the modelling, it appears that most of the outcropping metagabbros originate from the a similar deep seated feature, but stand out as different units at the surface. The depth extent of the main intrusion is moderate, and reaches approximately 1 km in its southern limit. The northern parts of the intrusion differ in both geometry and thickness. It becomes a more shallow feature, and appears to have

a total thickness of approximatly 300 m. Furthermore, the intrusion appears to be separated into two N-S elongated structures, separating the ultramafic from the mafic parts (Nilsson and Often, 2005). The ultramafic parts stands out as a deeper, bowl shaper structure, while the metagabbro forms a more elongated plate like body. This open for the possibility to interpret that the bodies are structurally separated. This could also explain the large magnetization contrasts between the ultramafic and mafic parts (Figure 6.5). However, due to the lack of outcrops, this remains speculations.

The correlation between the structural trends of the mafic and ultramafic intrusions and the lineament trends within the southern parts of the Gållebaike domain appear to be similar. The NNE-SSW trending faults apparently influencing both the Gallujavri and Stourra Grourpmet intrusion appear to be related to the reactived D_1 thrusting as described earlier. The observed arcuate trends of the mafic intrusions seen from the final 3D model appear to have been caused by the same dextral rotation of NE-SW trending faults zones, as for the adjacent supracrustal rocks. This indicates further the regional implications of these faults.

8.1.2 Uncertainties and limitations

Given the 3D modelling approach and complexity of the recorded geological evolution in the area, it is necessary to address the limitation of the developed 3D model. In the modelling, each layer is presented as a homogeneous unit, and is given a constant density. These bodies are modelled with sharp contacts to adjacent units, and assumed to have constant properties through out the region. This is a gross simplification when considering inherent complexity of the actual geology in the area. However, in order to develop a coherent 3D model of the 20 x 30 km area, it is impossible to include the heterogeneous nature of the lithological units, and such simplifications are necessary. This is particularly evident when modelling discontinuous and geological complex bodies, such isolated intrusions or refolded structure. It is therefore important to appreciate the physical scale and resolution of the developed 3D model, when the result is interpreted.

Due to the lack of constrains from field observations and outcrops in the area, there are even more limitations from field observations. By introducing as many constrains as possible, these limitations and uncertainties are minimized. The integration of both field mapping and geophysical analysis further constrains the structural interpretations. During this study, it was challenging to identify and isolate different deformation phases and structural evolution of the area, as most of the outcrops lacked overprinting relationships. However, correlations of structural trends in both field and geophysical data allowed to identify regional overprinting features. However, this requires a well constrained correlation between lithologies, structures and geophysical signature. In cases where key structures do not inherently display any characteristic geophysical signal, such relationships cannot

be establish. In the light of these evaluations, the approach combining geological mapping, high resolution aeromagnetic and gravity gradient data are considered as a effective approach to understand the 3D crustal architecture of the KGB.

8.2 Regional correlations

The results of this works allow for a comparison of the interpreted structural styles to other parts of the KGB and CLGB. Throughout the length of the KGB, it is a seemingly change and differentiation in structural styles and lithological distribution. As discussed by Davidsen (1994), the lithologies in the Lakselv valley are interpreted to present a continuous depositional sequence, with no inferred tectonic contacts between the units (See Figure 3.3). In particular, the interpretation that the lower parts of the stratigraphy, his Cår'gas Fm., contain features that are considered as the autochnous within the Iddjajav'ri, i.e. the Skuvvanvarri Fm. This differs from the Iddjajav'ri area, and further south, where the KGB has been interpreted to be thrusted on of the JGC Krill (1985); Braathen and Davidsen (2000).

Recent isotopic datings have shown deritral ages of 2700-2900 Ma for the Skuvvanvarri (M. Marker, pers.comm., aug. 2014), identical to ages obtained from the granites within the JGC. Hence, the Skuvvanvarri sediments appear to be sourced from the JGC. Both the geophysical and structural interpretation in this thesis supports the idea of a thrusted contact at the base of the KGB, as the contact appears to be influenced by significant ductile movement. Braathen and Davidsen (2000) reported that the thrust contact in the Karasjokka area, most likely had been reactivate several times during the rotation of the main paleostress orientation.

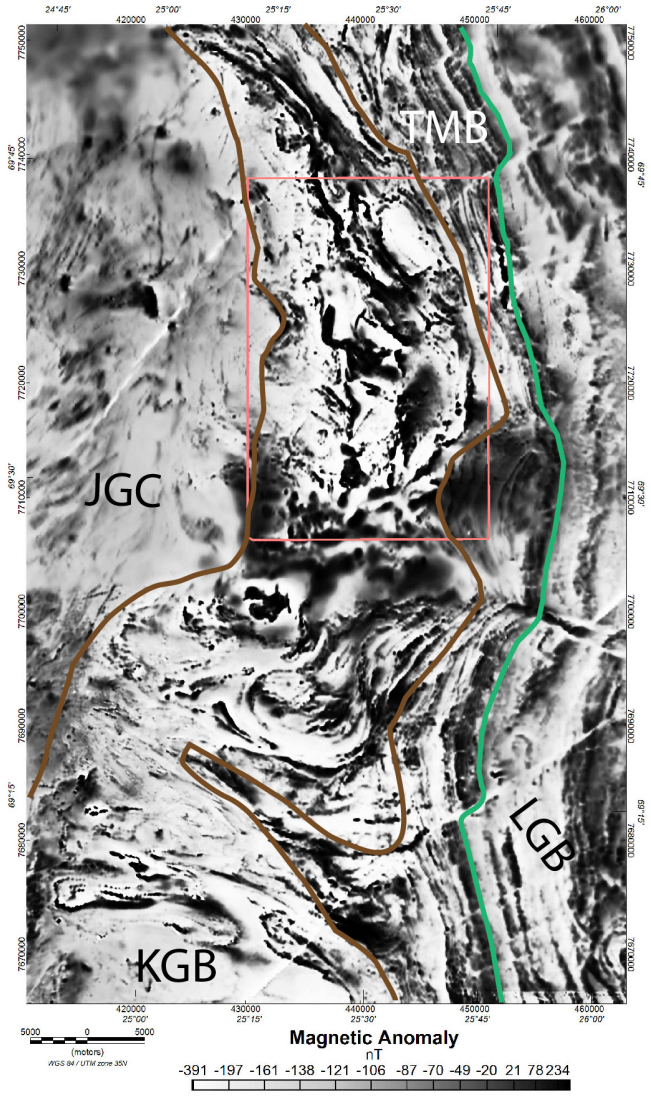

Figure 8.3: Magnetic anomaly, with tectonic outline based on (Krill, 1985) and this work. Brown line indicates the outline of the KGB, while the green line indicate the contact between the TMB and LGB. Pink box shows the boundaries of the 3D model from this study. The magnetic data indicate a change in structural style, south of the modelled area. The magnetic lineaments change orientation from mainly NNW-SSE to almost E-W. Abbreviations: JGC: Jergul Gneiss Complex; KGB: Karasjok Greenstone Belt; LGB: Levjok Granulate Belt: TMB: Tanaelv Migmatite Belt.

The structural styles appear to change between the Lakselv Valley, Iddjajav'ri area and the Karasjokka area (Davidsen, 1994; Braathen and Davidsen, 2000). The magnetic data (Figure 8.3) confirm the structural observations by Braathen and Davidsen (2000), and indicate that the supracrustal litodomain within the Karasjokka area is dominated by stratigraphic repetition due to isoclinal folding, which have been refolded by later phases. However, the northern parts of the Karasjokka river make up a clear transition to the Iddjajav'ri area, which appear to be less influenced by the same folding pattern observed further south (Figure 8.3). Structural studies from the Lakselv area show that the area was mainly affected by large scale thick-skinned folding and no large scale shear zones have been reported internally this area (Davidsen, 1994). Braathen and Davidsen (2000) did not observe any evidence for regional scale NE-SW trending faults. Their results differ from the interpretations from this study. Based on regional aeromagnetic data (Figure 8.3), this study proposes that the changes in apparent structural grain between the Iddjajav'ri area and Karasjokka area is caused by a fault zone parallel to the Karasjoka River. This explain seems to fit the change in the structural styles, evident both from field observation and aeromagnetic data (Figure 8.3).

Several earlier studies have recognized the KGB as the northern prolongation of the CLGB (Lehtonen et al., 1998; Evins and Laajoki, 2002). Recent 3D potential field studies and seismic reflection profiles have resulted in a significant higher data density in the Finnish part of the CLGB (Niiranen et al., 2014). As observed from Figure 1.2, the regional compiled aeromagnetic data show that the units within the KGB can be traced towards the Kittilä terrane. However, the area between the Karasjokka profile (Often, 1985) and Finnish boarder is very poor exposed and remote. Comparing the lithological units within the KGB to the stratigraphy further south, it appears that the lower parts of the KGB have close resemblance to the Sodankylä and Savukoski groups (Lehtonen et al., 1998; Hanski and Huma, 2005), based on the observed lithologies. These correlations have been proposed by Davidsen (1994) and Henriksen (1991), supported by radiometric datings from Krill et al. (1985). This correlation would also support the interpretation that the Bakkilvarri Fm. could be attributed to higher influx of metasedimentary units, as observed from the Savukoski Group (Hanski et al., 2001).

Datings by Marker et al. (2000) showed ages between 1971 and 2438 Ma for the Gållebaike Fm. Evaluating the margin of error of the Sm-Nd method used by Krill et al. (1985), these datings should be treated with care (M. Marker and A.G. Krill, pers.comm., Aug. 2014). From these ages, it is difficult to use any of these age datings with confidence. If the youngest ages are valid, the Gållebaike formations appear to correlate better with the Kittilä group in time, which has been dated to approximately 2.0 Ga. However, lithological units, and MORB affinity of the Kittilä group show that the depositional environment was different than from the Gållebaike Fm. Henriksen (1991); Davidsen (1994).

In terms tectonic setting, the youngest obtained ages place the deposition of the Iddjajav'ri group within the main collisional phase of the Lapland-Kola orogeny, a result that is of strong contrast to the interpretation from the Sodankylä and Savukoski Group within the CLGB, and the main tectonic model of the area (Hanski et al., 2001).

8.3 Mineral potential

Based on exploration within the KGB, the mafic and ultramafic inutrives appear to be related to promising magmatic Ni-Cu-PGE mineralizations. As the geophycsial interpretation of the area have shown that the intrusions hosted in the Gållebaike Fm. appear to be more prominent than earlier inferred, there might be larger potentials for economical mineralization. However, within the KGB, it has been challenging to establish the geophysical signature of mineralized mafic and ultramafic intrusions (Nilsson and Often, 2005). However, gravity gradients and 3D density modelling can be used to locate and estimate the sizes of the these intrusions.

The 3D modelling has shown that the Gallujavri intrusion may be part of a larger, deep seated intrusion, where the southern prolongation appears to be the largest. Both the 3D density modelling and magnetic interpretation show that the mafic to ultramafic intrusions located within the Iddjajav'ri area are most likely larger than what can be observed from the surface data. As the intensely magnetized intrusions often are related to ultramafic lithologies, this magnetic signature may used to identify prospects for magmatic Ni-Cu-PGE deposits.

As reported from the central parts of the CLGB, the orogenic gold deposits are mainly related to faults and shear zones that have been active in the ductile-brittle transition (Ward et al., 1989; Patison, 2007). Due to the close resemblance of lithologies and structures between the KGB and the Savukoski and Sodankylä Groups, the gold deposits in the CLGB may be used as analogs. Following the interpretations from this study, it appears to be a clear link between recorded deformation phases of the Iddjajav'ri area and the Finnish part of the CLGB (Hölttä et al., 2007; Ward et al., 1989; Väisänen, 2002). Within the CLGB, several of the large scale gold deposits have been located within reactivated large scale thrust zones, e.g. the Sirkka thrust zone (Eilu et al., 2007). In addition, the D_3 faults and shear zones that occurs at high angles to the D_1 thrusts, have shown to be related to significant gold mineralization (Patison, 2007; Patison et al., 2007). Within the Iddjajav'ri area, these reactivated, steep faults have been poorly investigated. If the structural evolution of these faults have been similar to the CLGB, they could be related to possible gold deposits. As seen both from the CLGB and KtGB, gold deposits are mostly related to pervasive albite-carbonate alterations (Ward et al., 1989; Sandstad et al., 2012).

In particular it is interseting to compare the similiarties between the Adjatavzi and the Tanaelv Fault against the Kiistala shear zone, hosting the Suurikuusikko Au-Cu deposit (Eilu et al., 2007). The mineralization within the Suurikuusikko deposit is hosted in the Kittilä Group, and are therefore somehwhat different from the lithologies within the Iddjajav'ri group. However, as the fault timing and deformation history are poorly constrained from the Iddjajav'ri area, and not throughly investigated by drilling, these indications remain speculative.

Chapter 9

Conclusion and outlook

A new 3D crustal model has been created for the northern parts of the KGB, based on 3D density modelling of Airborne Gravity Gradient data, integrated with qualitative interpretation of geophysical and geological data. The integration of high resolution geophysical data and surface observation have made it possible to identify several new structures not earlier known. The multiscale approach used here has allowed to link shallow and deeper structures throughout the area.

The new 3D model shows that the Karasjok Greenstone Belt is complex NNW-SSE striking crustal structure. The 3D model suggests that the belt reaches depths of approximately 3 km, and is emplaced as an east dipping structure between the Jergul Gneiss Complex in the west and Tanaelv Migmatite Belt in the east. The multiscale approach has revealed that the structural architecture of the KGB is far more complex than previously known. The first order structures are caused by west-vergent thrusting, developing local to regional thrust zones during the D1 deformation phase. This phase was caused by the main collisional phase of the Kola-Lapland orogeny. Internally, several thrust and shear zones have been identified, forming complex imbricate stacking and folding of the supracrustal rocks. This caused significant thickness variations of the stratigraphic units.

The volcanic units are concentrated in a wedge-shaped NW-SE trending belt within the eastern part of the area, and reflect the first order, short-wavelength gravity anomalies. Compared to the earlier estimates, this study proposes that the volcanic belt constitutes a significantly smaller part of the KGB. The 3D modelling has revealed that the outcropping tonalites within the northeastern parts extend as a N-S trending complex, and make up an important structural feature. The tonalites are considered to be at their largest towards the northeastern part of the belt, where they appear to reflect a large scale dome shaped structure. 3D modelling indicates that the depth of these structures extends to the base of the greenstone belt. This study suggests that they are either a part of a thrusted

basement sliver, or a deformed intermediate intrusion complex.

Internally, the present-day architecture appears to be a result of reactivations of earlier D_1 thrust structures. A later rotation of the main paleostress orientation caused reactivation of older thrust-related structures and development of two main fold phases. These structures caused development of complex overprinting structures within the region. The qualitative and 3D modelling suggest that NE-SW trending faults and shear zones have been important structures during the tectonic evolution of the KGB. These structures appear to have a more prolonged deformation history than earlier inferred. The Tanaelv and Adjatavzi Faults have been identified as the main NE-SW trending structure. They are interpreted to cause the arcuate shape of the southern part of the study area, caused by dextral rotation of the belt. As these faults most likely have been active several times, as both ductile and brittle faults, they may be prospective for epigenetic metal deposits.

The geophysical modelling has shown that the mafic to ultra-mafic intrusions make up a prominent arcuate trend within the central parts. From the geophysical data, they appear as structurally complex features, where their geometries have been controlled by NNW-SSE and NE-SW striking thrusts and faults. The intrusions are located only at moderate depths. If any of the mafic or ultramafic bodies are mineralized with Ni-Cu-PGE deposits, their size may be large enough to make up an economically viable deposit. In particular, the Gallujav'ri intrusion appear as a more deep seated feature than what can be observed from the surface observations, and are therefore a possible target for more exploration.

9.1 Suggestion for future work

In order to constrain and confirm the observed structures, more data are needed. Due to the lack of outcrops in the area, traditional mapping program purely based on field observations and outcrop hunting seems not to be worthwhile. Rather, an approach similar to what have been applied by the GTK in the Finnish parts of the Central Lapland Greenstone Belt, with large integrated mapping programs involving age datings, structural analysis and geophysical investigations, appear as a efficient method (see e.g. (Lehtonen et al., 1998) and Niiranen et al. (2014)). In terms of timing of geological events, it is clear that the area need better and more detailed structural analysis and isotopic dating to determine the relative ages. In particular, ages of the tonalite should be obtained, as this would either confirm or reject the possibility that the tonalite represent a thrusted-emplaced part of the Archean basement or an intrusion.

The acquisition of higher AMT and seismic reflection profiles could possibly yield further constrains of the deeper structures in the 3D model. In particular, seismic profiles could possibly confirm the depth of the supracrustal rocks within the KGB. A integrated approach of both potential field modelling and seis-

mic profiling has shown to produce reliable results in cases with high resolution seismic lines (Malehmir et al., 2007), even at exploration scale. However, recent seismic acquisition in the Masi area did not show promising results for shallow seismic investigations. The results from reflection seismic projects in Finland (FIRE, HUKKA and HIRE) was acquired with good results, and appear to have improved the crustal architecture of the Central Lapland Greenstone Belt.

For the 3D geophysical modelling and the geometry of the belt, the next step would be to incorporate the model in a joint magnetic and gravity inversion. A suitable approach would be a litho-constrained inversion integrated in GeoModeller. This approach would also benefit from the possibility to build a more detailed 3D geological model, using the structural results from this thesis. A lithoconstrained inversion approach as offered in GeoModeller would in addition allow the use of magnetic properties, and therefore further constrain the modelling result.

Appendix A

Appendix A

A.1 Geological Abbreviation

AC Adjatskaidi Complex

AF Adjatavzi Fault Zone

BI Biipovarri Intrusion

BNC Bakkilvarri Central Zone

BNE Bakkilvarri Northeastern Zone

BNW Bakkilvarri Northwestern Zone

CLGB Central Lapland Greenstone Belt

GC Geassacopma Complex

GE Gållebaike Eastern Zone

GI Gallujavri Intrusion

GW Gållebaike Western Zone

IOCG Iron oxide copper gold deposits

IT Inari Terrane

JGC Jergul Gneiss Complex

JH Jalgesvadda Hill

KGB Karasjok Greenstone Belt

KtGB Kautokeino Greenstone Belt

KiGB Kittilä Greenstone Belt

LGB Levajok Granulite Belt

LK Lassevarri Komatiite

RV Rivdnjesvada Complex

SG Stuorra Gourpmet Intrusion

TF Tanaelv Fault Zone

TMB Tanaelv Migmatite Belt

VMS Volcanogenic massive sulfide deposit

A.2 Other Abbreviations

AGG Airborne Gravity Gradient

AEM Airborne Electromagnetic

AM Aeromagnetic

DTM Digital Terrain Model

FDEM Frequency Domain Electromagnetic

FTG Full Tensor Gravity Gradiometry

GTK Geological Survey of Finland

HDT Horizontal Directive Tendency

NRM Natural Remanent Magnetization

NGU Geological Survey of Norway

Q-ratio Koenigsberger ratio

SGU Geological Survey of Sweden

THDR Total horizontal derivative

TDR Tilt derivative

SI Shape Index

Bibliography

Airo, M. and Mertanen, S. (2008). Magnetic signatures related to the orogenic gold mineralization , Central Lapland Greenstone Belt, Finland. *Journal of Applied Geophysics*, 64:14–24.

Airo, M.-L. (1995). Magnetic petrology and aeromagnetic interpretations. *In: Autio, S (Ed), Geological Survey of Finland, Special Paper*, 20:177–179.

Airo, M.-L. (2005). Regional interpretation of aerogeophysical data: Extracting compositional and structural features. *Aerogeophysics in Finland 1972–2004 (ed. M.L. Airo), Geological Survey of Finland, Special Paper,*, 39:176–197.

Airo, M.-L. (2007). Application of Aerogeophysical Data for Gold Exploration: Implications for Central Lapland Greenstone Belt. In Ojala, J. (ed.) Gold in the Central Lapland Greenstone Belt, Finland. *Geological Survey of Finland, Special Paper*, 44:171–192.

Airo, M.-L. and Kurimo, M. (1999). Paleoproterozoic Suukisjoki Mafic-Ultramafic intrusion in Northern Finland: Combined aerogeophysical, geological and tectonic studies. *Geological Survey of Finland, Special Paper*, 27:14–149.

Aitken, A. and Betts, P. (2009). Multi-scale integrated structural and aeromagnetic analysis to guide tectonic models: An example from the eastern Musgrave Province, Central Australia. *Tectonophysics*, 476:418–435.

Aitken, A., Betts, P., Schaefer, B., and Rye, S. (2008). Assessing uncertainty in the integration of aeromagnetic data and structural observations in the Deering Hills region of the Musgrave province. *Australian Journal of Earth Science*, 55:289–314.

Barbey, P., Convert, J., Moreau, B., Capdevila, R., and Hameurt, J. (1984). Petrogenesis and evolution of an early Proterozoic collisional orogenic belt: the granulite belt of Lapland and the Belomorides (fennoscandia). *Geological Survey of Finland*, 56:161–188.

Barnes, S.-J. and Often, M. (1990). Ti-rich komatiites from northern Norway. *Contrib Mineral Petrol*, 105:42–54.

Betts, P., Stewart, J., and Ailleres, L. (2007). Kinematic analysis of aeromagnetic data: Looking at geophysical data in a structural context. *Gondwana Research*, 11:83–111.

Betts, P., Valenta, R., and Finlay, J. (2003). Evolution of the Mount Woods inlier, northern Gawler Craton, Southern Australia: an integrated structural and aeromagnetic analysis. *Tectonophysics*, 366:83–111.

Bhattacharyya, B. (1966). Continuous spectrum of the total-magnetic-field anomaly due to a rectangular prismatic body,. *Geophysics*, 31:97–121.

Blakley, R. J. (1995). *Potential Field Theory in Gravity and Magnetic Applications*. Cambridge University Press.

Blakley, R. J. and Simpson, R. W. (1986). Approximating edges of source bodies from magnetic or gravity anomalies. *Geophysics*, 51(7):1494–1498.

Braathen, A. and Davidsen, B. (2000). Structure and stratigraphy of the Palaeoproterozoic Karasjok Greenstone Belt, northern Norway; regional implications. *Norwegian Journal of Geology*, 80:33–50.

Cagnard, F., Barbey, P., and Gapais, D. (2011). Transition between "Archaean-type" and "modern-type" tectonics: Insights from the Finnish Lapland Granulite Belt. *Precambrian Research*, 187:71–88.

Calcagno, P., Chilès, J., Courrioux, G., and Guillen, A. (2008). Geological modelling from field data and geological knowledge, part I — modelling method coupling 3d potential field interpolation and geological rules. *Phys. Earth. Planet. Inter.*, 171:147–157.

Carlos, D. U., Braga, M. A., Galbiatti, H. F., and Pereira, W. R. (2013). Airborne Gravity Gradiometry - data processing and interpretation. *Revista Brasileira de Geoffsica*, 31(3):427–453.

Cevallos, C., Kovac1, P., and Lowe, S. J. (2013). Application of curvatures to airborne gravity gradient data in oil exploration. *Geophysics*, 78(4):81–88.

Clark, D. (1997). Magnetic petrophysics and magnetic petrology: aids to geological interpretation of magnetic surveys. *AGSO Journal of Australian Geology and Geophysics*, 17(2):83–103.

Cooper, G. and Cowan, D. (2006). Enhancing potential field data using filters based on the local phase. *Computers and Geosciences*, 32:1585–1591.

Cooper, G. and Cowan, D. (2008). Edge enhancement of potential-field data using normalized statistics. *Geophysics*, 73:H1–H4.

Cordell, L. and Grauch, V. J. S. (1982). Mapping basement magnetization zones from aeromagnetic data in the san juan basin, new mexico. In *1982 SEG Annual Meeting*.

Daly, J., Balagansky, V., and Timmerman, M. (2001). Ion microprobe U-Pb zircon geochronology and isotopic evidence supporting a trans-crustal suture in the Lapland Kola Orogen, northern Fennoscandian Shield. *Precambrian Research*, 105:289–314.

Daly, J., Balagansky, V., Timmerman, M., and Whitehouse, M. (2006). Palaeoproterozoic collision and accretion of the northern Fennoscandian lithosphere, in: European Lithosphere Dynamics. *Geological Society, London, Memoirs*, 32:579–598.

Davidsen, B. (1994). Stratigrafi, petrologi og geokjemi med vekt på komatiittiske bergarter innen den nordligste delen av Karasjok grønnsteinsbelte, Brennelv, Finnmark. *Master Thesis, UiT*, pages 14–24.

de Wit, M. J. (1998). On Archean granites, greenstones, cratons and tectonics: does the evidence demand a verdict? *Precambrian Research*, 91:181–226.

Dransfield, M. (2007). Airborne Gravity Gradiometry in the Search for Mineral Deposits. *In Milkereit, B. (Ed.) Proceedings of Exploration 07: Fifth Decennial International Conference on Mineral Exploration*, pages 243–246.

Dransfield, M. (2010). Conforming Falcon gravity and the global gravity anomaly. *Geophysical prospecting*, 58:469–483.

Dransfield, M. and Zeng, Y. (2009). Airborne gravity gradiometry: Terrain corrections and elevation error. *Geophysics*, 74(5):137–142.

Dunlop, D. and Ozdemir, O. (1997). *Rock Magnetism*. Cambridge University Press.

Eilu, P., Pankka, H., Keinänen, V., Kortelainen, V., Niiranen, T., and Pulkkinen, E. (2007). Characteristics of gold mineralisation in the greenstone belts of Northern Finland. *Gold in the Central Lapland Greenstone Belt, Finland (ed. J. Ojala), Geological Survey of Finland, Special Paper*, 44:57–106.

Ellis, R. and Ebbing, J. (2013). Karasjok AGG Survey Example. In *Presented at the Gravity Gradients VOXI Workshop - 6th October 2013, Skukuza, Kruger National Park*.

Ellis, R. G., de Wet, B., and MacLeod, I. (2012). Inversion of magnetic data for remanent and induced sources. In *ASEG Extended Abstracts*. ASEG.

Elo, S., Lanne, E., Routoistenmäki, T., and Sindre, A. (1989). Interpretation of gravity anomalies along the POLAR Profile in the northern Baltic Shield. *Tectonophysics*, 162:135–150.

Elvebakken, G., Krill, A. G., Often, M., and Henriksen, H. (1985). Early Proterozoic shallow-marine albite-rich sandstone in the Karasjok Greenstone Belt. *Geological Survey of Norway Bulletin*, 405:113–119.

Evins, P. and Laajoki, K. (2002). Early proterozoic nappe formation: an example from Sodankylä, Finland, Northern Baltic Shield. *Geol. Mag.*, 139(1):79–87.

Evjen, H. (1932). The place of the vertical gradient in gravitational interpretations. *Geophysics*, 1:127–136.

Fugro (2011). *FALCON Airborne Gravity Gradiometer Survey for Store Norske Gull AS, Processing Report.*

Gaàl, G., Berthelsen, A., Gorbatschev, R., Kesola, R., Lethonen, M., Marker, M., and Raase, P. (1989). Structure and composition of the Precambrian crust along the POLAR profile in the northern Baltic Shield. *Tectonophysics*, 162:1–25.

Gaàl, G. and Gorbatschev, R. (1987). An outline of the Precambrian Evolution of the Baltic Shield. *Precambrian Research*, 35:15–52.

Geosoft (2005a). Montaj gridknit, Grid Extension for OASIS Montaj 6.1, Tutorial and User Guide. *Geosoft Incorporated.*

Geosoft (2005b). Montaj MAGMAP filtering, 2-D frequency domain processing of potential field data. extension for Oasis Montaj, v6.1. *Geosoft Incorporated*, page 66.

Glaznev, V., Raevsky, A., and Sharov, N. (1989). A model of the deep structure of the northeastern part of the Baltic shield based on joint interpretation of seismic, gravity, magnetic and heat flow data. *Tectonophysics*, 162:151–163.

Grant, F. (1985a). Aeromagnetics, geology and ore environments, 1. Magnetite in igneous, sedimentary and metamorphic rocks: An overview. *Geoexploration*, 23:303–333.

Grant, F. (1985b). Aeromagnetics, geology and ore environments, 2. Magnetite and ore environments. *Geoexploration*, 23:335–362.

GTK (2008). *Airborne Geophysical Survey Skuvvanvarri Finnmark, Norway,Technical Report.*

Götze, H. and Lahmeyer, B. (1988). Application of three-dimensional interactive modeling in gravity and magnetics. *Geophysics*, 53(8):1096–1108.

Gunn, P., Maidment, D., and Milligan, P. (1997). Interpreting aeromagnetic data in areas with limited outcrop. *AGSO Journal of Australian Geology*, 12:175–185.

Hanski, E. (2001). History of stratigraphical research in northern Finland. *Radiometric age determinations from Finnish Lapland and their bearing on the timing of Precambrian volcano-sedimentary sequences (ed. Matti Vaasjoki), Geological Survey of Finland, Special Paper*, 33:51–85.

Hanski, E., Huhma, H., and Vaasjoki, M. (2001). Geochronology of Northern Finland: A summary and discussion. *Radiometric age determinations from Finnish Lapland and their bearing on the timing of Precambrian volcano-sedimentary sequences (ed. Matti Vaasjoki), Geological Survey of Finland, Special Paper*, 33:51–85.

Hanski, E. and Huma, H. (2005). Central Lapland greenstone belt. *In: Precambrian geology of Finland, Key to the evolution of the Fennoscandian Shield, Ed: M. Lehtinen, P.A. Nurmi and O.T Rämö*, 14:139–183.

Heiland, C. (1940). *Geophysical Exploration.* Prentice-Hall, Inc.

Henkel, H. (1991). Magnetic crustal structures in northern Fennoscandia. *Tectonophysics*, 192:57–79.

Henkel, H. and Guzmàn, M. (1977). Magnetic features from fractures rocks. *Tectonophysics*, 115:173–181.

Henriksen, H. (1986). Bedrock map Iddjajavri 2034 II M 1:50 000, preliminary edition. *Geological Survey of Norway.*

Henriksen, H. (1991). Beskrivelse til det bergrunnsgeologiske kart 2034-II-M=1:50 000. *Un.pub. Geological Survey of Norway Bulletin*, pages 1–54.

Hinze, W. J., von Frese, R. R., and Saad, A. H. (2013). *Gravity and Magnetic Exploration, Principles, Practices and Application.* Cambridge University Press.

Hölttä, P., Väisänen, M., Väänänen, J., and Manninen, T. (2007). Paleoproterozoic metamorphism and deformation in Central Lapland, Finland. *In: Gold in the Central Lapland Greenstone Belt, Finland (ed. J. Ojala), Geological Survey of Finland, Special Paper*, 44:7–56.

Hofmann-Wellenhof, B. and Mortiz, H. (2005). *Physical Geodesy.* Springer Wien New York.

Janik, T., Kozlovskaya, E., Heikkinen, P., Yliniemi, J., and Silvennoinen, H. (2009). Evidence for preservation of crustal root beneath the Proterozoic Lapland-Kola orogen (northern fennoscandian shield) derived from P and S wave velocity models of POLAR and HUKKA wideangle reflection and refraction profiles and FIRE4 reflection transect. *Journal of Geophysical Research*, 114:B06308.

Jaques, A., Wellman, P., Whitaker, A., and Wyborn, D. (1997). High-resolution geophysics in modern geological mapping. *AGSO Journal of Australian Geology and Geophysics*, 17(2):159–173.

Kellogg, O. (1929). *Foundation of Potential Field Theory.* Berlin Verlag Von Julius Springer.

Koistinen, T., Stephens, M., Bogatcheva, V., Nordgulen, ., Wennerström, M., and Korhonen, J. (2002). Geological map of the Fennoscandian Shield, scale 1:2 000 000. *Espoo : Trondheim : Uppsala : Moscow: Geological Survey of Finland : Geological Survey of Norway : Geological Survey of Sweden : Ministry of Natural Resources of Russia.*

Korja, A., Lahtinen, R., and Nironen, M. (2006). The Svecofennian orogen: a collage of microcontinents and island arcs, in: Gee, d. g. and Stephenson, r. a. (eds). european lithosphere dynamics. *Geological Society of London, Special Publication*, 32:561–578.

Krill, A. G., , Bergh, S., Lindahl, I., W.Mearnes, Often, M., Olerud, S., Sandstad, J., Siedlecka, A., and Solli, A. (1985). Rb-Sr, U-Pb and Sm-Nd isotopic dates from Precambrian rocks of Finnmark. *Geological Survey of Norway Bulletin*, 405:37–54.

Krill, A. G. (1985). Svecokarelian Thrusting with Thermal Inversion in the Karasjok-Levajok Area of the Northern Baltic Shield. *Geological Survey of Norway Bulletin*, 405:88–101.

Lee, J. (2001). Falcon gravity gradiometry technology. *Exploration Geophysics*, 32:247–250.

Lehtonen, M., Airo, M., Eilu, P., Hanski, E., Kortelainen, V., Lanne, E., Manninen, T., Räsänen, P. R. J., and Virransalo, P. (1998). Kittilän vihreäkivialueen geologia. Lapin vulkaniittiprojektin raportti. Summary: The stratigraphy, petrology and geochemistry of the Kittilä greenstone area, northern Finland. A report of the Lapland Volcanite Project. *Geological Survey of Finland, Report of Investigations*, 140:139–183.

Luosto, U., Flueh, E., Lund, C., and Group, W. (1989). The crustal structure along the POLAR Profile from seismic refraction investigations. *Tectonophysics*, 162:51–85.

Luyendyk, A. (1997). Processing of airborne magnetic data. *AGSO Journal of Australian Geology and Geophysics*, 17(2):31–38.

Macedo, J. and Marshak, S. (1999). Controls on the geometry of fold-thrust belt salients. *Geological Society of America Bulletin*, 111:1808–1822.

Malehmir, A., Tryggvason, A., Lickorish, H., and Weihed, P. (2007). Regional structural profiles in the western part of the Palaeoproterozoic Skellefte Ore District, northern Sweden. *Precambrian Research*, 159:1–18.

Marker, M. (1985). Early proterozoic (c.2000-1900 ma) crustal structures of the northeastern Baltic Shield: tectonic division and tectogenesis. *Geological Survey of Norway Bulletin*, 405:75–88.

Marker, M., Kaulina, T., and Daly, J. (2000). New evidence for the Paleoproterozoic evolution of the Tanaelv and Karasjok belts based on Sm-Nd and recent U-Pb NORDSIM and TIMS dating from Finnmark, Norway. In *Svekalapko, An EUROPROBE project, 5th Workshop Lammi Finnland*. Univeristy of Oulu.

Marson, I. and Klingele, E. E. (1993). Advantages of using the vertical gradient of gravity for 3D interpretation. *Geophysics*, 58(11):1588–1595.

McEnroe, S. A. and Brown, L. (2004). A closer look at remanence dominated anomalies: rock-magnetic properties and magnetic mineralogy of the Russell Belt microcline-sillmanite gneisses, Northwest Adirondacks Mountains, new York. *Journal of Geophysical Research*, 56:437–456.

Midtun, R. D. (1988). Karasjokgrønnsteinbeltet: Regional geofysisk og geologisk tolkning. *Geological Survey of Norway Bulletin*, 88.

Miller, H. G. and Singh, V. (1994). Potential field tilt: a new concept for location of potential field sources. *Applied Geophysics*, 32:213–217.

Moisio, K. and Kaikkonen, P. (2012). Thermal and rheological structures along the seismic POLAR profile in the northern Fennoscandian shield. *Terra Nova*, 00:1–11.

Murphy, C. and Brewster, J. (2007). Target delineation using Full Tensor Gravity Gradiometry data. *ASEG, 2007, Extended Abstracts*, pages 1–3.

Niiranen, T., Lahti, I., Nykänen, V., and Karinen, T. (2014). Central Lapland Greenstone Belt 3D modeling project. *Report of Investigation, Geological Survey of Finland*, 209:78.

Nilsen, K. (1986). Bedrock map karasjok 2034 I M 1:50 000, preliminary edition. *Geological Survey of Norway*.

Nilsson, L. P. and Often, M. (2005). A summary report on the Cu-Ni-PGE occurences and their host rocks in the Precambrian of Finnmarks, Northern Norway. *Geological Society of Norway Report*, 085:79.

Nironen, M. (1997). The Svecofennian Orogen: a tectonic model. *Precambrian Research*, 86:21–44.

Often, M. (1985). The Early Proterozoic Karasjok Greenstone Belt, Norway: a preliminary description of lithology, stratigraphy and mineralization. *Geological Survey of Norway Bulletin*, 405:75–88.

Olesen, O., Brönner, M., Ebbing, J., Gellein, J., Gernigon, L., Koziel, J., Lauritsen, T., R.Myklebust, Pascal, C., Sand, M., Solheim, D., and Usov, S. (2010). New aeromagnetic and gravity compilations from Norway and adjacent areas: methods and applications. *Petroleum Geology Conference series*, 7:559–586.

Olesen, O., Roberts, D., Henkel, H., Lile, O., and Torsvik, T. (1990). Aeromagnetic and gravimetric interpretation of regional structural features in the Caledonides of West Finnmark and Northern Troms, north Norway. *Geological Survey of Norway Bulletin*, 405:1–24.

Olesen, O. and Sandstad, J. (1993). Interpretation of the Proterozoic Kautokeino Greenstone Belt, Finnmark, Norway from combined geophysical and geological data. *Geological Survey of Norway Bulletin*, 425:43–64.

Olesen, O. and Solli, A. (1985). Geophysical and geological interpretation of regional structures within the Precambrian Kautokeino Greenstone belt, Finnmark, North Norway. *Geological Survey of Norway Bulletin*, 405:119–130.

Parker, R. (1973). The Rapid Calculation of Potential Anomalies. *Geophysical Journal of the Royal Astronomical Society*, 31:447–455.

Paterson, N. R. and Reeves, C. V. (1985). Applications of gravity and magnetic surveys: The state-of-the-art in 1985. *Geophysics*, 50:2558–2594.

Patison, N. (2007). Structural controls on gold mineralization in the Central Lapland Greenstone Belt. *In Ojala, J. (ed.) Gold in the Central Lapland Greenstone Belt, Finland, Geological Survey of Finland, Special Paper*, 44:171–192.

Patison, N., Salamis, G., and Kortelainen, V. J. (2007). The Suurikuusikko Gold Deposit: Project development summary of Northern Europe's largest gold deposit. *In: Gold in the Central Lapland Greenstone Belt, Finland (ed. J. Ojala), Geological Survey of Finland, Special Paper*, 44:125–134.

Pedersen, L. and Rasmussen, T. (1990). The gradient tensor of potential field anomalies: Some implications on data collection and data processing of maps. *Geophysics*, 55(12):1558–1566.

Perrouty, S., Aillères, L., Jessell, M. W., Baratoux, L., Bourassa, Y., and Crawford, B. (2012). Revised Eburnean geodynamic evolution of the gold-rich southern Ashanti Belt, Ghana, with new field and geophysical evidence of pre-Tarkwaian deformations. *Precambrian Research*, 204:12–39.

Pharaoh, T. and Peatce, J. (1984). Geochemical evidence for the geotectonic setting of early Proterozoic metavolcanic sequences in Lapland. *Precambrian Research*, 25:283–308.

Pharaoh, T. and Walsh, N. (1987). Early Proterozoic Metavolcanic Suites of the Northernmost Part of the Baltic Shield. *Geological Society, London, Special Publications*, 33:41–58.

Roberts, D. (2003). The Scandinavian Caledonides: event chronology, palaeogeographic settings and likely modern analogues. *Tectonophysics*, 365:283–299.

Rybar, S. (1923). The Eötvös torsion balance and its application to the finding of mineral deposits. *Economical Geology*, 18:639–662.

Sandstad, J. S., Bjerkgård, T., Boyd, R., Ihlen, P., Korneliussen, A., Nilsson, L. P., Often, M., Eilu, P., and Hallberg, A. (2012). Metallogenic areas in Norway. *Mineral deposits and metallogeny of Fennoscandia (ed. P. Eilu), Geological Survey of Finland, Special Paper*, 53:14–149.

Schmidt, P. W., McEnroe, S. A., Clark, D. A., and Robinson, P. (2007). Magnetic properties and potential field modeling of the Peculiar Knob metamorphosed iron formation, south australia: An analog for the source of the intense Martian magnetic anomalies? *Journal of Geophysical Research*, 112:1–19.

Schmidt, S. and Götze, H. (1998). Interactive visualization and modification of 3D models using GIS functions. *Phys. Chem. Earth*, 23(3):289–296.

Siedlecka, A., Krill, A., Marker, M., Sandstad, J., Solli, A., Iversen, E., and Lieungh, B. (1985). Lithostratigraphy and correlation of the Archean and Early Proterozoic rocks of Finnmarksvidda and the Sør-Varanger district. *Geological Survey of Norway Bulletin*, 405:7–36.

Slotnick, M. (1932). Curvature of Equipotential Surfaces. *Bulletin of the American Association of Petroleum Geologist*, 16(12):1250–1259.

Verduzco, B., Fairhead, J. D., Green, C. M., and MacKenzie, C. (2004). New insights into magnetic derivates for strutural mapping. *The Leading Edge*.

Väisänen, M. (2002). Structural features in the central Lapland greenstone belt, northern Finland. *Geological Survey of Finland, archive report,K 21.42/2002/3.*, pages 135–150.

Ward, P., Härkönen, I., Nurmi, P. A., and Pankka), H. S. (1989). Structural studies in the Lapland greenstone belt, northern Finland and their application to gold mineralization. *Geological Survey of Finland, Special Paper*, 10:71–78.

Weihed, P., Arndt, N., Billström, K., Duchesne, J.-C., Eilu, P., Martinsson, O., Papunen, H., and Lahtinen, R. (2005). Precambrian geodynamics and ore formation: The Fennoscandian Shield. *Ore Geology Reviews*, 27:273–322.

Zhdanov, M. S., Ellis, R., and Mukherjee, S. (2004). Three-dimensional regularized focusing inversion of gravity gradient tensor component data. *Geophysics*, 69(4):925–937.